PHILOSOPHICAL TRANSACTIONS OF THE ROYAL SOCIETY A MATHEMATICAL, PHYSICAL & ENGINEERING SCIENCES

Derivation and Testing of a Molecular Orbital Description of Ligand Field Spectra

B. D. Bird, Elspeth A. Cooke, P. Day and A. F. Orchard

Phil. Trans. R. Soc. Lond. A 1974 **276**, 277-339
doi: 10.1098/rsta.1974.0024

DERIVATION AND TESTING OF A MOLECULAR ORBITAL DESCRIPTION OF LIGAND FIELD SPECTRA

BY B. D. BIRD, ELSPETH A. COOKE (*née* Grant), P. DAY AND A. F. ORCHARD
Inorganic Chemistry Laboratory, University of Oxford

(*Communicated by R. J. P. Williams, F.R.S.* – *Received* 15 *May* 1973 – *Revised* 10 *August* 1973)

CONTENTS

A model for describing the ligand-field spectra of cubic chromophores in a molecular orbital basis is derived and tested by carrying out least-squares-fits of the spectra of the tetrahedral ions CoX_4^{2-} (X = Cl, Br). Independent assignments of the ligand-field spectra of the latter ions are obtained by analysing the site-group splittings and vibrational fine-structure in the polarized spectra of Cs_3CoCl_5 and Cs_3CoBr_5 at 4.2 K. General expressions are calculated for the electron repulsion matrix elements of pairs of electrons occupying orbitals transforming as e, t_1 and t_2 in O_h and T_d point groups, without further assumption about the functional form of the orbitals. Tanabe & Sugano's (1954) matrices for d^1–d^5 configurations are rewritten in the more general form. The two-electron reduced matrix elements appearing in these expressions are further approximated in terms of orbital overlap populations (Mulliken 1955), one- and two-centre coulomb integrals and one-centre exchange integrals. An analogous reduction of the matrix elements of the molecular spin-orbit operator within a molecular orbital basis is also described. The energies of the spin-orbit baricentres of the ligand-field transitions are then calculated as functions of three orbital population parameters and the energy separation between the e and t_2 molecular orbitals. From the least-squares analysis of the independently assigned experimental spectra, empirical values of the four parameters are extracted, and their relation to the parameters of conventional ligand-field theory is discussed. The experimentally based molecular orbital parameters are further used to calculate spin-orbit splittings of the cubic Russell–Saunders ligand-field states, and the relative dipole strengths of transitions to those which are formally spin-forbidden from the ground state.

1. Introduction

The lower lying electronic excited states of open-shell transition metal complexes are conventionally divided into two types: ligand-field and charge transfer. To arrive at the former, electrons are excited from one orbital of predominantly d-character, localized on the metal, to another of the same type, while to form the latter, electrons are transferred from orbitals mainly localized on the ligands into the open shell or vice versa. Because the wavefunctions of the ligand field excited states have their greatest amplitude near the central metal ion it has been customary for a long time to treat them for analytical purposes as if they were composed of atomic d-functions, perturbed only to a limited extent by the surrounding ligands. Thus, for

example, the old electrostatic model of the crystal field, in which the atomic d-orbitals were held to be perturbed only by the field generated by the anionic or dipolar ligands, gave way first to a model which allowed for a radial expansion of the d-orbitals in the complex, parametrized empirically by reducing the magnitudes of the d-electron repulsion parameters below their free-ion values. With this model it has proved possible, over the years, to fit the energies of a very large number of ligand-field transitions in transition metal complexes of many types, to extract values for the energy differences between the d-orbitals of differing symmetry in the complex, and effective values of the d-shell electron repulsion energies.

Nevertheless, the existence of this apparent radial expansion of the d-shell when a transition metal ion is placed in a complex (the so-called nephelauxetic effect (Jørgensen 1962) is itself one of many strands of experimental evidence (see, for example, Jørgensen 1971) pointing to the conclusion that the open-shells in the ground- and ligand-field excited states of this kind of molecule, whilst having substantial metal d-orbital character, are sufficiently contaminated by admixture with ligand orbitals that a d-orbital basis alone is not adequate to describe them. Thus covalency must be taken explicitly into account. One of the earliest steps in this direction was taken by Koide & Pryce (1958), who argued that in octahedral complexes, for example, within the ligand field manifold the σ-antibonding e_g molecular orbital is expected to be more delocalized over the ligands than the π-antibonding t_{2g} and hence that different nephelauxetic scaling parameters would be required for the two sets of orbitals, a point also taken up by Jørgensen (1962). Lohr (1966) extended the Koide & Pryce analysis of the electron repulsion changes accompanying excitations within the ligand field manifold by considering explicitly l.c.a.o. wavefunctions in which the eigenvector of the metal d-function was sufficiently greater than those of the ligand functions that the electron repulsion integrals could be approximated by means of a Mulliken (1949) population analysis. Lohr neglected both two-centre metal-ligand, and one-centre ligand contributions to the resulting integrals. He did point out, however, that since the d-orbital population is changed when a transition takes place between two molecular orbitals having different d-eigenvectors, the Racah (1942) electron repulsion parameter A must be included, in contrast to the conventional ligand-field analysis which contains only B and C. This point was also examined by Balt (1967).

Lohr (1971) has subsequently elaborated his l.c.a.o.-m.o. parametrization of the ligand field electron repulsion integrals by recourse to the i.n.d.o. (intermediate neglect of differential overlap (Pople, Santry & Segal 1965)) approximation scheme, with the specific aim of accounting for the relative ordering of $^4A_{1g}$ and ^4E_g in the MnF_6^{4-} chromophore. Our aim, not dissimilar from, but more general than Lohr's, is to set up a model for describing ligand-field spectra within a molecular orbital framework, and to test it against a particular group of experimental data, in our case the complete set of excited states of the tetrahedral $3d^7$ ions CoX_4^{2-} (X = C, Br). For this purpose, we have made a completely new series of assignments for the doublet excited states of these molecules, based on an analysis of the site-group splittings and vibrational fine-structure of the lines in the polarized crystal spectra recorded at 4 K. Having obtained an independently based group of experimental assignments, the model may then be tested quite rigorously by carrying out a least-squares fit of the observed excited state energies to the disposable parameters (atomic orbital populations and orbital energy differences) of the theoretical model. The applicability of the model is assessed, both by the level of convergence of the fit, and the extent to which the resulting values of the parameters correspond to those obtained from molecular orbital calculations and to chemical experience.

PHILOSOPHICAL TRANSACTIONS OF THE ROYAL SOCIETY A MATHEMATICAL, PHYSICAL & ENGINEERING SCIENCES

In the following section we apply vector coupling methods to calculate quite general expressions for the electron repulsion matrix elements of pairs of electrons occupying orbitals of e, t_1 and t_2 symmetry in the O_h and T_d point groups, no other assumptions being made about the functional form of the orbitals. A set of integral approximations, roughly in the spirit of the n.d.d.o. (neglect of diatomic differential overlap) scheme (Pople *et al.* 1965), then leads to expressions for each of the electron repulsion integrals in terms of one- and two-centre Coulomb integrals and one-centre exchange integrals. In § 3, an analogous molecular orbital treatment of matrix elements of the molecular spin-orbit coupling operator is described. Section 4 sets out the new experimental data on the ligand-field spectra of Cs_3CoCl_5 and Cs_3CoBr_5 and the arguments which lead to the final set of empirical assignments. Confrontation between the electron repulsion and spin-orbit coupling theories of §§ 2 and 3, and the experimentally observed energies and intensities of § 4, takes place in § 5, where the results of the least-squares fitting are described. Finally we make some comments on the relation between the parameters extracted by the molecular orbital model and those of conventional ligand-field theory.

2. Molecular orbital treatment of electron repulsion

The most important factors which contribute to the energies of ligand-field and charge transfer excited states are one-electron orbital energy differences and changes in interelectronic repulsion energy. Our aim in this section is to set up the theoretical framework which will enable us to calculate the energies of such excited states, involving a number of unpaired electrons, in terms of one-electron and two-electron quantities. Working within a molecular orbital rather than a perturbed metal ion orbital basis increases the complexity of the problem very considerably, and we therefore wish to make the greatest possible use of arguments based on symmetry to relate the large number of integrals which would otherwise have to be evaluated or estimated. We use the vector coupling techniques originated by Racah (1942) and Wigner (1959), and first applied to transition metal ions by Tanabe & Sugano (1954), to write down expressions for all the matrix elements of electron repulsion between pairs of electrons occupying orbitals transforming under the representations e, t_1 and t_2 of the group O or T_d, with no limiting assumptions about the functional form of the orbitals. The formalism used throughout is that of Griffith (1962). Next we construct from these generalized two-electron matrix elements the complete set of electrostatic matrices for the configurations $(t_2e)^n$ for $n = 2$–5, where $(t_2e)^n$ denotes $t_2^{n_1}e^{n_2}$ with $n_1 + n_2 = n$. Application of the matrices to the cases $n = 6$–8 follows from a relation for hole-electron equivalence. Finally, and most important for detailed application of the matrices to extract information of chemical interest from observed spectra, we describe a set of approximations which enable us to express the generalized two-electron matrix elements in terms of a small number of orbital population parameters.

(*a*) *Symmetry considerations: two-electron matrix elements*

When calculating interelectron repulsion matrix elements in atomic spectroscopy the spherical harmonic addition theorem (Condon & Shortley 1935) is used to convert the two-electron operator G (equation (2.1)) into products of one-electron operators:

$$G = \sum_{j<k} \frac{e^2}{r_{jk}} = \sum_{j<k} \sum_{n=0}^{\infty} \frac{r_<^n}{r_>^{n+1}} \sum_{m=-n}^{n} \frac{4\pi}{2n+1} (-1)^m Y_{nm}(j)\, Y_{n-m}(k). \qquad (2.1)$$

The one-electron operators are proportional to the spherical harmonics $Y_{nm}(j)$, whose one-electron

matrix elements are easily reduced (Condon & Shortley 1935) to a small number of parameters, the well-known Slater–Condon–Shortley F^k. The number of F^k required is limited by group theoretical considerations.

In the case of molecular spectra, particularly of high symmetry (e.g. cubic) molecules a similar treatment is possible, as originally suggested by Griffith (1960). To deal with molecules it is necessary to transform the spherical harmonics to bases for the irreducible representations of the molecular point group, thus leading to the new expansion for G (Griffith 1962):

$$G = \sum_{if\phi} \sum_{j<k} g_{if\phi}(j)\, g^*_{if\phi}(k)$$
$$= \sum_{if} \sum_{j>k} g_{if}(j)\, g_{if}(k), \qquad (2.2)$$

where $g_{if}(j)$ is a one-electron operator acting on electron j which forms a suitable basis for the irreducible representation f with component ϕ. The radial part of the operator has been absorbed into the g. For molecular orbital functions there is no longer a convenient cut-off to the values of n in the spherical harmonic expansion since the molecular orbitals are not in general eigenfunctions of $\boldsymbol{L}$. Thus each irreducible representation f can occur repeatedly a large number of times, distinguished in the summation (2.2) by the subscript i. For this reason it is impossible to calculate the matrix elements of all the one-electron operators. However, they remain useful because they enable group-theoretical arguments to be applied to electrostatic matrix elements.

The general two-electron matrix element between two-electron wavefunctions which are not antisymmetrized can be expressed in terms of one-electron reduced matrix elements as follows:

$$\langle a\alpha(1)\, b\beta(2)|G|c\gamma(1)\, d\delta(2)\rangle = \sum_{if\phi} \langle a\alpha(1)|g^{(1)}_{if\phi}|c\gamma(1)\rangle\langle b\beta(2)|g^{(2)}_{if\phi}|d\delta(2)\rangle$$
$$= \sum_{f\phi} V\begin{pmatrix} a & c & f \\ \alpha & \gamma & \phi \end{pmatrix} V\begin{pmatrix} b & d & f \\ \beta & \delta & \phi \end{pmatrix} \sum_i \langle a\|g_{if}\|c\rangle\langle b\|g_{if}\|d\rangle, \qquad (2.3)$$

where, as throughout in this work, the definitions and notation of Griffith (1962) are used: a, b, c, d, f denote irreducible representations and α, β, γ, δ, ϕ denote components, assumed real. The coupling coefficients are the same for all values of i, and so the sum of products of reduced matrix elements in equation (2.3) can be separated as a single parameter of electron repulsion, depending solely on the orbitals involved and on the g_{if} contribution to G. Only those parameters may occur in which f is contained in the direct products $a \otimes c$, $b \otimes d$ and, furthermore, if $a = c$ or $b = d$, f is restricted to the symmetrized squares a^2 or b^2. The one electron-reduced matrix elements $\langle a\|g_{if}\|b\rangle$ will be denoted henceforth by a letter with a subscript i, as in table 1 (cf. Griffith 1961) and our parameters can be regarded as scalar products of vectors of these reduced matrix elements. For ligand field calculations, that is, calculations involving only t_2 and e orbitals, only ten such scalar products are permitted (k^2, kl, l^2, p^2, pq, q^2, r^2, s^2, st, t^2), thus generating the ten electron repulsion parameters required by a ligand field model in its most general form, a result first pointed out by Tanabe (1960).

For two-electron integrals involving t_1 and t_2 functions similar arguments indicate that 17 parameters are needed, three of which occur already in treating e and t_2 functions. For a combination of e and t_1 there are again ten integrals, five of which are new, while integrals involving functions of e, t_1, t_2 give rise to nine further parameters. Tables 2 to 5 list all these parameters, together with typical equivalent two-electron integrals, with the notation θ, ϵ for the components of e, x, y and z for t_1; and ξ, η and ζ for t_2.

TABLE 1. SINGLE ELECTRON REDUCED ELECTRON REPULSION MATRIX ELEMENTS

$$\langle t_2||g_{iA_1}||t_2\rangle = \sqrt{(3)}\,k_i$$
$$\langle e||g_{iA_1}||e\rangle = \sqrt{(2)}\,l_i$$
$$\langle e||g_{iT_1}||t_2\rangle = 2\sqrt{(3)}\,r_i$$
$$= -\langle t_2||g_{iT_1}||e\rangle$$
$$\langle t_1||g_{iA_1}||t_1\rangle = \sqrt{(3)}\,m_i$$
$$\langle t_1||g_{iE}||t_1\rangle = 2\sqrt{(3)}\,u_i$$
$$\langle t_1||g_{iE}||t_2\rangle = 2\sqrt{(3)}\,v_i$$
$$\langle t_1||g_{iT_2}||t_1\rangle = \sqrt{(6)}\,x_i$$
$$\langle t_1||g_{iT_2}||t_2\rangle = \sqrt{(6)}\,y_i$$
$$\langle e||g_{iT_1}||t_1\rangle = 2\sqrt{(3)}\,a_i$$
$$\langle e||g_{iT_2}||t_1\rangle = 2\sqrt{(3)}\,b_i$$

$$\langle e||g_{iE}||e\rangle = 2p_i$$
$$\langle t_2||g_{iE}||t_2\rangle = 2\sqrt{(3)}\,q_i$$
$$\langle e||g_{iT_2}||t_2\rangle = 2\sqrt{(3)}\,s_i$$
$$\langle t_2||g_{iT_2}||t_2\rangle = \sqrt{(6)}\,t_i$$
$$\langle t_1||g_{iA_2}||t_2\rangle = \sqrt{(3)}\,n_i$$
$$\langle t_1||g_{iT_1}||t_2\rangle = \sqrt{(6)}\,z_i$$
$$= -\langle t_2||g_{iE}||t_1\rangle$$
$$= -\langle t_2||g_{iT_2}||t_1\rangle$$
$$= -\langle t_1||g_{iT_2}||e\rangle$$

TABLE 2. THE TEN LIGAND ELECTRON REPULSION MATRIX ELEMENTS

$$a = \langle\xi\xi|\,G\,|\xi\xi\rangle = k.k+4q.q,$$
$$b = \langle\xi\eta|\,G\,|\xi\eta\rangle = k.k-2q.q,$$
$$c = \tfrac{1}{\sqrt{3}}\langle\xi\theta|\,G\,|\xi\epsilon\rangle = -p.q,$$
$$d = \langle\xi\epsilon|\,G\,|\xi\epsilon\rangle = k.l+p.q,$$
$$e = \langle\theta\theta|\,G\,|\theta\theta\rangle = l.l+p.p,$$
$$f = \langle\theta\epsilon|\,G\,|\epsilon\theta\rangle = p.p,$$
$$g = \langle\theta\eta|\,G\,|\eta\theta\rangle = 3r.r+s.s,$$
$$h = \tfrac{1}{\sqrt{3}}\langle\theta\eta|\,G\,|\eta\epsilon\rangle = -r.r+s.s,$$
$$i = \langle\theta\zeta|\,G\,|\eta\xi\rangle = -s.t,$$
$$j = \langle\xi\eta|\,G\,|\eta\xi\rangle = t.t,$$

where ξ, η, ζ indicate the components of t_2; θ, ϵ indicate the components of e (Griffith 1961), and in the following tables x, y, z indicate the components of t_1.

TABLE 3. THE INTERELECTRON REPULSION PARAMETERS BETWEEN t_1 AND t_2 ELECTRONS

$$\langle\xi\xi|\,G\,|\xi\xi\rangle = k.k+4q.q,$$
$$\langle\xi\eta|\,G\,|\xi\eta\rangle = k.k-2q.q,$$
$$\langle xx|\,G\,|xx\rangle = m.m+4u.u,$$
$$\langle xy|\,G\,|xy\rangle = m.m-2u.u,$$
$$\langle x\xi|\,G\,|\xi x\rangle = n.n+4v.v,$$
$$\langle xy|\,G\,|\xi\eta\rangle = n.n-2v.v,$$
$$\langle xy|\,G\,|\eta\xi\rangle = z.z-y.y,$$
$$\langle\xi x|\,G\,|\xi x\rangle = m.k+4u.q,$$
$$\langle x\eta|\,G\,|\eta x\rangle = z.z+y.y,$$
$$\langle\xi y|\,G\,|\xi y\rangle = m.k-2u.q,$$
$$\langle\xi z|\,G\,|\xi\zeta\rangle = -2\sqrt{(3)}\,v.q,$$
$$\langle xz|\,G\,|x\zeta\rangle = -2\sqrt{(3)}\,u.v,$$
$$\langle x\xi|\,G\,|y\eta\rangle = x.t,$$
$$\langle xx|\,G\,|y\eta\rangle = x.y,$$
$$\langle\xi x|\,G\,|\eta\eta\rangle = y.t,$$
$$\langle xy|\,G\,|yx\rangle = x.x,$$
$$\langle\xi\eta|\,G\,|\eta\xi\rangle = t.t.$$

PHILOSOPHICAL TRANSACTIONS OF THE ROYAL SOCIETY A MATHEMATICAL, PHYSICAL & ENGINEERING SCIENCES

TABLE 4. INTERELECTRON REPULSION PARAMETERS BETWEEN e AND t_1 ELECTRONS

$$\langle \theta x|\, G\,|\epsilon x\rangle = -\sqrt{(3)}\, p.u$$
$$\langle x\epsilon|\, G\,|x\epsilon\rangle = l.m+p.u$$
$$\langle \theta z|\, G\,|z\theta\rangle = 4a.a$$
$$\langle \epsilon z|\, G\,|z\epsilon\rangle = 4b.b$$
$$\langle \epsilon x|\, G\,|yz\rangle = b.x$$

TABLE 5. THE INTERELECTRON REPULSION PARAMETERS INVOLVING e, t_1, AND t_2 ELECTRONS

$$\langle \theta x|\, G\,|\epsilon\xi\rangle = -p.v$$
$$\langle \epsilon\xi|\, G\,|x\epsilon\rangle = -\sqrt{(3)}\, a.r+\sqrt{(3)}\, b.s$$
$$\langle \theta\xi|\, G\,|x\epsilon\rangle = -a.r+3b.s$$
$$\langle \theta y|\, G\,|z\xi\rangle = 2a.z$$
$$\langle \epsilon y|\, G\,|z\xi\rangle = 2b.y$$
$$\langle \theta\eta|\, G\,|x\zeta\rangle = \sqrt{(3)}\, b.t$$
$$\langle \theta x|\, G\,|\zeta y\rangle = 2s.x$$
$$\langle \theta x|\, G\,|\zeta\eta\rangle = 2s.y$$
$$\langle \epsilon x|\, G\,|\zeta\eta\rangle = 2.rz$$

For matrix elements of coupled two-electron functions the parametrization is particularly straightforward with the use of the W-coefficients (Griffith 1962). Thus

$$\langle a^2 ShM\theta|G|b^2 ShM\theta\rangle = \sum_{if} (-1)^{a+b+h+f}\, W\begin{pmatrix} a & a & h \\ b & b & f \end{pmatrix} \langle a\|g_{if}\|b\rangle^2, \tag{2.4a}$$

$$\langle a^2 ShM\theta|G|bcShM\theta\rangle = \frac{1}{\sqrt{2}} \sum_{if} (-1)^{a+b+f}\, W\begin{pmatrix} a & a & h \\ b & c & f \end{pmatrix} [(-1)^h + (-1)^f] \langle a\|g_{if}\|b\rangle \langle a\|g_{if}\|c\rangle,$$
$$= \sqrt{(2)} \sum_{if} (-1)^{a+b+h+f}\, W\begin{pmatrix} a & a & h \\ b & c & f \end{pmatrix} \langle a\|g_{if}\|b\rangle \langle a\|g_{if}\|c\rangle, \tag{2.4b}$$

$$\langle abShM\theta|G|cdShM\theta\rangle = \sum_{if} (-1)^{b+c+f} \Big[(-1)^h\, W\begin{pmatrix} a & b & h \\ d & c & f \end{pmatrix} \langle a\|g_{if}\|c\rangle \langle b\|g_{if}\|d\rangle$$
$$+ (-1)^S\, W\begin{pmatrix} a & b & h \\ c & d & f \end{pmatrix} \langle a\|g_{if}\|d\rangle \langle b\|g_{if}\|c\rangle \Big]. \tag{2.4c}$$

(b) Symmetry considerations: many-electron matrix elements

To evaluate integrals involving the wavefunctions of three or more electrons it is sometimes convenient to use a recursion method and express the integrals of N-electron wavefunctions in terms of $(N-1)$-electron wavefunctions. However, such a method can often be lengthy and a second, 'direct', method of decoupling a two-electron wavefunction from a $(N-2)$-electron part, to give simple two-electron integrals is then more suitable. In the case of the ligand field manifold the recursion method is most convenient because the matrix elements of $(t_2e)^3$ are constructed from those of $(t_2e)^2$, and so on up to $(t_2e)^8$. All the resultant matrices are useful and have application to systems of chemical interest. The recursion method was employed by Tanabe & Sugano (1954) in their work on the evaluation of ligand-field matrix elements. When the matrix elements of excited charge transfer configurations are to be evaluated, however, the number and complexity of the intermediate configurations in any recursive calculation scheme is so large that many of the intermediate results are of little chemical value. In such cases the direct method

is preferable and more rapid. We give here a brief account of the way in which we have applied these two methods to the present problem. For a more detailed account the reader is referred to Bird (1969).

(i) *Recursion method*

The basis of the recursion method is the conversion of the N-electron operator

$$G_N = \sum_{j<k}^{N} \frac{e^2}{r_{jk}}$$

to a $(N-1)$-electron operator $G_N = [N/(N-2)]\, G_{N-1}$, an operation made possible by the determinantal nature of the wavefunctions (Griffith 1961, 1962). By vector coupling methods the orbital of the Nth electron is separated, though it is important to notice that, because of the antisymmetrization in the wavefunction of the general configuration $(a^n b^p)$, with spin and symmetry S and h, the orbital separated may be either a or b. Thus

$$|a^n(S_1 h_1)\, b^p(S_2 h_2)\, ShM\theta\rangle = |(a^{n-1}b^p)\, a\rangle + |(a^n b^{p-1})\, b\rangle, \tag{2.5}$$

where a and b in the two separated wavefunctions are no longer antisymmetrized with the remaining $(N-1)$-electron wavefunctions. In more detail,

$$\begin{aligned}
|(a^{n-1}b^p)\, a\rangle &= \sqrt{\left(\frac{n}{N}\right)} \sum_{S_1' h_1', S_a h_a} D^a[a^{n-1}(S_1' h_1')\, b^p(S_2 h_2)\, S_a h_a;\, S_1 h_1, Sh] \\
&\qquad \times |a^{n-1}(S_1' h_1')\, b^p(S_2 h_2)\, S_a h_a .\, aShM\theta\rangle, \\
|(a^n b^{p-1})\, b\rangle &= \sqrt{\left(\frac{p}{N}\right)} \sum_{S_2' h_2', S_b h_b} D^b[a^n(S_1 h_1)\, b^{p-1}(S_2' h_2')\, S_b h_b;\, S_2 h_2, Sh] \\
&\qquad \times |a^n(S_1 h_1)\, b^{p-1}(S_2' h_2')\, S_b h_b .\, bShM\theta\rangle,
\end{aligned} \tag{2.6}$$

where

$$\begin{aligned}
&D^a[a^{n-1}(S_1' h_1')\, b^p(S_2 h_2)\, S_a h_a;\, S_1 h_1, Sh] \\
&\qquad = (-1)^{a+h_a+h_1+h_2+\frac{1}{2}+S_a+S_1+S_2+p} \sqrt{[\lambda(h_1)\, \lambda(h_a)\, (2S_a+1)\, (2S_1+1)]} \\
&\qquad\quad \times \langle a^{n-1}(S_1' h_1'), a|\}\, a^n S_1 h_1\rangle\, W\begin{pmatrix} h_1 & h_2 & h \\ h_a & a & h_1' \end{pmatrix} \overline{W}\begin{pmatrix} S_1 & S_2 & S \\ S_a & \frac{1}{2} & S_1' \end{pmatrix}
\end{aligned} \tag{2.7a}$$

and

$$\begin{aligned}
&D^b[a^n(S_1 h_1)\, b^{p-1}(S_2' h_2')\, S_b h_b;\, S_2 h_2, Sh] \\
&\qquad = (-1)^{b+h_1+h_2'+h+\frac{1}{2}+S_1+S_2'+S} \sqrt{[\lambda(h_2)\, \lambda(h_b)\, (2S_2+1)\, (2S_b+1)]} \\
&\qquad\quad \times \langle b^{p-1}(S_2' h_2'), b|\}\, b^p S_2 h_2\rangle\, W\begin{pmatrix} h_1 & h_2 & h \\ b & h_b & h_2' \end{pmatrix} \overline{W}\begin{pmatrix} S_1 & S_2 & S \\ \frac{1}{2} & S_b & S_2' \end{pmatrix}.
\end{aligned} \tag{2.7b}$$

The W coefficients are the $6j$ symbols, the spin analogues of the W coefficients. The fractional parentage coefficients defined by Griffith (1962) are also used. Integration over the coordinates of the Nth electron, taking account of the usual orthonormality rules, leads to reduction of the matrix element

$$\begin{aligned}
M &= \langle a^n(S_1 h_1)\, b^p(S_2 h_2)\, ShM\theta|G_N|a^{n'}(S_3 h_3)\, b^{p'}(S_4 h_4)\, ShM\theta\rangle \\
&= \sqrt{\left(\frac{nn'}{N-2}\right)} \sum_{\substack{S_1' h_1', S_3' h_3' \\ S_a h_a}} D^a[a^{n-1}(S_1' h_1')\, b^p(S_2 h_2)\, S_a h_a;\, S_1 h_1, Sh]\, D^a[a^{n'-1}(S_3' h_3')\, b^{p'}(S_4 h_4)\, S_a h_a;\, S_3 h_3, Sh] \\
&\quad \times \langle a^{n-1}(S_1' h_1')\, b^p(S_2 h_2)\, S_a h_a|G_{N-1}|a^{n'-1}(S_3' h_3')\, b^{p'}(S_4 h_4)\, S_a h_a\rangle \\
&\quad + \sqrt{\left(\frac{pp'}{N-2}\right)} \sum_{\substack{S_2' h_2', S_4' h_4' \\ S_b h_b}} D^b[a^n(S_1 h_1)\, b^{p-1}(S_2' h_2')\, S_b h_b;\, S_2 h_2, Sh]\, D^b[a^{n'}(S_3 h_3)\, b^{p'-1}(S_4' h_4')\, S_b h_b;\, S_4 h_4, Sh] \\
&\quad \times \langle a^n(S_1 h_1)\, b^{p-1}(S_2' h_2')\, S_b h_b|G_{N-1}|a^{n'}(S_3 h_3)\, b^{p'-1}(S_4' h_4')\, S_b h_b\rangle.
\end{aligned} \tag{2.8}$$

Equation (2.8) is similar to the Tanabe–Sugano reduction formula (1954), though in a different notation. A computer program (Bird 1969) performed the 'aufbau' calculation for the matrix elements of the ligand-field manifold, and the results for $(t_2e)^2$ to $(t_2e)^5$ appear in tables 6–9. The diagonal matrix elements of electron repulsion for these configurations have also been listed recently by Richardson, Soules, Vaught & Powell (1971), who used a somewhat different notation. However, they have only given the off-diagonal elements for $(t_2e)^2$ and $(t_2e)^3$, so we have thought it worth presenting the complete set of matrices in tables 6–9.

TABLE 6. GENERALIZED ELECTROSTATIC MATRICES FOR $(t_2e)^2$

e^2	$^3A_2$	$e-3f$
t_2e	$^3T_2$	$d-c-g-3h$
t_2e	$^1T_1$	$d+3c+g-h$

$^1A_1$	e^2	t_2^2	$^1T_2$	t_2^2	t_2e
e^2	$e+f$	$\sqrt{6}(g+h)$	t_2^3	$b+j$	$2i$
t_2^2		$a+2j$	t_2e		$d-c+g+3h$
^1E	e^2	t_2^2	$^3T_1$	t_2^2	t_2e
e^2	$e-f$	$2h$	t_2^2	$b-j$	$-2\sqrt{(3)}i$
t_2^2		$a-j$	t_2e		$d+3c-g+h$

Note: the c and h used here are $-\frac{1}{\sqrt{3}}$ times the c and h of Griffith (1961).

TABLE 7. GENERALIZED ELECTROSTATIC MATRICES FOR $(t_2e)^3$

$(t_2e)^3\ ^2T_2$ matrix

t_2^3	$t_2^2(^3T_1)\,e$	$t_2^2(^1T_2)\,e$	$t_2e^2(^1A_1)$	$t_2e^2(^1E)$			
$a+2b$	$-3i$	$5i$	$2g+2h$	$-2h$	t_2^3	$t_2^3\ ^4A_2$	$3b-3j$
	$b+2d+g+2h-j$	$-3h$	$3i$	$-3i$	$t_2^2(^3T_1)\,e$	$t_2^2(^3T_1)\,e\ ^4T_2$	$b+2d-2g-4h-j$
		$b+4c+2d-g+j$	$-i$	$-i$	$t_2^2(^1T_2)\,e$	$t_2^2(^1E)\,e\ ^2A_1$	$a-2c+2d-g-3h-j$
			$2c+2d+e+f-g-h$	$-4c-2h$	$t_2e^2(^1A_1)$	$t_2^2(^1E)\,e\ ^2A_2$	$a+6c+2d-g+h-j$
				$2c+2d+e-f-g-h$	$t_2e^2(^1E)$		

$(t_2e)^3\ ^2E$ matrix

t_2^3	$t_2^2(^1A_1)\,e$	$t_2^2(^1E)\,e$	e^3	
$3b$	$-2\sqrt{(6)}\,i$	$+\sqrt{(6)}\,i$	0	t_2^3
	$a+2c+2d-g-h+2j$	$-4c-2h$	$\sqrt{(3)}\,(g+h)$	$t_2^2(^1A_1)\,e$
		$a+2c+2d-g-h-j$	$-2\sqrt{(3)}\,h$	$t_2^2(^1E)\,e$
			$3c-5f$	e^3

$(t_2e)^3\ ^2T_1$ matrix

t_2^3	$t_2^2(^3T_1)\,e$	$t_2^2(^1T_2)\,e$	$t_2e^2(^3A_2)$	$t_2e^2(^1E)$	
$a+2b-2j$	$-\sqrt{(3)}\,i$	$-\sqrt{(3)}\,i$	0	$-2\sqrt{(3)}\,h$	t_2^3
	$b+4c+2d+g-j$	$3h$	$-\sqrt{(3)}\,i$	$3i$	$t_2^2(^3T_1)\,e$
		$b+2d-g-2h+j$	$-\sqrt{(3)}\,i$	i	$t_2^2(^1T_2)\,e$
			$2c+2d+e-3f+g+h$	$-2\sqrt{(3)}\,h$	$t_2e^2(^3A_2)$
				$2c+2d+e-f-g-h$	$t_2e^2(^1E)$

$(t_2e)^3\ ^4T_1$ matrix

$t_2^2(^3T_1)\,e$	$t_2e^2(^3A_2)$	
$b+4c+2d-2g-j$	$-2\sqrt{(3)}\,i$	$t_2^2(^3T_1)\,e$
	$2c+2d+e-3f-2g-2h$	$t_2e^2(^3A_2)$

TABLE 8. GENERALIZED ELECTROSTATIC MATRICES FOR $(t_2e)^4$

$t_2^3(^4A_2)\ e\ ^5E$	$3b+3c+3d-3g-3h-3j$
$t_2^2(^3T_1)\ e^2(^3A_2)\ ^5T_2$	$b+4c+4d+e-3f-4g-4h-j$
$t_2^3(^2E)\ e\ ^3A_1$	$3b+3c+3d-2y-2h$

$(t_2e)^4\ ^3A_2$ matrix

$t_2^3(^2E)\ e$	$t_2^2(^1A_1)\ e^2(^3A_2)$	
$3b+3c+3d-2g$	$-4\sqrt{(3)}\,i$	$t_2^3(^2E)\ e$
	$a+4c+4d+e-3f-2g-2h+2j$	$t_2^2(^1A_1)\ e^2(^3A_2)$

$(t_2e)^4\ ^3T_2$ matrix

$t_2^3(^2T_2)\ e$	$t_2^3(^2T_1)\ e$	$t_2^2(^3T_1)\ e^2(^3A_2)$	$t_2^2(^3T_1)\ e^2(^1E)$	t_2e^3	
$a+2b+3c+3d-2g-3h$	$\sqrt{(3)}\,(2c+h)$	$-\sqrt{(6)}\,i$	$\sqrt{(3)}\,i$	$\sqrt{(2)}\,(g+2h)$	$t_2^3(^2T_2)\ e$
	$a+2b+3c+3d-2g-h-2j$	$-\sqrt{(2)}\,i$	$-i$	$\sqrt{(6)}\,h$	$t_2^3(^2T_1)\ e$
		$b+4c+4d+e-3f-j$	$-2\sqrt{(2)}\,h$	$-2\sqrt{(3)}\,i$	$t_2^2(^3T_1)\ e^2(^3A_2)$
			$b+4c+4d+e-f-2g-2h-j$	$\sqrt{(6)}\,i$	$t_2^2(^3T_1)\ e^2(^1E)$
				$5c+3d+3e-5f-2g-2h$	t_2e^3

$(t_2e)^4\ ^3E$ matrix

$t_2^3(^4A_2)\ e$	$t_2^3(^2E)\ e$	$t_2^2(^1E)\ e^2(^3A_2)$	
$3b+3c+3d+g+h-3j$	$4h$	0	$t_2^3(^4A_2)\ e$
	$3b+3c+3d-2g-2h$	$\sqrt{(6)}\,i$	$t_2^3(^2E)\ e$
		$a+4c+4d+e-3f-2g-2h-j$	$t_2^2(^1E)\ e^2(^3A_2)$

$(t_2e)^4\ ^3T_1$ matrix

t_2^4	$t_2^3(^2T_1)\ e$	$t_2^3(^2T_2)\ e$	$t_2^2(^3T_1)\ e^2(^1A_1)$	$t_2^2(^3T_1)\ e^2(^1E)$	$t_2^2(^1T_2)\ e^2(^3A_2)$	t_2e^3	
$a+5b-3j$	$\sqrt{(2)}\,i$	$-\sqrt{(6)}\,i$	$-\sqrt{(2)}\,(g+h)$	$-2\sqrt{(2)}\,h$	0	0	t_2^4
	$a+2b+3c+3d-2g-3h-2j$	$-\sqrt{(3)}\,(2c+h)$	$-i$	$-i$	$\sqrt{(3)}\,i$	$-\sqrt{(6)}\,h$	$t_2^3(^2T_1)\ e$
		$a+2b+3c+3d-2g-h$	$-\sqrt{(3)}\,i$	$\sqrt{(3)}\,i$	$-5i$	$\sqrt{(2)}\,g$	$t_2^3(^2T_2)\ e$
			$b+4c+4d+e+f-2g-2h-j$	$4c+2h$	0	$-\sqrt{(6)}\,i$	$t_2^2(^3T_1)\ e^2(^1A_1)$
				$b+4c+4d+e-f-2g-2h-j$	$-2\sqrt{(3)}\,h$	$-\sqrt{(6)}\,i$	$t_2^2(^3T_1)\ e^2(^1E)$
					$b+4c+4d+e-3f-2g-2h+j$	$\sqrt{(2)}\,i$	$t_2^2(^1T_2)\ e^2(^3A_2)$
						$c+3d+3e-5f-2g-2h$	t_2e^3

TABLE 8 (*cont.*)

$(t_2e)^4\,{}^1A_1$ matrix

t_2^4	$t_2^3(^2E)\,e$	$t_2^2(^1A_1)\,e^2(^1A_1)$	$t_2^2(^1E)\,e^2(^1E)$	e^4	
$2a+4b$	$-4\sqrt{(6)}\,i$	$2\sqrt{(2)}\,(g+h)$	$-2\sqrt{(2)}\,h$	0	t_2^4
	$3b+3c+3d+6h$	$-4\sqrt{(3)}\,i$	$2\sqrt{(3)}\,i$	0	$t_2^3(^2E)\,e$
		$a+4c+4d+e+f-2g-2h+2j$	$-4(2c+h)$	$\sqrt{(6)}\,(g+h)$	$t_2^2(^1A_1)\,e^2(^1A_1)$
			$a+4c+4d+e-f-2g-2h-j$	$-2\sqrt{(6)}\,h$	$t_2^2(^1E)\,e^2(^1E)$
				$6e-10f$	e^4

$(t_2e)^4\,{}^1A_2$ matrix

$t_2^3(^2E)\,e$	$t_2^2(^1E)\,e^2(^1E)$	
$3b+3c+3d-6h$	$-2\sqrt{(3)}\,i$	$t_2^3(^2E)\,e$
	$a+4c+4d+e-f-2g-2h-j$	$t_2^2(^1E)\,e^2(^1E)$

$(t_2e)^4\,{}^1E$ matrix

t_2^4	$t_2^3(^2E)\,e$	$t_2^2(^1E)\,e^2(^1A_1)$	$t_2^2(^1A_1)\,e^2(^1E)$	$t_2^2(^1E)\,e^2(^1E)$	
$2a+4b-3j$	$2\sqrt{(3)}\,i$	$-\sqrt{(2)}\,(g+h)$	$-2h$	$4h$	t_2^4
	$3b+3c+3d$	$\sqrt{(6)}\,i$	$-4\sqrt{(3)}\,i$	0	$t_2^3(^2E)\,e$
		$a+4c+4d+e+f-2g-2h-j$	$-\sqrt{(2)}\,(4c+2h)$	$-\sqrt{(2)}\,(4c+2h)$	$t_2^2(^1E)\,e^2(^1A_1)$
			$a+4c+4d+e-f-2g-2h+2j$	0	$t_2^2(^1A_1)\,e^2(^1E)$
				$a+4c+4d+e-f-2g-2h-j$	$t_2^2(^1E)\,e^2(^1E)$

$(t_2e)^4\,{}^1T_1$ matrix

$t_2^3(^2T_1)\,e$	$t_2^3(^2T_2)\,e$	$t_2^2(^1T_2)\,e^2(^1E)$	t_2e^3	
$a+2b+3c+3d+3h-2j$	$-\sqrt{(3)}\,(2c+h)$	$\sqrt{(3)}\,i$	$-\sqrt{(6)}\,h$	$t_2^3(^2T_1)\,e$
	$a+2b+3c+3d-3h$	$5i$	$\sqrt{(2)}\,g$	$t_2^3(^2T_2)\,e$
		$b+4c+4d+e-f-2g-2h+j$	$\sqrt{(2)}\,i$	$t_2^2(^1T_2)\,e^2(^1E)$
			$c+3d+3e-5f-4h$	t_2e^3

$(t_2e)^4\,{}^1T_2$ matrix

t_2^4	$t_2^3(^2T_1)\,e$	$t_2^3(^2T_2)$	$t_2^2(^3T_1)\,e^2(^3A_2)$	$t_2^2(^1T_2)\,e^2(^1E)$	$t_2^2(^1T_2)\,e^2(^1A_1)$	t_2e^3	
$a+5b-j$	$\sqrt{(6)}\,i$	$5\sqrt{(2)}\,i$	0	$-2\sqrt{(2)}\,h$	$-\sqrt{(2)}\,(g+h)$	0	t_2^4
	$a+2b+3c+3d-3h-2j$	$2\sqrt{(3)}\,c+\sqrt{(3)}\,h$	$-\sqrt{(3)}\,i$	$-\sqrt{(3)}\,i$	$\sqrt{(3)}\,i$	$\sqrt{(6)}\,h$	$t_2^3(^2T_1)\,e$
		$a+2b+3c+3d+3h$	$-3i$	$-5i$	$-5i$	$\sqrt{(2)}\,(g+2h)$	$t_2^3(^2T_2)\,e$
			$b+4c+4d+e-3f+2g+2h-j$	$6h$	0	$-3\sqrt{(2)}\,i$	$t_2^2(^3T_1)\,e^2(^3A_2)$
				$b+4c+4d+e-f-2g-2h+j$	$4c+2h$	$-\sqrt{(2)}\,i$	$t_2^2(^1T_2)\,e^2(^1E)$
					$b+4c+4d+e+f-2g-2h+j$	$\sqrt{(2)}\,i$	$t_2^2(^1T_2)\,e^2(^1A_1)$
						$5c+3d+3e-5f+4h$	t_2e^3

TABLE 9. GENERALIZED ELECTROSTATIC MATRICES FOR $(t_2e)^5$

$t_2^3(^4A_2)\,e^2(^3A_2)\,{}^6A_1$	$3b+6c+6d+e-3f-6g-6h-3j$
$t_2^3(^4A_2)\,e^2(^3A_2)\,{}^4A_1$	$3b+6c+6d+e-3f-g-h-3j$
$t_2^3(^4A_2)\,e^2(^1A_1)\,{}^4A_2$	$3b+6c+6d+e+f-3g-3h-3j$

$(t_2e)^5\,{}^4T_1$ matrix

$t_2^4(^3T_1)\,e$	$t_2^3(^2T_2)\,e^2(^3A_2)$	$t_2^2(^3T_1)\,e^3$	
$a+5b+2c+4d-3g-3h-3j$	$-\sqrt{(6)}\,i$	$-g+h$	$t_2^4(^3T_1)\,e$
	$a+2b+6c+6d+e-3f-4g-4h$	$\sqrt{(6)}\,i$	$t_2^3(^2T_2)\,e^2(^3A_2)$
		$b+4c+6d+3e-5f-4g-4h-j$	$t_2^2(^3T_1)\,e^3$

$(t_2e)^5\,{}^4T_2$ matrix

$t_2^4(^3T_1)\,e$	$t_2^3(^2T_1)\,e^2(^3A_2)$	$t_2^2(^3T_1)\,e^3$		
$a+5b+6c+4d-3g-3h-3j$	$\sqrt{(2)}\,i$	$-y-3h$	$t_2^4(^3T_2)\,e$	
	$a+2b+6c+6d+e-3f-4g-4h-2j$	$\sqrt{(2)}\,i$	$t_2^3(^2T_1)\,e^2(^3A_2)$	
		$b+8c+6d+3e-5f-4g-4h-j$	$t_2^2(^3T_1)\,e^3$	

$(t_2e)^5\,{}^4E$ matrix

$t_2^3(^2E)\,e^2(^3A_2)$	$t_2^3(^4A_2)\,e^2(^1E)$	
$3b+6c+6d+e-3f-4g-4h$	$2\sqrt{(3)}\,h$	$t_2^3(^2E)\,e^2(^3A_2)$
	$3b+6c+6d+e-f-3g-3h-3j$	$t_2^3(^4A_2)\,e^2(^1E)$

$(t_2e)^5\,{}^2A_1$ matrix

$t_2^4(^1E)\,e$	$t_2^3(^1E)\,e^2(^1E)$	$t_2^3(^4A_2)\,e^2(^3A_2)$	$t_2^2(^1E)\,e^3$	
$2a+4b+8c+4d-2g-3j$	$-\sqrt{(6)}\,i$	0	$-g-5h$	$t_2^4(^1E)\,e$
	$3b+6c+6d+e-f-3g-3h$	$4\sqrt{(3)}\,h$	$-\sqrt{(6)}\,i$	$t_2^3(^2E)\,e^2(^1E)$
		$3b+6c+6d+e-3f+2g+2h-3j$	0	$t_2^3(^4A_2)\,e^2(^3A_2)$
			$a+10+6d+3e-5f-3g-h-j$	$t_2^2(^1E)\,e^3$

$(t_2e)^5\,{}^2A_2$ matrix

$t_2^4(^1E)\,e$	$t_2^3(^2E)\,e^2(^1E)$	$t_2^2(^1E)\,e^3$	
$2a+4b+4d-2g-4h-3j$	$\sqrt{(6)}\,i$	$-g+3h$	$t_2^4(^1E)\,e$
	$3b+6c+6d+e-f-3g-3h$	$\sqrt{(6)}\,i$	$t_2^3(^2E)\,e^2(^1E)$
		$a+2c+6d+3e-5f-3g-5h-j$	$t_2^2(^1E)\,e^3$

$(t_2e)^5\,{}^2E$ matrix

$t_2^4(^1A_1)\,e$	$t_2^4(^1E)\,e$	$t_2^3(^2E)\,e^2(^1A_1)$	$t_2^3(^2E)\,e^2(^3A_2)$	$t_2^3(^2E)\,e^2(^1E)$	$t_2^3(^1E)\,e^3$	$t_2^2(^1A_1)\,e^3$	
$2a+4b+4c+4d-2g-2h$	$4c+2h$	$2\sqrt{(3)}\,i$	$6i$	$2\sqrt{(6)}\,i$	$2h$	$2g+2h$	$t_2^4(^1A_1)\,e$
	$2a+4b+4c+4d-2g-2h-3j$	$-\sqrt{(3)}\,i$	$3i$	0	$-(g+h)$	$2h$	$t_2^4(^1E)\,e$
		$3b+6c+6d+e+f-3g-3h$	0	0	$-\sqrt{(3)}\,i$	$-2\sqrt{(3)}\,i$	$t_2^3(^2E)\,e^2(^1A_1)$
			$3b+6c+6d+e-3f-g-h$	$2\sqrt{(6)}\,h$	$-3i$	$-6i$	$t_2^3(^2E)\,e^2(^3A_2)$
				$3b+6c+6d+e-f-3g-3h$	0	$-2\sqrt{(6)}\,i$	$t_2^3(^2E)\,e^2(^1E)$
					$a+6c+6d+3e-5f-3g-3h-j$	$4c+2h$	$t_2^2(^1E)\,e^3$
						$a+6c+6d+3e-5f-3g-3h+2j$	$t_2^2(^1A_1)\,e^3$

PHILOSOPHICAL TRANSACTIONS OF THE ROYAL SOCIETY A MATHEMATICAL, PHYSICAL & ENGINEERING SCIENCES

PHILOSOPHICAL TRANSACTIONS OF THE ROYAL SOCIETY A MATHEMATICAL, PHYSICAL & ENGINEERING SCIENCES

		$t_2^4(^3T_1)$ e	$t_2^4(^1T_2)$ e	$t_2^3(^2T_1)$ e$^2(^1A_1)$	$t_2^3(^2T_1)$ e$^2(^1E)$	$t_2^3(^2T_2)$ e$^2(^3A_2)$	$t_2^3(^2T_2)$ e$^2(^1E)$	$t_2^2(^1T_2)$	$t_2^2(^3T_1)$ e^3	
		$a+5b+2c+4d$ $-3h-3j$	$3h$	$\frac{1}{2}\sqrt{(6)}\,i$	$\frac{1}{2}\sqrt{(6)}\,i$	$-\frac{1}{2}\sqrt{(6)}\,i$	$\frac{3}{2}\sqrt{(2)}\,i$	0	$-g+h$	$t_2^4(^3T_1)$ e
			$a+5b+6c+4d$ $-2g-h-j$	$\frac{1}{2}\sqrt{(6)}\,i$	$-\frac{1}{2}\sqrt{(6)}\,i$	$-\frac{5}{2}\sqrt{(6)}\,i$	$\frac{5}{2}\sqrt{(2)}\,i$	$-g-3h$	0	$t_2^4(^1T_2)$ e
				$a+2b+6c+6d$ $+e+f-3g$ $-3h-2j$	0	0	$2\sqrt{(3)}\,(2c+h)$	$-\frac{1}{2}\sqrt{(6)}\,i$	$-\frac{1}{2}\sqrt{(6)}\,i$	$t_2^3(^2T_1)$ e$^2(^1A_1)$
					$a+2b+6c+6d$ $+e-f-3g$ $-3h-2j$	0	0	$-\frac{1}{2}\sqrt{(6)}\,i$	$+\frac{1}{2}\sqrt{(6)}\,i$	$t_2^3(^2T_1)$ e$^2(^1E)$
						$a+2b+6c+6d$ $+e-3f-g-h$	$-2\sqrt{(3)}\,h$	$+\frac{5}{2}\sqrt{(6)}\,i$	$+\frac{1}{2}\sqrt{(6)}\,i$	$t_2^3(^2T_2)$ e$^2(^3A_2)$
							$a+2b+6c+6d$ $+e-f-3g$ $-3h$	$-\frac{5}{2}\sqrt{(2)}\,i$	$-\frac{3}{2}\sqrt{(2)}\,i$	$t_2^3(^2T_2)$ e$^2(^1E)$
								$b+8c+6d+3e$ $-5f-3g-2h$ $+j$	$3h$	$t_2^2(^1T_2)$ e^3
									$b+4c+6d+3c$ $-5f-g-4h$ $-j$	$t_2^2(^3T_1)$ e^3

$(t_2e)^5\,{}^2T_2$ matrix

t_2^5	$t_2^4(^3T_1)$ e	$t_2^4(^1T_2)$ e	$t_2^3(^2T_1)$ e$^2(^3A_2)$	$t_2^3(^2T_1)$ e$^2(^1E)$	$t_2^3(^2T_2)$ e$^2(^1A_1)$	$t_2^3(^2T_2)$ e$^2(^1E)$	$t_2^2(^1T_2)$ e^3	$t_2^2(^3T_1)$ e^3	t^2e^4	
$2a+8b-4j$	$+3\sqrt{(2)}\,i$	$-\sqrt{(2)}\,i$	0	$-2\sqrt{(3)}\,h$	$2(g+h)$	$-2h$	0	0	0	t_2^5
	$a+5b+6c+4d$ $+3h-3j$	$-3h$	$\frac{1}{2}\sqrt{(2)}\,i$	$-\frac{1}{2}\sqrt{(6)}\,i$	$\frac{3}{2}\sqrt{(2)}\,i$	$-\frac{3}{2}\sqrt{(2)}\,i$	0	$-g-3h$	0	$t_2^4(^3T_1)$ e
		$a+5b+2c+4d$ $-2g-3h-j$	$-\frac{3}{2}\sqrt{(2)}\,i$	$\frac{1}{2}\sqrt{(6)}\,i$	$-\frac{5}{2}\sqrt{(2)}\,i$	$-\frac{5}{2}\sqrt{(2)}\,i$	$-g+h$	0	0	$t_2^4(^1T_2)$ e
			$a+2b+6c+6d$ $+e-3f-g-h$ $-2j$	$2\sqrt{(3)}\,h$	0	0	$-\frac{3}{2}\sqrt{(2)}\,i$	$+\frac{1}{2}\sqrt{(2)}\,i$	0	$t_2^3(^2T_1)$ e$^2(^3A_2)$
				$a+2b+6c+6d$ $+e-f-3g$ $-3h-2j$	$-2\sqrt{(3)}\,(2c+h)$	0	$+\frac{1}{2}\sqrt{(6)}\,i$	$-\frac{1}{2}\sqrt{(6)}\,i$	$-2\sqrt{(3)}\,h$	$t_2^3(^2T_1)$ e$^2(^1E)$
					$a+2b+6c+6d$ $+e+f-3g$ $-3h$	0	$-\frac{5}{2}\sqrt{(2)}\,i$	$+\frac{3}{2}\sqrt{(2)}\,i$	$2(g+h)$	$t_2^3(^2T_2)$ e$^2(^1A_1)$
						$a+2b+6c+6d$ $+e-f-3g$ $-3h$	$+\frac{5}{2}\sqrt{(2)}\,i$	$+\frac{3}{2}\sqrt{(2)}\,i$	$2h$	$t_2^3(^2T_2)$ e$^2(^1E)$
							$b+4c+6d+3e$ $-5f-3g-4h$ $+j$	$-3h$	$-\sqrt{(2)}\,i$	$t_2^2(^1T_2)$ e^3
								$b+8c+6d+3e$ $-5f-g+2h$ $-j$	$3\sqrt{(2)}\,i$	$t_2^2(^3T_1)$ e^3
									$4c+4d+6c$ $-10f-2g-2h$	t_2e^4

In the conventional ligand-field approximation the results reduce to those listed by Griffith (1961), apart from some phase differences, and in addition, some of the matrices were further checked by performing hand calculations on $(t_2e)^3$ without using a vector coupling method. Finally, since the computer program proceeds from $(t_2e)^3$ to $(t_2e)^8$, the hole-equivalence rules (Griffith 1961) may be checked. It is thus unnecessary to provide tables for $(t_2e)^6$ to $(t_2e)^8$, since they can be derived from the hole-equivalent case, by adding

$$(n-3)\,(a+4b-3j)+(2(n-3)+3(p-2))\,(2c+2d-g-h)+(p-2)\,(3e-5f) \qquad (2.8c)$$

to the diagonal elements, and changing the phases of the wavefunctions according to the Griffith (1961) description.

(ii) *Direct method*

This method directly reduces a N-electron integral to a set of two-electron integrals:

$$G_N = \tfrac{1}{2}N(N-1)\,G_2.$$

Vector coupling procedures are used to decouple two electrons, and the remaining $(N-2)$-electron wavefunction is integrated out:

$$|a^n(S_1h_1)\,b^p(S_2h_2)\,ShM\theta\rangle = |(a^{n-2}b^p)\,a^2\rangle + |(a^{n-1}b^{p-1})\,ab\rangle + |(a^nb^{p-2})\,b^2\rangle. \qquad (2.9)$$

There is no antisymmetrization between the $(N-2)$-electron function and the two-electron function, but each is individually antisymmetrized. The detailed forms of each of the three functions in equation (2.9) are given in equation (2.10), with the same notation as in the previous section:

$$|(a^{n-2}b^p)\,a^2\rangle = \sqrt{\left(\frac{n(n-1)}{N(N-1)}\right)}\sum_{\substack{S_1'h_1',\,S_ah_a\\ S_a'h_a'}} D^{a^2}[a^{n-2}(S_1'h_1')\,b^p(S_2h_2)\,S_a'h_a';\,S_1h_1,S_ah_a,Sh]$$
$$\times\,|a^{n-2}(S_1'h_1')\,b^p(S_2h_2)\,S_a'h_a'.a^2(S_ah_a)\,ShM\theta\rangle, \qquad (2.10a)$$

$$|(a^{n-1}b^{p-1})\,ab\rangle = \sqrt{\left(\frac{2np}{N(N-1)}\right)}\sum_{\substack{S_1'h_1',\,S_2'h_2'\\ S_bh_b,\,S_{ab}h_{ab}}} D^{ab}[a^{n-1}(S_1'h_1')\,b^{p-1}(S_2'h_2')\,S_bh_b;\,S_1h_1,S_2h_2,S_{ab}h_{ab},Sh]$$
$$\times\,|a^{n-1}(S_1'h_1')\,b^{p-1}(S_2'h_2')\,S_bh_b.ab(S_{ab}h_{ab})\,ShM\theta\rangle, \qquad (2.10b)$$

$$|(a^nb^{p-2})\,b^2\rangle = \sqrt{\left(\frac{p(p-1)}{N(N-1)}\right)}\sum_{\substack{S_2'h_2',\,S_bh_b\\ S_b'h_b'}} D^{b^2}[a^n(S_1h_1)\,b^{p-2}(S_2'h_2')\,S_b'h_b';\,S_2h_2,S_bh_b,Sh]$$
$$\times\,|a^n(S_1h_1)\,b^{p-2}(S_2'h_2')\,S_b'h_b'.b^2(S_bh_b)\,ShM\theta\rangle, \qquad (2.10c)$$

where

$$D^{a^2}[a^{n-2}(S_1'h_1')\,b^p(S_2h_2)\,S_a'h_a';\,S_1h_1,S_ah_a,Sh]$$
$$=(-1)^{S_1+S_2+S_a+S_a'+h_1+h_2+h_a+h_a'}\sqrt{[\lambda(h_1)\,\lambda(h_a')\,(2S_1+1)\,(2S_a'+1)]}\,\langle a^{n-2}(S_1'h_1')\,a^2(S_ah_a)|\}\,a^nS_1h_1\rangle$$
$$\times\,W\begin{pmatrix}h_1 & h_2 & h\\ h_a' & h_a & h'\end{pmatrix}\overline{W}\begin{pmatrix}S_1 & S_2 & S\\ S_a' & S_a & S_1'\end{pmatrix} \qquad (2.11a)$$

$$D^{ab}[a^{n-1}(S_1'h_1')\,b^{p-1}(S_2'h_2')\,S_bh_b;\,S_1h_1,S_2h_2,S_{ab}h_{ab},Sh]$$
$$=(-1)^{p+1}\sqrt{[\lambda(h_1)\,\lambda(h_2)\,\lambda(h_b)\,\lambda(h_{ab})\,(2S_1+1)\,(2S_2+1)\,(2S_b+1)\,(2S_{ab}+1)]}$$
$$\times\,\langle a^{n-1}(S_1'h_1')\,a|\}\,a^nS_1h_1\rangle\,\langle b^{p-1}(S_2'h_2')\,b|\}\,b^pS_2h_2\rangle\,X\begin{pmatrix}h & h_1 & h_2\\ h_b & h_1' & h_2'\\ h_{ab} & a & b\end{pmatrix}\overline{X}\begin{pmatrix}S & S_1 & S_2\\ S_b & S_1' & S_2'\\ S_{ab} & \frac{1}{2} & \frac{1}{2}\end{pmatrix}, \qquad (2.11b)$$

$$D^{b^2}[a^n(S_1h_1)\,b^{p-2}(S_2'h_2')\,S_b'h_b';\,S_2h_2,S_bh_b,Sh]$$
$$=(-1)^{S_1+S_2'+S_b+h_1+h_2'+h_b+h_b'}\sqrt{[\lambda(h_2)\,\lambda(h_b')\,(2S_2+1)\,(2S_b'+1)]}$$
$$\times\,\langle b^{p-2}(S_2'h_2')\,b^2(S_bh_b)|\}\,b^p(S_2h_2)\rangle\,W\begin{pmatrix}h_1 & h_2 & h\\ h_b & h_b' & h_2'\end{pmatrix}\overline{W}\begin{pmatrix}S_1 & S_2 & S\\ S_b & S_b' & S_2'\end{pmatrix}. \qquad (2.11c)$$

The $\bar{X}$ coefficients in equation (2.11 b) are also known as $9j$ symbols, while the X coefficients are their space analogues defined by Griffith (1962). The fractional parentage coefficients

$$\langle a^{n-2}(S_1'h_1')\, a^2(S_ah_a)|\}\, a^nS_1h_1\rangle,$$

where $a = \mathrm{t}_2$, are given by Griffith (1961, table A 35), though with some phase differences. Those involving t_1, which we have derived for the present work, are set out in table 10.

By a procedure similar to the recursion method, the N-electron matrix elements can be reduced to two-electron matrix elements multiplied by the D factors of equation (2.11). A total of nine matrix elements may be formed in principle from the three recoupled wavefunctions of equation (2.10), though only three, at most, will be non-zero, depending on the difference between the configurations on the right- and left-hand sides of the matrix element. The reduction is illustrated below for the most general case:

$$\begin{aligned}
&\langle a^n(S_1h_1)\, b^p(S_2h_2)\, Sh|G_N|a^{n'}(S_3h_3)\, b^{p'}(S_4h_4)\, Sh\rangle \\
&\quad = \tfrac{1}{2}n(n-1) \sum_{\substack{S_1'h_1', S_3'h_3' \\ S_ah_a, S_4'h_4'}} D^{a^2}[a^{n-2}(S_1'h_1')\, b^p(S_2h_2)\, S_a'h_a'; S_1h_1S_ah_aSh] \\
&\qquad \times D^{a^2}[a^{n'-2}(S_3'h_3')\, b^{p'}(S_4h_4)\, S_a'h_a'; S_3h_3S_ah_aSh]\, \langle a^2S_ah_a|G_2|a^2S_ah_a\rangle \\
&\qquad + np \sum_{\substack{S_1'h_1', S_2'h_2' \\ S_3'h_3', S_4'h_4' \\ S_bh_b, S_{ab}, h_{ab}}} D^{ab}[a^{n-1}(S_1'h_1')\, b^{p-1}(S_2'h_2')\, S_bh_b; S_1h_1S_2h_2S_{ab}h_{ab}Sh] \\
&\qquad \times D^{ab}[a^{n'-1}(S_3'h_3')\, b^{p'-1}(S_4'h_4')\, S_bh_b; S_3h_3S_4h_4S_{ab}h_{ab}Sh]\, \langle abS_{ab}h_{ab}|G_2|abS_{ab}h_{ab}\rangle \\
&\qquad + \tfrac{1}{2}p(p-1) \sum_{\substack{S_2'h_2', S_4'h_4' \\ S_b'h_b', S_bh_b}} D^{b^2}[a^n(S_1h_1)\, b^{p-2}(S_2'h_2')\, S_b'h_b'; S_2h_2S_bh_bSh] \\
&\qquad \times D^{b^2}[a^{n'}(S_3h_3)\, b^{p'-2}(S_4'h_4')\, S_b'h_b'; S_4h_4S_bh_bSh]\, \langle b^2S_bh_b|G_2|b^2S_bh_b\rangle. \qquad (2.12)
\end{aligned}$$

If $n = n'$, and therefore $p = p'$ (i.e. the two configurations are the same), then all three terms contribute, but if $n = n' + 1$ we have only the terms

$$\langle (a^{n-2}b^p)\, a^2|G|(a^{n-1}b^{p-1})\, ab\rangle \quad \text{and} \quad \langle (a^{n-1}b^{p-1})\, ab|G|(a^nb^{p-2})\, b^2\rangle,$$

while if $n = n' + 2$, then only $\langle (a^{n-2}b^p)\, a^2|G|(a^nb^{p-2})\, b^2\rangle$ is non-zero.

If inter-electron repulsion between excited configurations $b^{2\lambda-1}a^{n+1}$ and $c^{2\lambda-1}a^{n+1}$, where a^n is an open ground configuration, is considered, equation (2.12) is inadequate. Although each excited configuration has only two open shells, it is necessary to include the closed shells c^2 and b^2 in the configurations, thus posing the problem of reducing electrostatic matrix elements over three open shells. No treatment of this problem appears to have been published before, so we give a somewhat more extended account of the way in which the direct method of reduction can be used. Electrostatic matrix elements involving three shells are needed both for treating charge transfer configurations themselves, and for dealing with the interaction between charge transfer and ligand field states.

The coupling of three shells together is a two stage process, the final result of which may be written

$$|a^p(S_1d)\, b^q(S_2e)\, S_3f, c^r(S_4g)\, Sh\rangle. \qquad (2.13)$$

Two electrons may be decoupled from (2.13) in six possible permutations: a^2, b^2, c^2, ab, ac, bc. The methods by which this is done are essentially the same as in the two open-shell problem,

TABLE 10. COEFFICIENTS OF FRACTIONAL PARENTAGE

$\langle a^{n-2}(S_1h_1)\, a^2(S_2h_2)|\}\, a^nSh\rangle$ for $a = t_1$

$\langle t_1^2(S_1h_1)\, t_1^2(S_2h_2)|\}\, t_1^4\, {}^1A_1\rangle$

S_2h_2 \ S_1h_1	$^1A_1$	^1E	$^3T_1$	$^1T_2$
$^1A_1$	$\frac{\sqrt{2}}{3}$	0	0	0
^1E	0	$-\frac{1}{3}$	0	0
$^3T_1$	0	0	$\frac{-1}{\sqrt{2}}$	0
$^1T_2$	0	0	0	$\frac{-1}{\sqrt{6}}$

$\langle t_1^2(S_1h_1)\, t_1^2(S_2h_2)|\}\, t_1^4\, {}^1E\rangle$

S_2h_2 \ S_1h_1	$^1A_1$	^1E	$^3T_1$	$^1T_2$
$^1A_1$	0	$\frac{-1}{3\sqrt{2}}$	0	0
^1E	$\frac{-1}{3\sqrt{2}}$	$\frac{\sqrt{2}}{3}$	0	0
$^3T_1$	0	0	$\frac{-1}{\sqrt{2}}$	0
$^1T_2$	0	0	0	$\frac{-1}{\sqrt{6}}$

$\langle t_1^2(S_1h_1)\, t_1^2(S_2h_2)|\}\, t_1^4\, {}^3T_1\rangle$

S_2h_2 \ S_1h_1	$^1A_1$	^1E	$^3T_1$	$^1T_2$
$^1A_1$	0	0	$\frac{-1}{3\sqrt{2}}$	0
^1E	0	0	$-\frac{1}{3}$	0
$^3T_1$	$\frac{-1}{3\sqrt{2}}$	$-\frac{1}{3}$	$\frac{1}{\sqrt{3}}$	$\frac{-1}{\sqrt{6}}$
$^1T_2$	0	0	$\frac{-1}{\sqrt{6}}$	0

$\langle t_1^2(S_1h_1)\, t_1^2(S_2h_2)|\}\, t_1^4\, {}^1T_2\rangle$

S_2h_2 \ S_1h_1	$^1A_1$	^1E	$^3T_1$	$^1T_2$
$^1A_1$	0	0	0	$\frac{-1}{3\sqrt{2}}$
^1E	0	0	0	$-\frac{1}{3}$
$^3T_1$	0	0	$\frac{-1}{\sqrt{2}}$	0
$^1T_2$	$\frac{-1}{3\sqrt{2}}$	$-\frac{1}{3}$	0	$\frac{1}{\sqrt{6}}$

$\langle t_1^3(S_1h_1)\, t_1^2(S_2h_2)|\}\, t_1^5\rangle$

S_2h_2 \ S_1h_1	$^4A_1$	^2E	$^2T_1$	$^2T_2$
$^1A_1$	0	0	$\frac{1}{\sqrt{15}}$	0
^1E	0	0	$\frac{-1}{\sqrt{30}}$	$\frac{1}{\sqrt{10}}$
$^3T_1$	$\frac{-1}{\sqrt{5}}$	$\frac{-1}{\sqrt{10}}$	$\frac{-\sqrt{3}}{\sqrt{20}}$	$\frac{-\sqrt{3}}{\sqrt{20}}$
$^1T_2$	0	$\frac{-1}{\sqrt{10}}$	$\frac{-1}{\sqrt{20}}$	$\frac{-1}{\sqrt{20}}$

giving equations similar to (2.10*a–c*). The decoupling of c^2 is particularly easy, being a straightforward elaboration of equation (2.10*c*):

$$|(a^pb^qc^{r-2})\, c^2\rangle = \sqrt{\left(\frac{r(r-1)}{N(N-1)}\right)} \sum_{S_5i,\, S_6k,\, S_7l} (-1)^{h+f+i+k+S+S_3+S_5+S_6} \sqrt{[\lambda(g)\, \lambda(l)\, (2S_4+1)\, (2S_7+1)]}$$
$$\times W\begin{pmatrix} h & g & f \\ i & k & k \end{pmatrix} \overline{W}\begin{pmatrix} S & S_4 & S_3 \\ S_5 & S_7 & S_6 \end{pmatrix} \langle c^{r-2}(S_5i)\, c|\}\, c^rS_4g\rangle$$
$$\times |a^p(S_1d)\, b^q(S_2e)\, S_3f, c^{r-2}(S_5i)\, S_7l\, .\, c^2(S_6k)\, Sh\rangle. \qquad (2.14)$$

a^2 and b^2 are decoupled from S_3f as in equations (2.10*a*) and (2.10*c*) and further reordering and recoupling of the states within the kets gives

$$|(a^{p-2}b^qc^r)\, a^2\rangle = \sqrt{\left(\frac{p(p-1)}{N(N-1)}\right)} \sum_{\substack{S_5i,\, S_6k \\ S_7l,\, S_8n}} (-1)^{d+e+g+f+l+n+S_1+S_2-S_3+S_4-S_7+S_8}$$
$$\times \sqrt{[\lambda(d)\, \lambda(f)\, \lambda(l)\, \lambda(n)\, (2S_1+1)\, (2S_3+1)\, (2S_7+1)\, (2S_8+1)]}$$
$$\times \langle a^{p-2}(S_5i)\, a^2(S_6k)|\}\, a^pS_1d\rangle\, W\begin{pmatrix} d & e & f \\ l & k & i \end{pmatrix} W\begin{pmatrix} f & g & h \\ n & k & l \end{pmatrix} \overline{W}\begin{pmatrix} S_1 & S_2 & S_3 \\ S_7 & S_6 & S_5 \end{pmatrix}$$
$$\times \overline{W}\begin{pmatrix} S_3 & S_4 & S \\ S_8 & S_6 & S_7 \end{pmatrix} |a^{p-2}(S_5i)\, b^q(S_2e)\, S_7l, c^r(S_4g)\, S_8n\, .\, a^2(S_6k)\, Sh\rangle. \qquad (2.15)$$

$$|(a^p b^{q-2} c^r)\, b^2\rangle = \sqrt{\left(\frac{q(q-1)}{N(N-1)}\right)} \sum_{\substack{S_5 i,\, S_6 k \\ S_7 l,\, S_8 n}} (-1)^{d+g+i+n+S_1+S_4+S_5+2S_7+S_8}$$
$$\times \sqrt{[\lambda(e)\,\lambda(f)\,\lambda(l)\,\lambda(n)\,(2s_2+1)\,(2S_3+1)\,(2S_7+1)\,(2S_8+1)]}$$
$$\times \langle b^{q-2}(S_5 i)\, b^2(S_6 k)|\}\, b^q S_2 e\rangle\, W\begin{pmatrix} l & k & f \\ a & d & i \end{pmatrix} W\begin{pmatrix} l & k & f \\ h & g & n \end{pmatrix} \overline{W}\begin{pmatrix} S_7 & S_6 & S_3 \\ S_2 & S_1 & S_5 \end{pmatrix}$$
$$\times \overline{W}\begin{pmatrix} S_7 & S_6 & S_3 \\ S & S_4 & S_8 \end{pmatrix} |a^p(S_1 d)\, b^{q-2}(S_5 i)\, S_7 l, c^r(S_4 g)\, S_8 n.\, b^2(S_6 k)\, Sh\rangle. \qquad (2.16)$$

Equation (2.10*b*) can be applied to decouple *ab* from $S_3 f$ and, with a further decoupling and reordering, gives

$$|(a^{p-1} b^{q-1} c^r)\, ab\rangle = \sqrt{\left(\frac{2pq}{N(N-1)}\right)} \sum_{\substack{S_6 k,\, S_5 i,\, S_7 l \\ S_8 n,\, S_9 s}} (-1)^{l+g+n+S_4+S_7+S_8+q+1}$$
$$\times \sqrt{[\lambda(d)\,\lambda(e)\,\lambda(f)\,\lambda(l)\,\lambda(n)\,(2S_1+1)\,(2S_2+1)\,(2S_3+1)\,(2S_7+1)\,(2S_9+1)]}$$
$$\times \langle a^{p-1}(S_6 k)\, a|\}\, a^p S_1 d\rangle \langle b^{q-1}(S_5 i)\, b|\}\, b^q S_2 e\rangle$$
$$\times W\begin{pmatrix} f & g & h \\ n & s & l \end{pmatrix} \overline{W}\begin{pmatrix} S_3 & S_4 & S \\ S_8 & S_9 & S_7 \end{pmatrix} X\begin{pmatrix} f & d & e \\ l & k & i \\ s & a & b \end{pmatrix} \overline{X}\begin{pmatrix} S_3 & S_1 & S_2 \\ S_7 & S_6 & S_5 \\ S_9 & \frac{1}{2} & \frac{1}{2} \end{pmatrix}$$
$$\times |a^{p-1}(S_6 k)\, b^{q-1}(S_5 i)\, S_7 l, c^r(S_4 g)\, S_8 n.\, ab(S_9 s)\, Sh\rangle. \qquad (2.17)$$

The procedure for decoupling *bc* and *ac* is more lengthy. To decouple *bc*, *b* is first decoupled from $S_3 f$ by using (2.6), and the ket is then recoupled to give

$$|b, [a^p(S_1 d)\, b^{q-1}(S_5 i)\, S_7 l.\, c^r(S_4 q)]\, S_b h_b Sh\rangle.$$

We then decouple *c* from $S_b h_b$ by using (2.6) again, and with further recoupling, obtain an expression involving four W and four $\overline{W}$ coefficients. This is simplified to X and $\overline{X}$ coefficients by using Griffith's (1962) definition, eliminating a summation over $S_b h_b$ and giving finally:

$$|(a^p b^{q-1} c^{r-1})\, bc\rangle = \sqrt{\left(\frac{2qr}{N(N-1)}\right)} \sum_{\substack{S_5 i,\, S_6 k,\, S_7 l \\ S_8 n,\, S_9 s}} (-1)^{b+d+f+i+\frac{1}{2}+S_1+S_3+S_5+r-1}$$
$$\times \sqrt{[\lambda(e)\,\lambda(f)\,\lambda(g)\,\lambda(l)\,\lambda(n)\,\lambda(S)\,(2S_2+1)\,(2S_3+1)\,(2S_4+1)\,(2S_7+1)}$$
$$\times (2S_8+1)\,(2S_9+1)]\, \langle b^{q-1}(S_5 i)\, b|\}\, b^q S_2 e\rangle\, \langle c^{r-1}(S_6 k)\, c|\}\, c^r S_4 g\rangle$$
$$\times W\begin{pmatrix} l & b & f \\ e & d & i \end{pmatrix} \overline{W}\begin{pmatrix} S_7 & \frac{1}{2} & S_3 \\ S_2 & S_1 & S_5 \end{pmatrix} X\begin{pmatrix} h & f & g \\ n & l & k \\ s & b & c \end{pmatrix} \overline{X}\begin{pmatrix} S & S_3 & S_4 \\ S_8 & S_7 & S_6 \\ S_9 & \frac{1}{2} & \frac{1}{2} \end{pmatrix}$$
$$\times |a^p(S_1 d)\, b^{p-1}(S_5 i)\, S_7 l, c^{r-1}(S_6 k)\, S_8 n.\, bc(S_9 s)\, Sh\rangle. \qquad (2.18)$$

The sixth and last of these expressions is for *ac*, and is obtained in an analogous way to that for *bc*:

$$|(a^{p-1} b^q c^{r-1})\, ac\rangle = \sqrt{\left(\frac{2pr}{N(N-1)}\right)} \sum_{\substack{S_5 i,\, S_6 k,\, S_7 l \\ S_8 n,\, S_9 s}} (-1)^{\frac{1}{2}+S_1+S_2+S_7+d+e+a+l+q+r-1}$$
$$\times \sqrt{[\lambda(d)\,\lambda(f)\,\lambda(g)\,\lambda(l)\,\lambda(n)\,\lambda(s)\,(2S_1+1)\,(2S_3+1)\,(2S_4+1)\,(2S_7+1)}$$
$$\times (2S_8+1)\,(2S_9+1)]\, \langle a^{p-1}(S_5 i)\, a|\}\, a^p S_1 d\rangle\, \langle c^{r-1}(S_6 k)\, e|\}\, c^r S_4 g\rangle$$
$$\times W\begin{pmatrix} d & e & f \\ l & a & i \end{pmatrix} \overline{W}\begin{pmatrix} S_1 & S_2 & S_3 \\ S_7 & \frac{1}{2} & S_5 \end{pmatrix} X\begin{pmatrix} h & f & g \\ n & l & k \\ s & a & c \end{pmatrix} \overline{X}\begin{pmatrix} S & S_3 & S_4 \\ S_8 & S_7 & S_6 \\ S_9 & \frac{1}{2} & \frac{1}{2} \end{pmatrix}$$
$$\times |a^{p-1}(S_5 i)\, b^q(S_2 e)\, S_7 l, c^{r-1}(S_6 k)\, S_8 n.\, ac(S_9 s)\, Sh\rangle. \qquad (2.19)$$

Combining the expressions (2.14) to (2.19) the general electrostatic matrix element for three open shells is broken down into 36 possible parts, only a fraction of which, however, will be non-zero in any particular case. Thus, only six are non-zero for configurationally diagonal matrix elements. If shells differ in only one electron there are three such contributions to the reduction of the matrix element, and only one contribution if a shell differs in two electrons between the two halves of the matrix element.

The expressions are very general and can be applied not only to interaction between singly excited configurations, but also to doubly and triply excited configurations and even double excitations from two different configurations. The complexity of the expressions necessitates computer programming, and thus a completely generalized program has been written which will reduce any electrostatic matrix element over three open shells down to the two-electron parameters described in § 2 (*a*). It is described by Bird (1969). We have thus set up the apparatus needed to reduce electrostatic matrix elements of states derived from configurations containing either two or three open shells, transforming as e, t_1 or t_2, down to combinations of the two-electron matrix elements of tables 1–5. No explicit functional form for the orbitals need be invoked, and the results are therefore applicable at all levels of approximation of the two-electron parameters.

(*c*) *Integral approximations not determined by symmetry*

The two-electron electrostatic matrix elements obtained by means of the arguments outlined in the last two sections cannot be treated further using group theory and to evaluate them in greater detail, and relate them to atomic quantities, some approximation scheme must be adopted. For calculations within the ligand field manifold, involving orbitals localized predominantly on a central metal ion, the electrostatic matrix elements may be related most simply to the Slater–Condon F^k of the free gaseous metal ion, multiplied by a proportionality constant, called the nephelauxetic parameter (Jørgensen 1962). This approach only takes into account indirectly the participation of the ligands in the orbitals containing the unpaired electrons, and fails to separate the effects of bonding, i.e. the extent of delocalization on to the ligands, or to differentiate π- and σ-effects, from the properties of the ligands themselves. Neither is there any obvious way in which the nephelauxetic model could be applied to charge transfer transitions.

We therefore adopt a l.c.a.o.-m.o. approach using integral approximations of a type analogous to those incorporated in a number of recent m.o. calculation schemes for metal complexes (Nicholson 1970). Overlap is not neglected, but use is made of the approximation (2.20) (Richardson & Rundle 1956):

$$\phi_{a_n}(i)\,\phi_{c_m}(j) \simeq \tfrac{1}{2}S_{ac}[\phi_{a_n}(i)\,\phi_{a_n}(j) + \phi_{c_m}(i)\,\phi_{c_m}(j)], \tag{2.20}$$

where $\phi_{a_n}(i)$ denotes an atomic orbital a on nucleus n, occupied by electron i, and S_{ac} is the overlap integral between the two atomic orbitals. If $i = j$, equation (2.20) represents the well known Mulliken approximation (Mulliken 1949), the level of approximation of which has been widely discussed (see, for example, Nicholson 1970). The major *ad hoc* correction required to (2.20), for $i = j$, would be to reinstate the one-centre exchange integrals, whose size is far greater than the magnitude of any other errors incurred by the approximation. An approximation of the form (2.20) for $i = j$, sometimes called the Ruedenberg approximation (Ruedenberg 1951), is more severe than the Mulliken approximation since it ignores one-centre Coulomb integrals which must therefore be reinstated.

When applied to the l.c.a.o.-m.o. expansion of Coulomb and exchange integrals between

m.os, the approximation (2.20) leads to expressions which are considerably simplified by employing Mulliken populations (Mulliken 1955):

$$n_p(a_n) = c_p(a_n) \sum_{b_m} c_p(b_m)\, S_{a_n b_m}, \tag{2.21}$$

where $n_p(a_n)$ is the contribution to the population on centre n by one electron in m.o. Ψ_p through its constituent a.o. ϕ_{a_n}, having a coefficient $c_p(a_n)$. Equation (2.21) leads to a simple density function for one molecular electron:

$$\Psi_p(1)\, \Psi_p(1) = \sum_{a_n} n_p(a_n)\, \phi^2_{a_n} \tag{2.22}$$

from which we obtain the Coulomb integral

$$\begin{aligned} J_{pq} &= \iint \Psi_p(1)\, \Psi^*_q(2)\, (e^2/r_{12})\, \Psi_p(1)\, \Psi^*_q(2)\, d\tau_1\, d\tau_2 \\ &= \langle pq|pq\rangle = \sum_{a_n,\, b_m} n_p(a_n)\, n_q(b_m)\, J_{a_n b_m}. \end{aligned} \tag{2.23}$$

As we noted above, the Mulliken approximation neglects one-centre exchange integrals. This is a result of the orthogonality of functions ϕ_{a_n}, ϕ_{b_n}. However, such integrals occur in the expansion (2.23) of J_{pq} and we therefore add a correction to the density function (2.22) such that terms of the form $n_p(a_n)\, n_q(b_n)\, K_{a_n b_n}$ are introduced into the expression for J_{pq}. The resulting expression then differs only from that obtained by neglect of differential overlap in replacing the squares of m.o. coefficients by population factors, i.e. $n_p(a_n)$ replaced $c^2_p(a_n)$. Almost certainly it represents an improvement in situations where neglect of overlap may not be realistic. It can be seen that when the overlap region makes a significant contribution to n_p, neglect of overlap would lead to too high a value for c_p.

To expand exchange integrals over m.os, K_{pq}, into sums of exchange integrals over atomic orbitals one possibility would be to make use of the Ruedenberg approximation (equation (2.20) with i and j referring to different electrons) though, as we remarked above, an *ad hoc* correction would then be needed to reinstate one-centre Coulomb integrals, which are much larger than the two-centre exchange integrals. Consequently we prefer to base our approach on making exchange corrections to the Mulliken approximation, and in any case incur no greater error if instead we let

$$\Psi_p(1)\, \Psi_q(1) = \sum_{a_n,\, b_m} [n_p(a_n)\, n_q(b_n)]^{\frac{1}{2}}\, \phi_{a_n}(1)\, \phi_{b_n}(2). \tag{2.24}$$

This expression cannot be derived rigorously from Mulliken's expression, but it does lead to the elegant reduction, not only of exchange integrals, but also of the general integrals $\langle pq|rs\rangle$ which occur in configuration interaction calculations. It has similarities to the zero overlap approximations (strictly speaking, to the 'neglect-of-diatomic-differential overlap' procedure of Pople, Santry & Segal (1965)), but makes some attempt to correct for the deficiencies in these by substituting $[n_p(a_n)]^{\frac{1}{2}}$ for $c_p(a_n)$.

With the approximation (2.24) the general molecular electrostatic integral $\langle pq|rs\rangle$ may be written as the sum of terms each involving a one-centre or two-centre Coulomb or exchange integral multiplied by functions of population factors. In evaluating these sums, the coordinate system and symmetry adapted combinations of metal and ligand wavefunctions of Ballhausen & Gray (1964), for tetrahedral complexes, were employed. Numerical estimates of the one-centre terms may be obtained from atomic spectra or atomic Hartree–Fock calculations. The two-centre Coulomb terms are approximated to the interaction of point charges situated at the atomic centres. Two-centre exchange integrals are neglected.

PHILOSOPHICAL TRANSACTIONS OF THE ROYAL SOCIETY A MATHEMATICAL, PHYSICAL & ENGINEERING SCIENCES

TABLE 11 (*a*). THE LIGAND FIELD INTERELECTRON REPULSION PARAMETERS IN THE l.c.a.o.-m.o. APPROXIMATION OF § 2 (*c*)

$$a = n_t^2(A+4B+3C) + (1-n_t)\,n_t(2/R) + \tfrac{1}{4}(1-n_t)^2\,(J_{av}+3J_{LL}+2K_{av})$$
$$b = n_t^2(A-2B+C) + (1-n_t)\,n_t(2/R) + \tfrac{1}{4}(1-n_t)\,(J_{av}+3J_{LL}) + \tfrac{1}{8}(2n_\sigma - n_\pi)^2\,K_{av}$$
$$c = 2Bn_e n_t - n_\pi/8(1-n_e)\,K_{av}$$
$$d = n_e n_t(A-2B+C) + (n_t(1-n_e)+n_e(1-n_t))\,(1/R) + \tfrac{1}{4}(1-n_t)\,(1-n_e)\,(J_{av}+3J_{LL}) + \tfrac{3}{8}n_\pi(1-n_e)\,K_{av}$$
$$e = n_e^2(A+4B+3C) + 2n_e(1-n_e)\,(1/R) + \tfrac{1}{4}(1-n_e)^2\,(J_{av}+3J_{LL}) + \tfrac{1}{2}(1-n_e)^2\,K_{av}$$
$$f = n_e^2(4B+C) + \tfrac{1}{4}(1-n_e)^2\,K_{av}$$
$$g = n_e n_t(B+C) + \tfrac{1}{16}n_\pi(1-n_e)\,(J_{av}-J_{LL}+K_{av}) + \tfrac{1}{16}(1-n_t)\,(1-n_e)\,K_{av}$$
$$h = n_e n_t B + \tfrac{1}{16}n_\pi(1+n_e)\,(J_{av}+K_{av}-J_{LL})$$
$$i = n_t\sqrt{(3n_e n_t)}\,B + \tfrac{1}{16}(2n_\sigma - n_\pi)\,\sqrt{[n_\pi(1-n_e)]}\,(J_{av}-K_{av}-J_{LL})$$
$$j = n_t^2(3B+C) + \tfrac{1}{16}(2n_\sigma - n_\pi)^2\,(J_{av}-J_{LL}+K_{av}) + \tfrac{1}{4}(1-n_t)^2\,K_{av}.$$

TABLE 11 (*b*). INTERELECTRON REPULSION INTEGRALS INVOLVING t_1

t_1/t_2 integrals

$$mm = \tfrac{1}{4}(J_{av}+K_{av}+3J_{LL}) \qquad uu = \tfrac{1}{16}K_{av}$$
$$xx = \tfrac{1}{16}(J_{av}+5K_{av}-J_{LL}) \qquad nn = \text{zero}$$
$$uq = -\tfrac{1}{16}n_\pi K_{av} \qquad vv = \tfrac{1}{16}(1-n_t)\,K_{av}$$
$$mk = n_t(1/R) + \tfrac{1}{4}(1-n_t)\,(J_{av}+3J_{LL}) + \tfrac{1}{4}n_\pi K_{av}$$
$$zz = \tfrac{3}{16}n_\pi K_{av} + \tfrac{1}{16}(1-n_t)\,K_{av}$$
$$tx = -\tfrac{1}{16}(2n_\sigma - n_\pi)\,(J_{av}-J_{LL}) - \tfrac{3}{16}n_\pi K_{av}$$
$$yy = \tfrac{3}{16}n_\pi(J_{av}-J_{LL}) + \tfrac{3}{16}(1-n_t)\,K_{av}$$
$$qv = -\tfrac{1}{16}\sqrt{(n_\pi)}\,(2n_\sigma - n_\pi)\,K_{av} \qquad uv = -\tfrac{1}{16}\sqrt{(n_\pi)}\,K_{av}$$
$$xy = -\tfrac{\sqrt{3}}{16}\sqrt{(n_\pi)}\,(J_{av}+K_{av}-J_{LL})$$
$$ty = \tfrac{\sqrt{3}}{16}\sqrt{(n_\pi)}\,(2n_\sigma - n_\pi)\,(J_{av}+K_{av}-J_{LL}).$$

TABLE 11 (*c*)

e/t_1 integrals

$$lm = n_e(1/R) + \tfrac{1}{4}(1-n_e)\,(J_{av}+K_{av}+3J_{LL})$$
$$pu = -\tfrac{1}{8}(1-n_e)\,K_{av}$$
$$aa = \tfrac{1}{16}(1-n_e)\,K_{av}$$
$$bb = \tfrac{1}{16}(1-n_e)\,(J_{av}+2K_{av}-J_{LL})$$
$$bx = -\tfrac{1}{16}\sqrt{(1-n_e)}\,(J_{av}-K_{av}-J_{LL}).$$

$e/t_1/t_2$ integrals

$$pv = \tfrac{1}{8}\sqrt{(n_\pi)}\,(1-n_e)\,K_{av}$$
$$ar = \tfrac{1}{8}\sqrt{(n_\pi)}\,(1-n_e)\,K_{av}$$
$$bs = -\tfrac{1}{16}\sqrt{(n_\pi)}\,(1-n_e)\,(J_{av}-K_{av}-J_{LL})$$
$$az = -\tfrac{1}{8}\sqrt{[n_\pi(1-n_e)]}\,K_{av}$$
$$by = \tfrac{\sqrt{3}}{16}\sqrt{[n_\pi(1-n_e)]}\,(J_{av}+K_{av}-J_{LL})$$
$$bt = \tfrac{1}{16}(2n_\sigma - n_\pi)\,\sqrt{[(1-n_e)]}\,(J_{av}-J_{LL}) - \tfrac{3}{16}n_\pi\sqrt{[(1-n_e)]}\,K_{av}$$
$$sx = \tfrac{1}{16}\sqrt{[n_\pi(1-n_e)]}\,(J_{av}+3K_{av}-J_{LL})$$
$$sy = -\tfrac{\sqrt{3}}{16}n_\pi\sqrt{[(1-n_e)]}\,(J_{av}+K_{av}-J_{LL}) + \tfrac{\sqrt{3}}{16}n_\sigma\sqrt{[(1-n_e)]}\,K_{av}$$
$$rz = \tfrac{1}{16}(n_\sigma - 2n_\pi)\,\sqrt{[(1-n_e)]}\,K_{av}.$$

The resulting expressions for the interelectron repulsion integrals over the ligand field manifold defined in table 2 are given in table 11 (*a*), while in sections (*b*) and (*c*) of that table are listed the expressions for the interelectron repulsion integrals involving t_1 orbitals. In table 11 (*a*) we have given the integrals in terms of Griffith's (1961) nomenclature $a, \ldots, j$ since these are better known than the parameters $kk, \ldots, st$, etc., but in sections (*b*) and (*c*) of table 11 we revert to the notation set out in tables 3–5. The symbols used in table 11 for the population factors and integrals are as follows:

$n_t = n_{t2}(d)$, the population in the metal d-orbitals due to one electron in a t_2 m.o.
$n_e = n_e(d)$, the population in the metal d-orbitals due to one electron in an e m.o.
$n_\pi = n_{t_2}(p_x, p_y)$, the total population in all the ligand p_π orbitals due to one electron in a t_2 m.o.
$n_\sigma = n_{t_2}(p_z)$, the total population in all the ligand p orbitals due to one electron in a t_2 m.o.
J_{av}, the average one-centre ligand Coulomb integral. N.B. the average ligand Coulomb integral is used, rather than $J(p_x, p_x)$ and $J(p_x, p_y)$ in order to preserve invariance to the group operations.
K_{av}, the average one-centre ligand exchange integral.
J_{LL}, the Coulomb integral between orbitals on different ligands, approximated as $\sqrt{(6)}/4R$ (a.u.)
A, B, C, Racah interelectron repulsion parameters for the metal d-orbitals.
R, the metal-ligand distance (a.u.)

Inserting the expressions in table 11 into the matrices of tables 6–9, we now have the means in principle to fit the term energies in a ligand-field spectrum so as to extract m.o. population factors and hence eigenvectors, in a completely empirical fashion. Unlike an earlier attempt at a similar m.o. parametrization of ligand field spectra by Lohr (1966) repulsion between ligand electrons is explicitly included, as also is the contribution of the metal Racah parameter A. In addition, in the expressions (*b*) and (*c*) of table 11 we have the means of parametrizing the electron repulsion splittings of charge transfer configurations and the interaction between charge transfer and ligand field configurations. The application of all these results to the spectra of tetrahalogenocobaltates(II) is described in § 5.

3. Molecular orbital treatment of spin-orbit coupling

Ions of the first transition series have spin-orbit coupling constants in the range 50–800 cm^{-1} (see, for example, Figgis 1966), and since the linewidths of the ligand field spectra of transition metal complexes, particularly in crystals at low temperatures, are often much less than this, resolved fine structure due to spin-orbit splitting of the Russell–Saunders terms is frequently observed. Also the appearance of bands attributable to Russell–Saunders terms which are formally spin forbidden requires us to consider the effect of off-diagonal matrix elements of the spin-orbit operator, mixing in small amounts of spin-allowed terms. Charge transfer terms, too, are frequently split by spin-orbit coupling, particularly when the ligand has a large spin-orbit coupling constant, e.g. bromide or iodide.

In conventional ligand-field theory only spin-orbit coupling at the central metal ion is considered, sometimes scaled down by a 'relativistic nephelauxetic parameter' (Jørgensen 1962), to take account of covalency. In the spirit of our attempt to parametrize ligand field spectra directly in terms of m.o. eigenvectors, however, we also give an m.o. treatment of spin-orbit coupling, which takes into account the spin-orbit interactions both at the metal and ligand

centres. As in the case of electron repulsion, we require expressions for one-electron matrix elements in terms of m.o. eigenvectors and atomic spin-orbit coupling constants, plus a method of constructing many electron matrix elements from them.

(*a*) *One-electron integrals*

The spin-orbit Hamiltonian of a molecule can be approximated (Blume & Watson 1962, 1963; Misetich & Buch 1964) as

$$\mathscr{H}_{so} = \sum_{N,i} \zeta_N \boldsymbol{l}_i \cdot \boldsymbol{s}_i = \sum_i \boldsymbol{u}_i \cdot \boldsymbol{s}_i, \tag{3.1}$$

where ζ_N is the spin-orbit coupling constant of nucleus N, incorporated into the molecular operator $\boldsymbol{u}_i$ for electron i. Equation (3.1) permits us to write simple expressions for matrix elements of spin-orbit coupling between m.os in terms of m.o. eigenvectors and atomic spin-orbit coupling coefficients. Population factors, used in the m.o. treatment of electron repulsion, are not appropriate here since in general the overlap region does not contribute significantly to the spin-orbit coupling. This is because the operator equivalent of ζ_N approximately depends on $\langle r_{iN}^{-3} \rangle$, where r_{iN} is the distance from electron i to nucleus N. For example, Misetich & Watson (1966) calculated the many-centre terms contributing to spin-orbit coupling in $KNiF_3$, and found them to be negligible. To a good approximation, one may therefore confine the l.c.a.o.-m.o. expansion of the matrix element of $\boldsymbol{u}$ simply to the one-centre terms (Bird & Day 1968).

If Ψ_1 is an m.o. expanded in terms of a.os ϕ:

$$\Psi_1 = \sum_\alpha c_{1\alpha} \phi_{1\alpha}, \tag{3.2}$$

then the matrix element u which connects Ψ_1 and Ψ_2 can be written

$$\begin{aligned} \langle \Psi_1 | \boldsymbol{u} | \Psi_2 \rangle &= \sum_{\alpha,\beta,N} c_{1\alpha} c_{2\beta} \langle \phi_{1\alpha} | \zeta_N \boldsymbol{l} | \phi_{2\beta} \rangle \\ &= \sum_N c_{1N} c_{2N} \langle \phi_{1N} | \zeta_N \boldsymbol{l} | \phi_{2N} \rangle, \end{aligned} \tag{3.3}$$

where ϕ_{1N} and ϕ_{2N} are a.os (e.g. p_x, p_y) on the same centre N. The one-centre terms are then simply multiples of ζ_N provided that appropriate coordinate transformations are carried out to make the molecular coordinate system, normally coincident with that of the central metal ion, compatible with the local coordinate system of the nucleus in question. We have employed the coordinate system of Ballhausen & Gray (1964) for tetrahedral complexes.

The resulting matrix elements of the molecular spin-orbit operator are most succinctly expressed in terms of reduced matrix elements, and in table 12 these are listed for all combinations of e, t_1 and t_2 m.os. The m.o. eigenvectors in the expressions for $\langle \Psi_a \| \boldsymbol{s} \cdot \boldsymbol{u} \| \Psi_b \rangle$ in table 12 are labelled a_k and b_k for Ψ_a and Ψ_b, where $k = 1, 2, 3$ for metal d, ligand σ- and ligand π-orbitals respectively. The contribution to the matrix elements from ligand s has been neglected.

(*b*) *Many-electron integrals*

From the one-electron reduced matrix elements of table 12 many-electron matrix elements may be constructed using the methods described by Griffith (1962). As the procedures we have used for this purpose follow Griffith's quite precisely, no further description of them is needed here.

TABLE 12. REDUCED MATRIX ELEMENTS OF SPIN-ORBIT COUPLING FOR TETRAHEDRAL SYMMETRY

$$\langle \tfrac{1}{2}e\|su\|\tfrac{1}{2}t_1\rangle = \tfrac{1}{2}\sqrt{(6)}\, a_3 b_3 \zeta_L,$$
$$\langle \tfrac{1}{2}e\|su\|\tfrac{1}{2}t_2\rangle = -\tfrac{1}{2}\sqrt{(6)}\,[(\sqrt{(2)}\, a_3 b_2 + a_3 b_3)\,\zeta_L + 2\sqrt{(3)}\, a_1 b_1 \zeta_d],$$
$$\langle \tfrac{1}{2}t_1\|su\|\tfrac{1}{2}t_1\rangle = -\tfrac{3}{2} a_3 b_3 \zeta_L,$$
$$\langle \tfrac{1}{2}t_1\|su\|\tfrac{1}{2}t_2\rangle = -\tfrac{1}{2}\sqrt{(3)}\,(\sqrt{(2)}\, b_2 + b_3)\, a_3 \zeta_L,$$
$$\langle \tfrac{1}{2}t_2\|su\|\tfrac{1}{2}t_2\rangle = 3a_1 b_1 \zeta_d + \tfrac{3}{2}[\sqrt{(2)}\,(a_2 b_3 + a_3 b_2) - a_3 b_3]\,\zeta_L.$$

ζ_d and ζ_L are the spin-orbit coupling constants for metal d and ligand p orbitals.

4. THE SPECTRA OF TETRAHALOGENOCOBALTATES(II)

In seeking systems to test the molecular orbital ligand-field scheme which we have derived in the previous sections, a number of considerations have to be satisfied. First, it is necessary to choose molecules whose ligand-field spectra can be assigned as far as possible empirically, i.e. from experimental evidence independent of the theoretical framework which we wish to test. We therefore seek a ligand-field spectrum which is well resolved, so that we can locate the absorption maxima accurately, whose transitions have associated with them a reasonable amount of vibrational, spin-orbit or other fine structure which will provide extra evidence of assignment, and, most important, which contains a large enough number of transitions that the parameters in our model will be over-determined. Without including spin-orbit coupling, the theory contains four freely disposable parameters, Δ, n_e, n_{t_2} and n_π, so we require a ligand-field spectrum in which the baricentres of at least four Russell–Saunders terms can be unambiguously located.

To achieve the most favourable resolution compatible with measurements over a wide range of spectral energies it would be desirable to use data recorded on a crystal at liquid helium temperature: we would then also be able to use the selection rules for linearly polarized light as a further assignment tool. The need to use crystal data brings with it another desideratum, namely that the transition metal ion should occupy a site of the highest possible point symmetry compatible with our wish, if possible, to be able to observe polarized transitions. The molecular orbital expressions for the ligand-field matrix elements have been derived for the cubic point groups, and could therefore be tested by comparison with the spectrum of an octahedral or tetrahedral molecule. However, the ligand-field transitions in the former are only made allowed by vibrational–electronic interaction, a complication which we wish to avoid. Among tetrahedral complexes of the 3d-elements, those of cobalt(II) form an attractive group for our purpose. The terms of the free ion are ^4P, ^4F, ^2P, ^2D, ^2F, ^2G and ^2H. In a tetrahedral ligand-field the ground-state term is an orbital singlet, $^4A_2(F)$, so that to first order it will not be affected by spin-orbit coupling. As well as three quartet excited states, $^4T_1(F)$, $^4T_2(F)$ and $^4T_1(P)$, no less than 14 doublets are potentially observable; they are derived as follows:

$$^2P \rightarrow {}^2T_1,$$
$$^2D \rightarrow {}^2E + {}^2T_2,$$
$$^2F \rightarrow {}^2A_2 + {}^2T_1 + {}^2T_2,$$
$$^2G \rightarrow {}^2A_1 + {}^2E + {}^2T_1 + {}^2T_2,$$
$$^2H \rightarrow {}^2E + 2{}^2T_1 + {}^2T_2.$$

To test the molecular orbital expressions for the matrix elements of the spin-orbit operator, it is also convenient to be able to vary the spin-orbit coupling constant of the ligand, a procedure

which is easily possible by focusing on the halide complexes CoX_4^{2-} (X = Cl, Br, I), since the atomic spin-orbit coupling constants of the three halogens increase from 587 cm^{-1} for chlorine to 2455 cm^{-1} (Br) and 5070 cm^{-1} (I). In the past the ligand-field spectra of the tetrahalogenocobaltate(II) ions have been measured often, and under a wide variety of conditions. A survey of the available evidence, the main features of which are summarized in the next section, nevertheless revealed large gaps in the experimentally based assignments of these spectra, gaps which the following sections attempt to fill.

(*a*) *Summary of previous work*

As early as 1937, Dreisch & Trommer (1937) examined the spectrum of Co(II) in concentrated HCl and observed a band at 6300 cm^{-1} which they attributed to a transition of $CoCl_4^{2-}$. Later Ballhausen & Jørgensen (1955) observed the higher-energy spin-allowed band at 15 000 cm^{-1} in this complex. The solution spectra of a large number of tetrahedral Co(II) complexes were studied by Cotton, Goodgame & Goodgame (1961), but their work was handicapped by the low resolution of the spectra, particularly in the region of the doublets. At about the same time, Weakliem (1962) studied the ligand-field spectrum of Co(II) in some wurtzite lattices. At 77 K he observed some of the spin-forbidden bands arising from the doublet terms of the free ion, but being primarily concerned with the quartet bands, he examined only the spin-allowed visible band under high resolution at 4 K.

Because of its high crystal symmetry (tetragonal) and point symmetry (D_{2d}), Cs_3CoCl_5 is probably the most convenient crystal in which to study the spectrum of $CoCl_4^{2-}$. The spectrum of $CoCl_4^{2-}$ in Cs_3CoCl_5 was first measured at 1.8 K by Pelletier-Allard (1961, 1965*a*, *b*). She carried out some point charge crystal-field calculations but, lacking vibrational data on the crystal, she could not unravel the complicated vibronic structure and locate the band origins. The lowest energy quartet ligand-field transitions of $CoCl_4^{2-}$ in Cs_3CoCl_5, $^4T_1(F)$ and $^4T_2(F)$ were examined by Belgers, Bongers, Van Stapele & Zijlstra (1964) and Van Stapele, Belgers, Bongers & Zijlstra (1966) in connexion with their work on the paramagnetic resonance spectrum of the crystal. The remaining quartet $^4T_1(P)$, was also examined by Jesson (1968), using Cs_3ZnCl_5 as a host lattice. Ferguson (1963) was the first to tackle the doublet spectrum of $CoCl_4^{2-}$ in some detail. He measured spectra in three crystalline environments, $Cs_2(Zn, Co)Cl_4$,

$$(NMe_4)_2(Zn, Co)Cl_4\ (Me = CH_3) \quad \text{and} \quad (QH)_2(Zn, Co)Cl_4\ (QH = \text{quinolinium}),$$

and used a four parameter crystal field model used to interpret the data. Unfortunately the low crystal and point symmetries prevented him from making firm assignments, except for some of the levels derived from ^2F. Data on the doublet spectrum of Cs_3CoCl_5 are also contained in the thesis of Stoneman (1964) but he, too, had no detailed vibrational information on the crystal, and thus was unable to assign much of the vibronic fine structure.

The work reported in the present paper, which was undertaken with the aim of locating the origins of the doublet ligand-field transitions, and determining their assignments, extends the previous experiments outlined above in a number of important respects. First, we have measured the spectrum of Cs_3CoBr_5, as well as remeasuring that of Cs_3CoCl_5, and are thus in a position to distinguish spin-orbit splittings from vibrational intervals, which are expected to vary in quite a different way with the mass of the halide ions. Indeed, in many instances the vibronic structure of the bands in Cs_3CoBr_5 has proved easier to disentangle than that of the corresponding bands in the chloride, so that assignments obtained for the former may then be used to throw light on the latter. Secondly, we are fortunate in having available detailed vibrational information on

the electronic ground states of both crystals, in the form of single-crystal Raman spectra, the polarizations of which enabled a factor-group analysis to be performed. Thus we have data, not simply on the complex anions viewed as tetrahedral units, but on the extent to which the normal modes of the tetrahedra are split by the low symmetry environment in the crystal, and by intermolecular interactions, an index of the latter being also provided by the many lattice modes which are observed in the Raman spectrum. The third respect in which the present work extends previous observations on the ligand-field spectra of tetrahedral cobalt(II) complexes lies in the quantitative use we have made of observations on the temperature dependence of the intensities of certain transitions. E.s.r. experiments (Belgers *et al.* 1964; Van Stapele *et al.* 1966) have established that in Cs_3CoCl_5 and Cs_3CoBr_5 the ground states exhibit zero field splittings of a few wave numbers so that, linewidths permitting, pairs of lines whose relative intensities vary with temperature according to the Boltzman law, should be found throughout the spectrum. The appearance of such lines is a great help in separating ground from excited state zero field splittings.

(*b*) *Experimental*

Blue tetragonal prisms of Cs_3CoX_5 (X=Cl, Br) were prepared by evaporating an aqueous solution of caesium halide and the appropriate cobalt halide in stoichiometric amounts at room temperature. Analysis for halide gave the following results:

Cs_3CoCl_5: found Cl, 28.07; calc. for Cs_3CoCl_5, Cl, 27.93 %,

Cs_3CoBr_5: found, Br, 46.72; calc. for Cs_3CoBr_5, Br, 46.61 %.

The crystals developed as rectangular prisms, approximately 2–3 mm edge, with (110) and (001) faces most pronounced. Debris and surface flaws in the crystals were removed by polishing with talc on a velvet polishing pad, and they were mounted with a thin layer of grease over a hole in a copper sheet, which was then bolted to the base of an Oxford Instrument Co. optical cryostat, using an indium gasket to ensure good thermal contact with the liquid helium reservoir.

The temperature of the crystal mount was measured by a 0.03 at. % Fe/Au versus chromel thermocouple. One junction was embedded in the indium gasket between the crystal mount and the cryostat and the other was immersed in liquid nitrogen. This thermocouple, first discussed by Berman & Huntley (1963), is very stable and reproducible. The potential difference varies almost linearly with temperature throughout the range 200–300 K. The potential difference, which was recorded by a Servoscribe, could be measured to an accuracy of ± 0.01 mV, approximately equivalent to ± 1 K in the range 4–77 K. A plot of thermoelectric power per degree against temperature was derived for this thermocouple by Berman, Brock & Huntley (1964). Our thermocouple was calibrated by fitting their plot to a set of experimentally determined fixed points.

The spectra were recorded by a Cary 14 spectrophotometer fitted with an intense (600 W quartz iodine) light source. The incident light was polarized by a calcite Glan prism placed in front of the cryostat.

(*c*) Cs_3CoCl_5 *and* Cs_3CoBr_5: *preliminaries*

The structure of Cs_3CoCl_5 was first determined by Powell & Wells (1935) and refined more recently by Figgis, Gerloch & Mason (1964). The crystals belong to the space group D_{4h}^{18} and have four molecules per unit cell (see figure 1). The site group of the Co(II) is D_{2d} and the tetrahedron of halide ligands experiences a small tetragonal elongation. A full analysis of the crystal

structure of Cs_3CoBr_5 has not been carried out, but an X-ray powder photograph (Belgers 1965) showed that the compound is isomorphous with Cs_3CoCl_5 and enabled the unit cell dimensions to be determined (see figure 1).

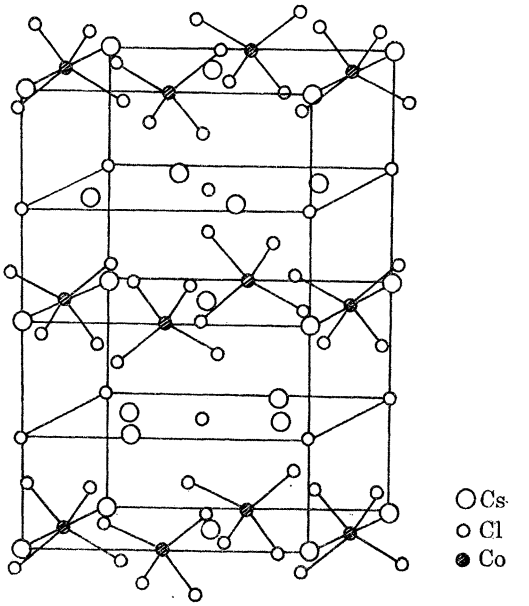

FIGURE 1. The unit cell of Cs_3CoX_5 (Powell & Wells 1935).

By polishing the crystals either parallel or perpendicular to the unique c axis it was possible to examine the axial spectrum (both electric vector and magnetic vector in the xy plane), the σ spectrum (electric vector in xy, magnetic vector parallel to z), and the π spectrum (electric vector parallel to z, magnetic vector in xy). The axial and σ spectra were identical, establishing that the observed transitions are electric dipole in origin.

Surveys of the axial (σ) spectra of Cs_3CoCl_5 and Cs_3CoBr_5 in the ligand-field doublet region are illustrated in figure 2. In principle, since the spectra are those of pure crystals, additional features due to exciton or magnon effects may be present. A small negative exchange interaction has been invoked to explain the shift to higher field of the e.s.r. lines of Cs_3CoCl_5 as the temperature is lowered from 77 to 4 K (Belgers *et al.* 1964) and also to account for deviations of magnetic susceptibilities from theoretical values for a number of tetrahedral chloro-complexes of Co(II) (Figgis *et al.* 1964) including Cs_3CoCl_5 (Belgers *et al.* 1964). However, the Néel temperatures of the two materials are so low ($T_N = 0.52$ K for Cs_3CoCl_5 (Wielinga, Blöte, Roest & Huiskamp 1967) that at 4.2 K magnon sidebands will not be present. Exciton effects may manifest themselves as small splittings or shifts in band positions in the two polarizations, but in view of the weakness of exchange forces in these crystals they are not expected to contribute much to the appearance of the spectra. Much more important is the need to separate and assign the vibronic fine-structure which is such a prominent feature of most of the bands: and thus to identify the band origins. Information is therefore required about the vibrational properties of the lattices.

Table 13 contains the results of a single crystal Raman study of both Cs_3CoCl_5 and Cs_3CoBr_5 undertaken by Dr T. R. Gilson of Southampton University (1970, personal communication). In a species of strictly T_d symmetry there are four internal vibrational modes: $\nu_1(a_1)$, $\nu_2(e)$, $\nu_3(t_2)$ and $\nu_4(t_2)$. All four are Raman active, but only ν_3 and ν_4 are infrared active. The cobalt

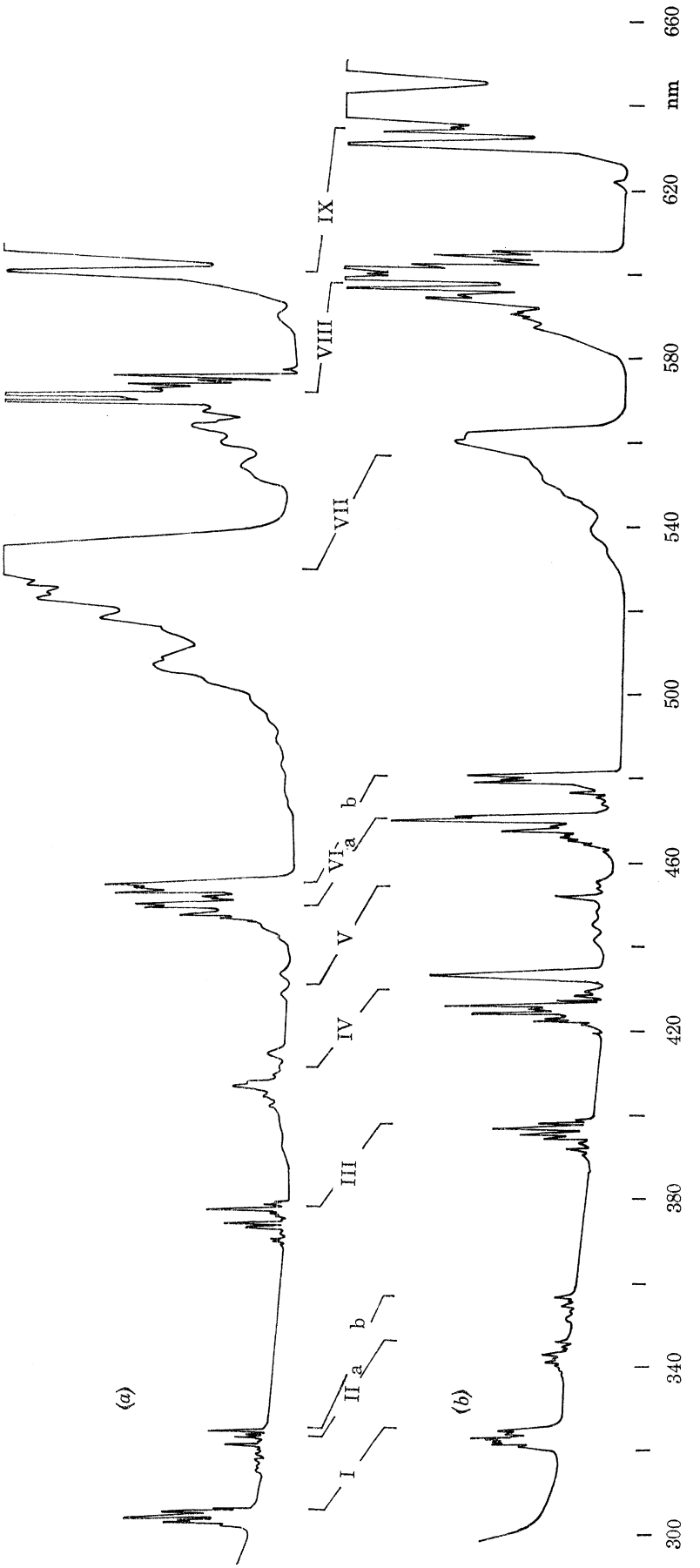

FIGURE 2. Axial absorption spectra of (*a*) Cs_3CoCl_5 and (*b*) Cs_3CoBr_5 at 4.2 K. The regions labelled with roman numerals correspond to those in §4 (*d*).

ion site in Cs_3CoCl_5 and Cs_3CoBr_5, however, is not T_d but D_{2d}, and this results in the lifting of the degeneracy of e to give $a_1 + b_1$ and of t_2 to give $b_2 + e$. Thus, ν_2, ν_3 and ν_4 may each be expected to split into two components, and in addition, lattice modes will arise from motions of the ions within the unit cell. The Raman spectra were analysed by carrying out a factor group analysis. Symmetry considerations and comparison of frequencies of the internal modes in T_d with those in D_{2d} and in the factor group D_{4h} enable the observed Raman bands for Cs_3CoCl_5 and Cs_3CoBr_5 to be classified into lattice modes and internal modes and the latter to be correlated with the internal modes in T_d symmetry. The vibrational frequencies coexcited with the electronic transitions will be labelled as indicated in table 13 to emphasize the relation with strictly tetrahedral symmetry. (Thus, $\nu_2(a_{1g})$ is a mode which transforms as a_{1g} in D_{4h} and correlates with the $\nu_2(e)$ mode in T_d.)

In a site of T_d point symmetry, the ground state for a d^7 ion is $^4A_2$. Spin-orbit coupling does not lift the spin-degeneracy, and the ground state transforms as Γ_8 in T_d^*. Lowering the symmetry to D_{2d}^*, however, splits $\Gamma_8(T_d)$ into two Kramers doublets belonging to Γ_6 and Γ_7 representations. For both Cs_3CoCl_5 and Cs_3CoBr_5, this zero field splitting has been studied in detail by e.s.r. spectroscopy (Belgers *et al.* 1964; Van Stapele *et al.* 1966). The separation of the doublets is 8.6 cm^{-1} in Cs_3CoCl_5 and 10.8 cm^{-1} in Cs_3CoBr_5 with the spin state $\Gamma_7(\pm\frac{3}{2})$ lying at lower energy in both cases. This state transforms as Γ_6 when the orbital symmetry is included. Since the Γ_7 levels are thermally accessible from the ground levels, the intensities of the observed peaks in the electronic spectra may show temperature dependence because of changes in the Boltzmann distribution of population between these levels.

To facilitate description, the electronic spectra are divided into the distinct regions indicated in figure 2. These will be discussed separately, starting at high energy since the bands are more clearly resolved and simpler to assign than the bands at low energy. The frequencies of the observed peaks are listed in tables A and B† and each peak will be referred to by its number in these tables. The frequencies listed in the tables have been corrected for the absolute error in the spectrometer readings, determined by calibration with a mercury discharge lamp. The most important remaining source of error is the reading error of the peak positions on the charts. Since the spectrometer chart record is linear in wavelength, the reading error is linear in angstroms and is estimated to be not greater than ± 0.05 nm for well-defined peaks over the whole spectrum. The peaks are reproducible to within 0.01 nm so that the maximum limits of error range from 1.5 cm^{-1} at 15 000 cm^{-1} to 5 cm^{-1} at 33 000 cm^{-1}.

To identify each band in detail, it is useful to describe corresponding bands of the bromo- and chloro-complexes together since this highlights the similarities and differences between them and helps in the identification of vibrational intervals. The origins of transitions are located by considering energy separations, polarization ratios and intensities. As a guide to the number of transitions expected and also their rough relative dispositions, we have used Ferguson's (1963) ligand-field splitting diagram for tetrahedral d^7 complexes, which was calculated from a conventional four parameter model. For convenience, this diagram is reproduced in figure 3. Vibrational progressions accompanying the transitions are identified on the assumption that the polarization ratio is similar for each component of the progression. There may be ambiguities in the characterization of some vibronic structure because certain frequency intervals correspond to several possible combinations of known modes. In such cases the number of modes invoked

† Tables A and B have been deposited with the Royal Society. Copies may be purchased from the British Library Lending Division, Boston Spa, Yorkshire LS23 7BQ, I.K. (reference number SUP 10012).

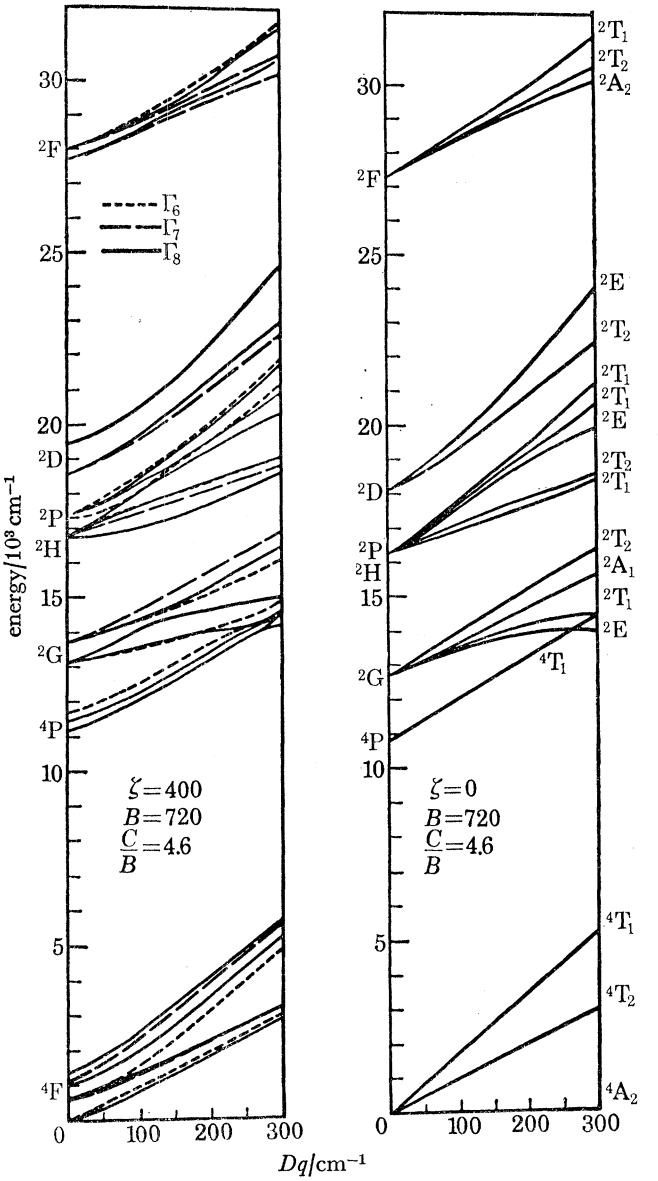

FIGURE 3. Calculated energy levels of Co^{2+} in a crystal field of T_d symmetry with and without spin-orbit coupling. (Reproduced by permission from *J. chem. Phys.* (1963), **39**, 116.)

within the transition is kept to a minimum. Tables A and B list the frequencies calculated by assuming particular identifications of the origins, with the further assumption that the excited state vibrational frequencies are equal to those of the ground state. The excellent agreement between theory and experiment in the large majority of cases is good evidence that for these spectra the assumption is a good one.

(*d*) *Description of the spectra*

(i) *Region I* (figures 4 and 5)

The highest energy band is moderately intense in both complexes. The spectrum in Cs_3CoBr_5 starts with the weak *z* polarized peak, 125 which is not observed in the chloro-complex. This is assigned to transition A. With this exception, the pattern of origins is similar in the two complexes.

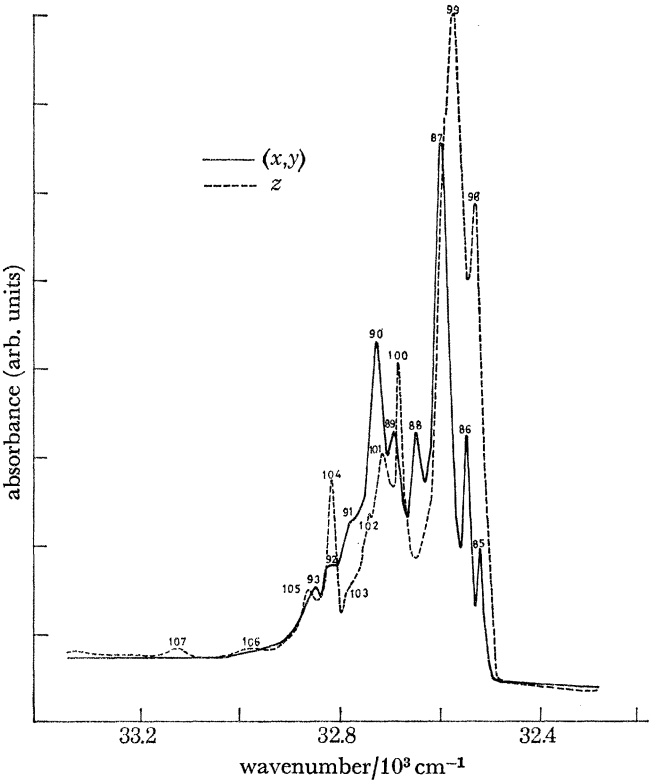

FIGURE 4. The spectrum of Cs_3CoCl_5 at 4.2 K, region I.

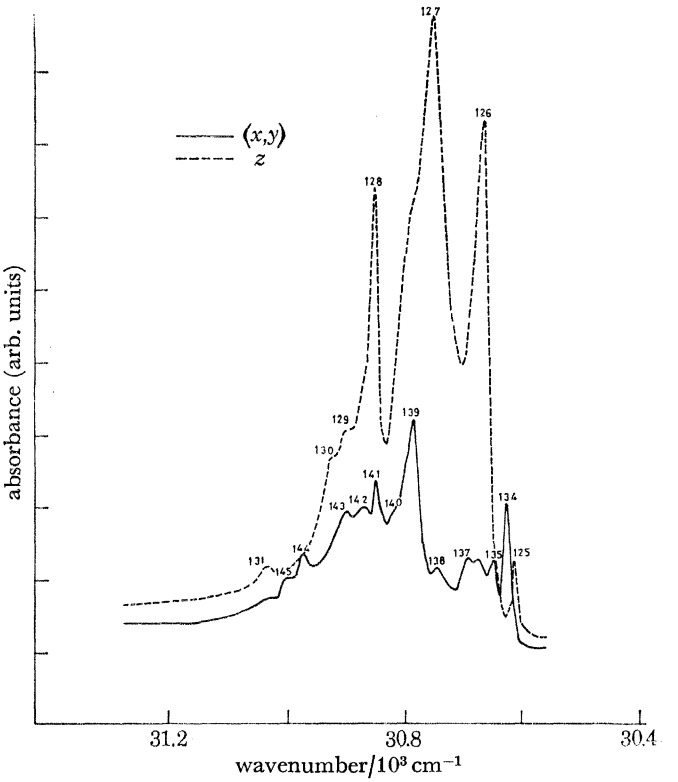

FIGURE 5. The spectrum of Cs_3CoBr_5 at 4.2 K, region I.

In Cs_3CoCl_5 the (x, y) spectrum consists of three origins, peaks 85, 86 and 87, assigned to transitions A, C and E respectively. Transitions B and D occur in z polarizations only (peaks 98 and 99). The vibrational structure associated with B, C and D is in frequencies corresponding to $\nu_1(a_{1g})$ as the frequency is the same as $2\nu_4(b_{2g})$ (see table 13). The separation of the origins of transitions B and C is 13 cm^{-1} while that of the origins of D and E is 25 cm^{-1} with the (x, y) polarized band at higher energy in both cases. These shifts are outside the limits of error of the measurements. The vibrational structure associated with B and C involves the same frequencies for both transitions and the polarization ratio is constant throughout. This suggests that these transitions may arise from the same electronic excitation. For D and E, on the other hand, the vibrational structures are quite different.

TABLE 13. SINGLE CRYSTAL RAMAN SPECTRUM OF Cs_3CoCl_5 AND Cs_3CoBr_5 (Gilson 1970)

symmetry species in factor group D_{4h}	Cs_3CoCl_5		Cs_3CoBr_5	
	frequency (cm^{-1})	label	frequency (cm^{-1})	label
a_{1g}	54	ν_{L1}	24	ν_{L1}
	121	$\nu_2(a_{1g})$	76	$\nu_2(a_{1g})$
	284	$\nu_1(a_{1g})$	174	$\nu_1(a_{1g})$
b_{1g}	95	$\nu_2(b_{1g})$	46	ν_{L2}
			59	$\nu_2(b_{1g})$
b_{2g}	47	ν_{L2}	52†	ν_{L3}
	142	$\nu_4(b_{2g})$	95	$\nu_4(b_{2g})$
	310	$\nu_3(b_{2g})$		
e_g	37	ν_{L3}	20	ν_{L4}
	72†	ν_{L4}	36	ν_{L5}
	126	$\nu_4(e_g)$	51	ν_{L6}
	309	$\nu_3(e_g)$	58	ν_{L7}
			85	$\nu_4(e_g)$

† Possibly a doublet.

In Cs_3CoBr_5, transitions A, C and D occur in z polarization and B, C and E in (x, y). Transition C is weak in (x, y), but corresponds well with C in z. There is an analogy between the separation (30 cm^{-1}) of D and E in Cs_3CoBr_5 and the separation of D and E in Cs_3CoCl_5, and in both crystals the transitions D and E have associated fine structure in $\nu_4(b_{2g})$ and $\nu_4(e_g)$ respectively.

(ii) *Region II* (figures 6 and 7)

In Cs_3CoBr_5 this region embraces two distinct band groups while in Cs_3CoCl_5 only one is seen. The lower energy region in Cs_3CoBr_5, II *b*, consists simply of a single transition (origin in 116*xy*, 105*z*) associated with progression in $\nu_1(a_{1g})$. Region II *a* probably contains three transitions: A (123*xy*, 113*z*) and B (124*xy*, 114*z*) are present in both polarizations while C (127*xy*) is only observed in (x, y). The dominant vibrational mode associated with all three transitions is $\nu_1(a_{1g})$. It is also possible that B is not a separate transition but $A + \nu_L$. Region II in Cs_3CoCl_5 is more complex. A very weak peak, 79, ascribed to transition A, is observed in z polarization only, about 500 cm^{-1} below the main peaks. Transition B (origin in 70*xy*, 80*z*) is predominantly (x, y) polarized while transitions D and E (origins in 86*z* and 93*z* respectively) are strongly z polarized. Peaks 73*xy* and 83*z* are ascribed to transition C. The most striking difference between the spectra of the bromo- and chloro-complexes in this region is the occurrence of transition E in Cs_3CoCl_5. It has no counterpart in Cs_3CoBr_5.

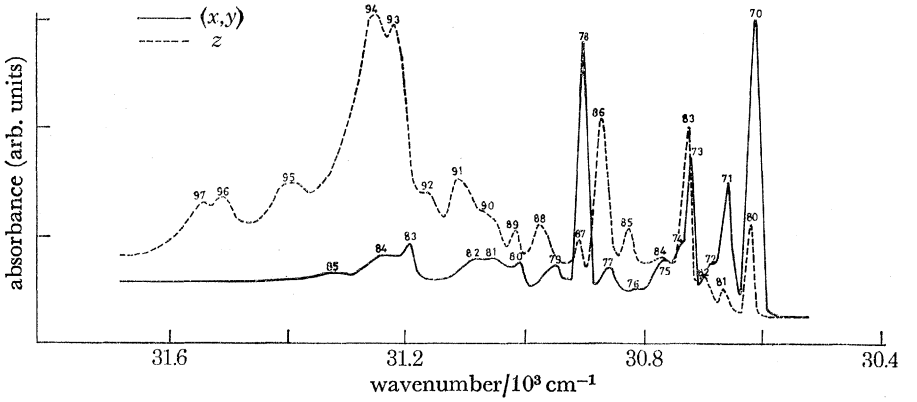

FIGURE 6. The spectrum of Cs_3CoCl_5 at 4.2 K, region II.

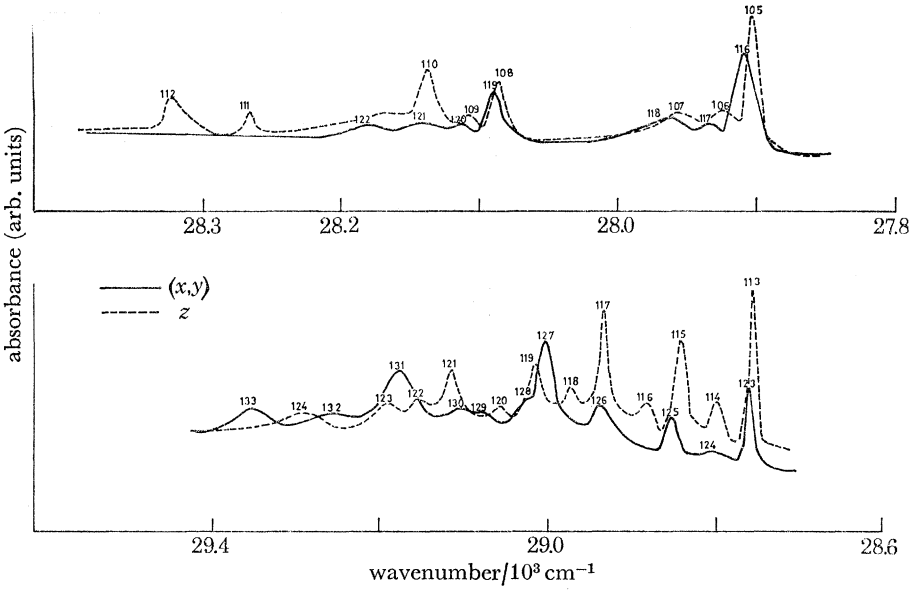

FIGURE 7. The spectrum of Cs_3CoBr_5 at 4.2 K, region II.

(iii) *Region III* (figures 8 and 9)

This band is well separated from its neighbours and the spectra of the two crystals correspond quite closely. Transition A (origin in $51xy$ in Cs_3CoCl_5, $98xy$ in Cs_3CoBr_5) is weak and observed in (x, y) polarization only; transition B (origin in $52xy$, $62z$ in Cs_3CoCl_5, $99xy$, $91z$ in Cs_3CoBr_5) is also weak, but it is present in both polarizations; transition C (origin in $63z$ in Cs_2CoCl_5, $92z$ in Cs_3CoBr_5) is slightly more intense and occurs in z polarization only; lastly, transition D (origin in $53xy$ in Cs_3CoCl_5, $100xy$ in Cs_3CoBr_5) is the most intense and is only observed in (x, y) polarization. In both complexes vibrational fine structure consists of a progression in $\nu_1(a_{1g})$ with other modes superimposed on it. It is interesting to note that the most intense component of the progression based on B in Cs_3CoCl_5 is $0'' \rightarrow 1'$ in both polarizations while, in Cs_3CoBr_5, $0'' \rightarrow 1'$ is the most intense in x, y polarization only. For all other transitions the maximum intensity is in $0'' \rightarrow 0'$. The temperature dependence of the origins A, B, C and D in both complexes is of interest. In the range 4 to 77 K, A and C increased in intensity as the temperature increased, D decreased, and B showed little change in z polarization but increased in (x, y). Dr M. Leask

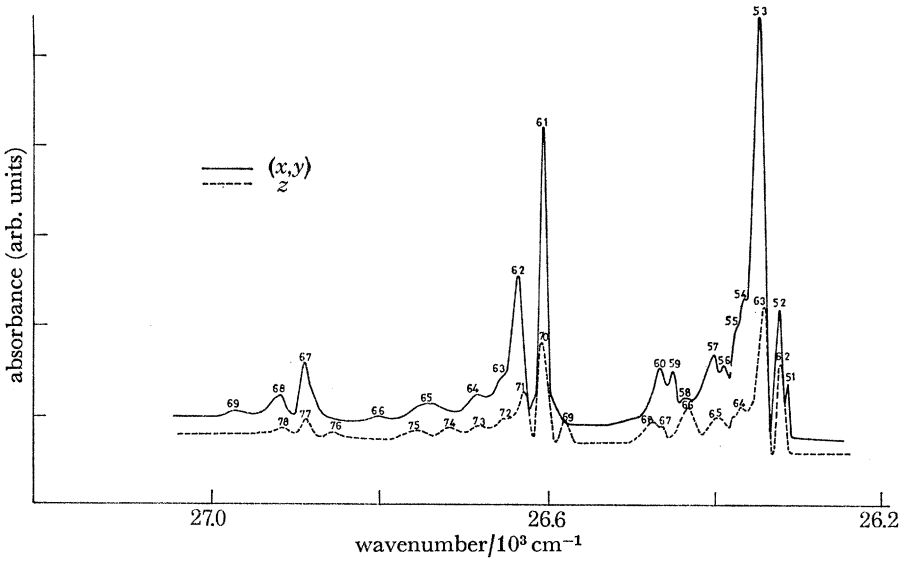

FIGURE 8. The spectrum of Cs_3CoCl_5 at 4.2 K, region III.

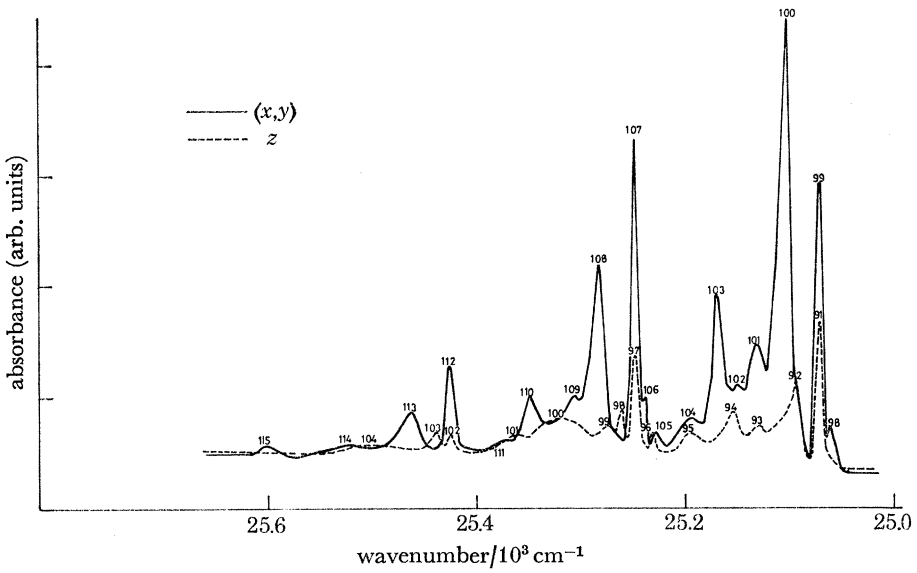

FIGURE 9. The spectrum of Cs_3CoBr_5 at 4.2 K, region III.

of the Clarendon Laboratory, Oxford, measured the spectrum of A and B in Cs_3CoBr_5 in the range of 1.3–4 K (Leask 1970, personal communication) and showed that A vanished at low temperatures but that B was still present. The higher resolution of his instrument also permitted a more accurate measurement of the separation of these two origins, giving a value of 8.4 cm^{-1}.

(iv) *Region IV* (figures 10 and 11)

In both crystals, three electronic transitions can be identified: transition A at low energy (origin in 44*xy*, 54*z* in Cs_3CoCl_5; 80*xy*, 74*z* in Cs_3CoBr_5) is very intense and strongly *z* polarized; transition B (47*xy*, 57*z* in Cs_3CoCl_5, 85*xy*, 80*z* in Cs_3CoBr_5) is rather weak; and transition C (48*xy*, 58*z* in Cs_3CoCl_5; 86*xy*, 81*z* in Cs_3CoBr_5) is moderately intense in both polarizations. The origins of transition B were located by comparison of the fine structure in the two crystals and

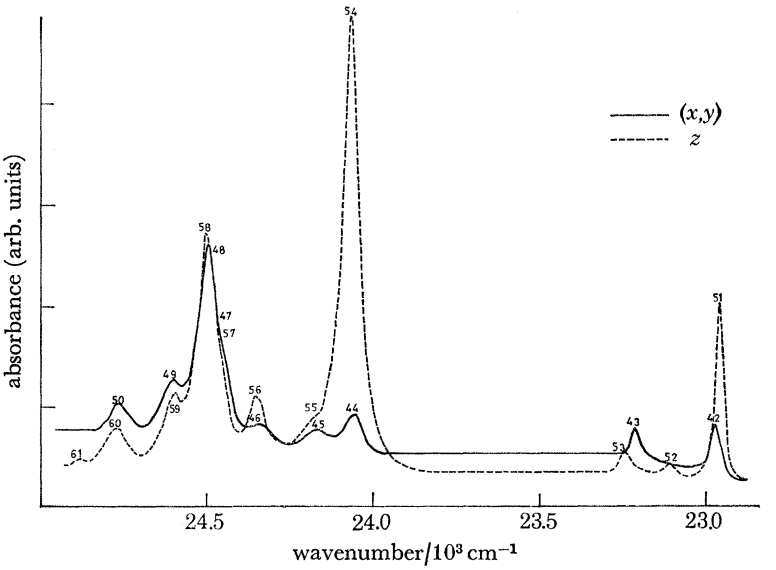

FIGURE 10. The spectrum of Cs_3CoCl_5 at 4.2 K, regions IV and V.

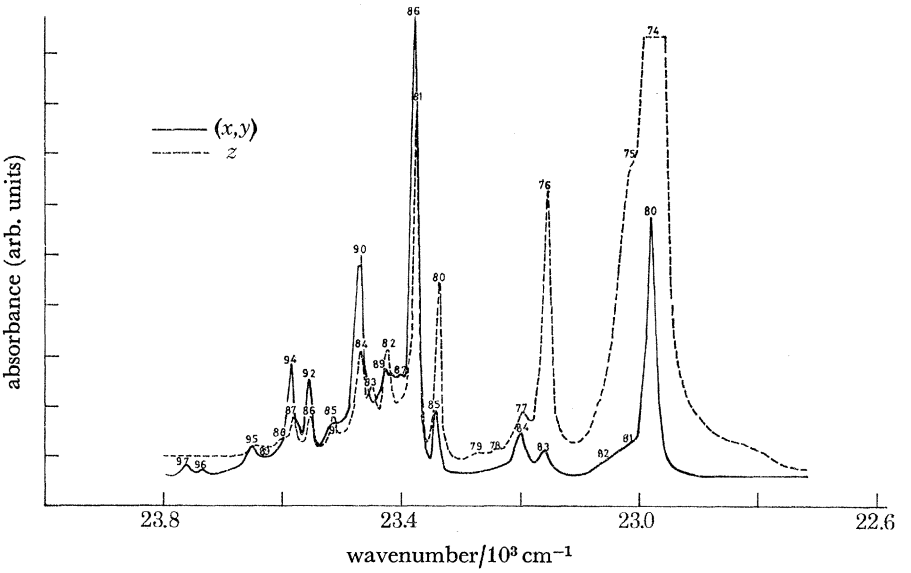

FIGURE 11. The spectrum of Cs_3CoBr_5 at 4.2 K, region IV.

by studying the temperature dependence of the band intensities. A well-defined progression in $\nu_1(a_{1g})$ is associated with transition A in Cs_3CoBr_5, with peak 80z corresponding to the $0'' \rightarrow 2'$ component. In (x, y) polarization, however, the intensity of the corresponding peak, 85, is too high for such an assignment. Both 85xy and 80z increased in intensity with increasing temperature and the analogous peaks in Cs_3CoCl_5, 47xy and 57z, behaved similarly. In the chloro-complex, however, the separation of 47xy and 57z from the origin of transition A does not correspond to a vibrational interval. This region therefore contains another transition, B, which in Cs_3CoBr_5 is accidentally degenerate with the $0'' \rightarrow 2'$ component of a progression in $\nu_1(a_{1g})$. This hypothesis was confirmed by a quantitative study of the temperature dependence of the oscillator strength, the results of which are shown in figure 12.

The spectrum of Cs_3CoCl_5 in this region is remarkable for its lack of vibrational structure. The bands remain smooth and broad at all temperatures and the fine structure involves a_{1g} modes only. In Cs_3CoBr_5, on the other hand, the bands are much sharper and, in addition to the dominant $\nu_1(a_{1g})$ mode, several peaks can be assigned to $\nu_4(b_{2g})$.

(v) *Region V* (figures 12 and 13)

In Cs_3CoCl_5 the spectrum in this region is very weak and all the bands are broad. Transition A (origin in $51z$) and transition B (origin in $42xy$) are oppositely polarized and separated by $13\,cm^{-1}$. $43xy$ is assigned tentatively to a third transition, C, because the separation of $43xy$ from $42xy$ does not correspond to a vibrational interval. The spectrum in Cs_3CoBr_5 is more intense, especially in z polarization, and there is more fine structure, but only two origins can be assigned. Transition A (origin in $70xy$, $63z$) is predominantly z polarized, while transition B (origin in $73xy$) is observed in (x, y) polarization only.

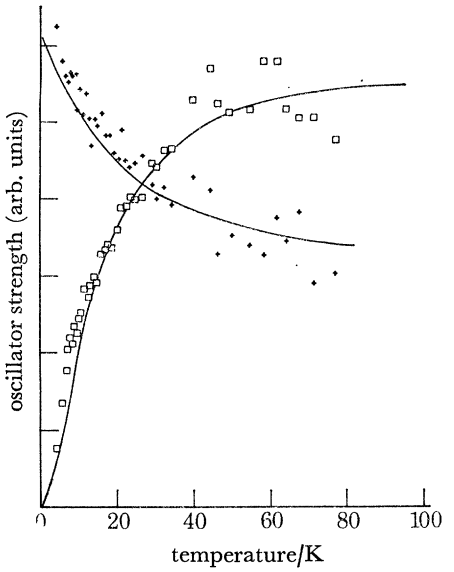

FIGURE 12. Temperature dependence of peaks $85xy$ (□) and $86xy$ (+) in the spectrum of Cs_3CoBr_5. ——, Theoretical curves for $\Delta E = 11\,cm^{-1}$.

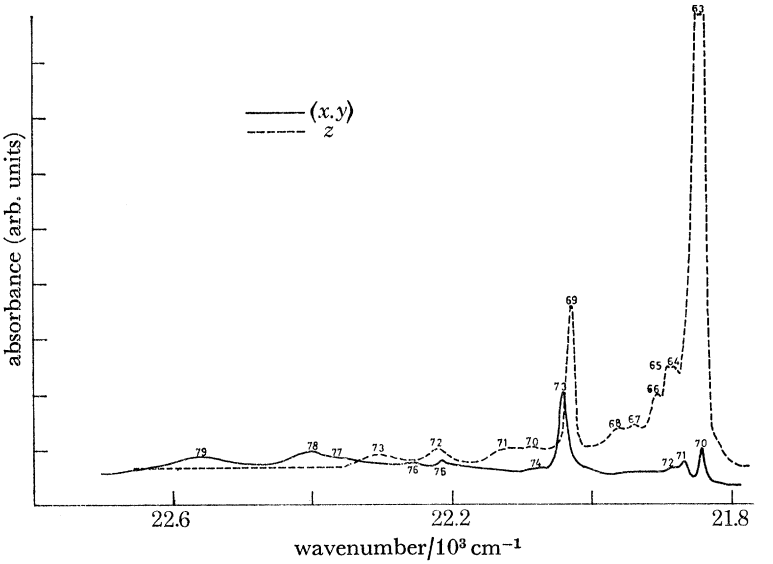

FIGURE 13. The spectrum of Cs_3CoBr_5 at 4.2 K, region V.

(vi) *Region VI* (figures 14, 15 and 16)

In Cs_3CoCl_5 the intense spectrum in this region may be further subdivided into a group of sharp (x, y) polarized peaks at low energy with broader, strongly z polarized peaks at higher energy. In Cs_3CoBr_5 these two groups are clearly separated and much vibrational fine structure can be seen. Region VI*b* in Cs_3CoBr_5 commences with a pair of bands of opposite polarization, separated by $10\,cm^{-1}$ (peaks $35xy$, $33z$ and $36xy$, $34z$), which are assigned to transitions A and B. In Cs_3CoCl_5 only one band occurs in (x, y) (peak $30xy$) but there are two weak bands separated by $9\,cm^{-1}$ in a polarization (peaks $35z$, $37z$). Because of its high intensity, peak $41z$ in Cs_3CoCl_5 is assigned as the origin of transition C and likewise, by analogy, peak $39z$ in Cs_3CoBr_5. Region VI*a* in Cs_3CoBr_5 commences with an intense (x, y) polarized transition, A (origin in $54xy$, $46z$), matched by a rather less intense peak, $34xy$, in Cs_3CoCl_5 (transition D). Peaks $47z$ in Cs_3CoBr_5 and $45z$ in Cs_3CoCl_5, which are both rather broad and extremely intense, are assigned to transitions B

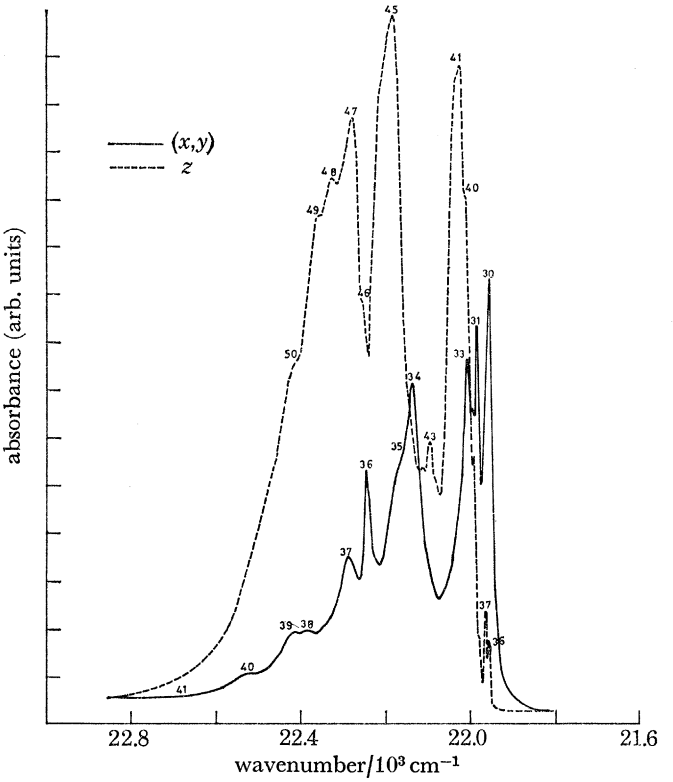

FIGURE 14. The spectrum of Cs_3CoCl_5 at 4.2 K, region VI.

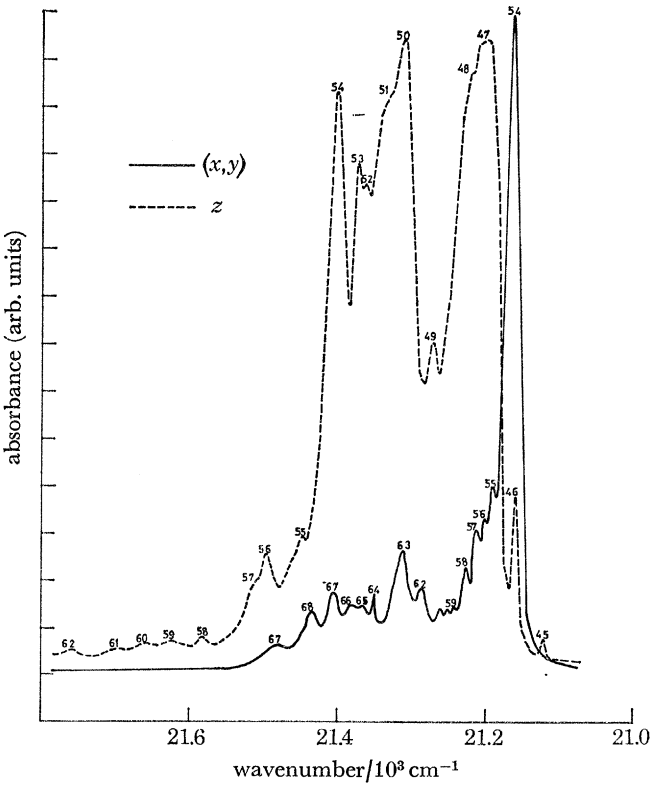

FIGURE 15. The spectrum of Cs_3CoBr_5 at 4.2 K, region VI*a*.

PHILOSOPHICAL TRANSACTIONS OF THE ROYAL SOCIETY A MATHEMATICAL, PHYSICAL & ENGINEERING SCIENCES

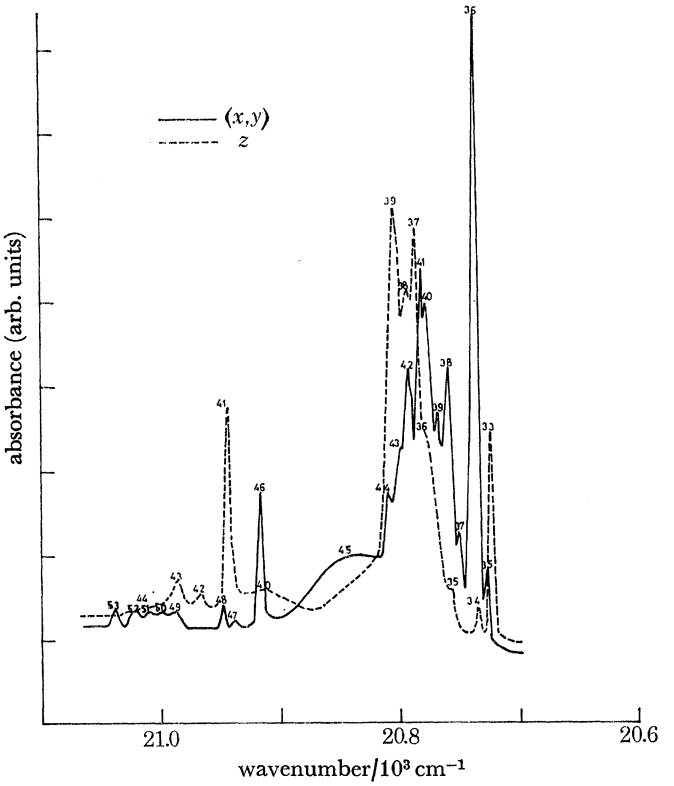

FIGURE 16. The spectrum of Cs_3CoBr_5 at 4.2 K, region VI*b*.

and E respectively. Comparison of the band structure of region VI*a* in Cs_3CoBr_5 with that of region VI in Cs_3CoCl_5 suggests that the *z* polarized peaks 50*z* in Cs_3CoBr_5 and 47*z* in Cs_3CoCl_5, may also be origins and, accordingly, they are assigned to transitions C and F respectively.

(vii) *Region VII* (figures 17 and 18)

In this region the spectra of both Cs_3CoCl_5 and Cs_3CoBr_5 are very broad and intense, and little vibrational structure can be assigned. There are three main broad regions of absorption in (x, y)

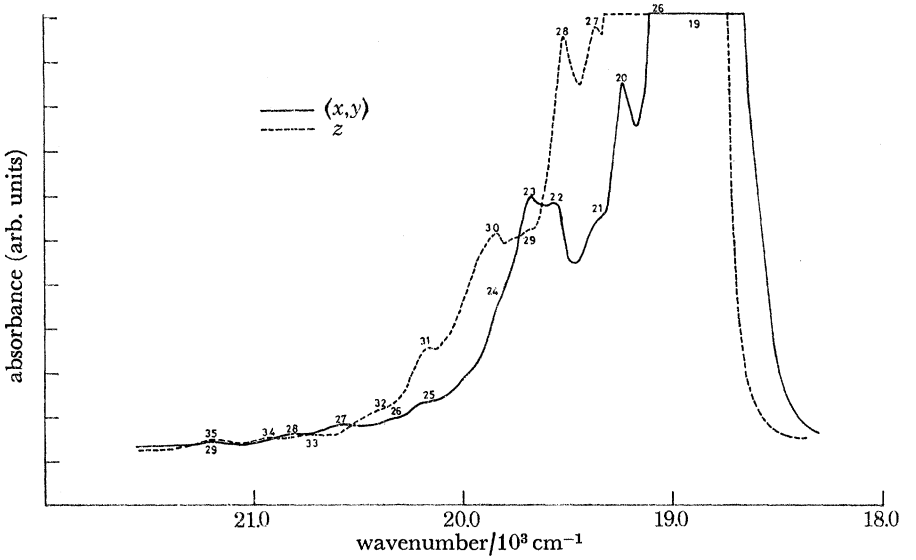

FIGURE 17. The spectrum of Cs_3CoCl_5 at 4.2 K, region VII.

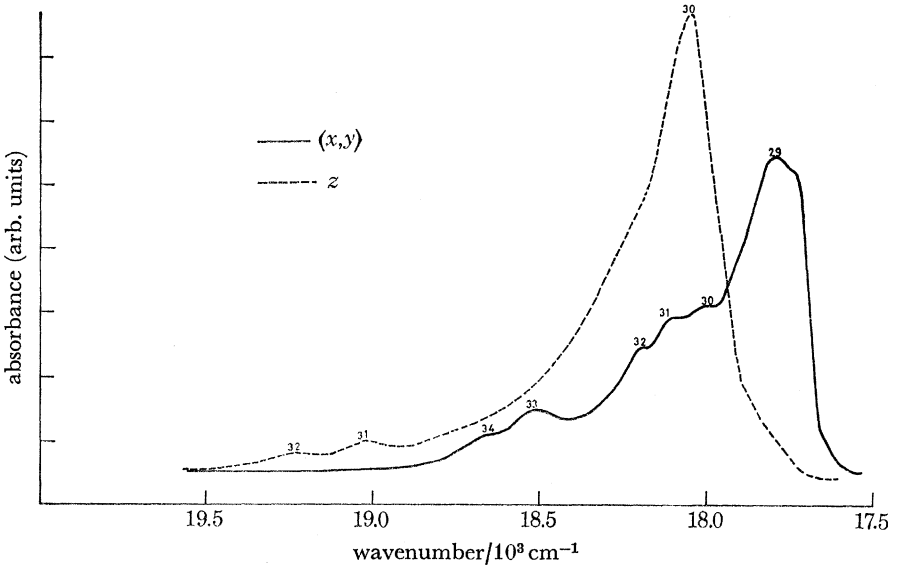

FIGURE 18. The spectrum of Cs_3CoBr_5 at 4.2 K, region VII.

polarization. Peaks 19*xy* in Cs_3CoCl_5 and 29*xy* in Cs_3CoBr_5 are assigned to transition A, peaks 20*xy* in Cs_3CoCl_5 in 31*xy* in Cs_3CoBr_5 to transition C, and peaks 22*xy* in Cs_3CoCl_5 and 33*xy* in Cs_3CoBr_5 to transition D. The most intense peaks in *z* polarization (26*z* in Cs_3CoCl_5, 30*z* in Cs_3CoBr_5) are assigned to transition B. The magnetic circular dichroism (m.c.d.) spectrum of Cs_3CoCl_5 in this region (Collingwood, Day & Denning 1970, unpublished observations) shows that peaks 19, 22, 23, 28 and 29*xy* have the opposite sign of m.c.d. from peaks 20, 21, 26 and 27*xy*.

(viii) *Region VIII* (figures 19 and 20)

This region consists of a long and complex series of bands with sharp peaks at low energy and broad, strongly *z* polarized bands at higher energy. The sharp peak 8*xy* in Cs_3CoBr_5 has no counterpart in *z* polarization or in Cs_3CoCl_5 and is assigned to transition A. Transition B (origins

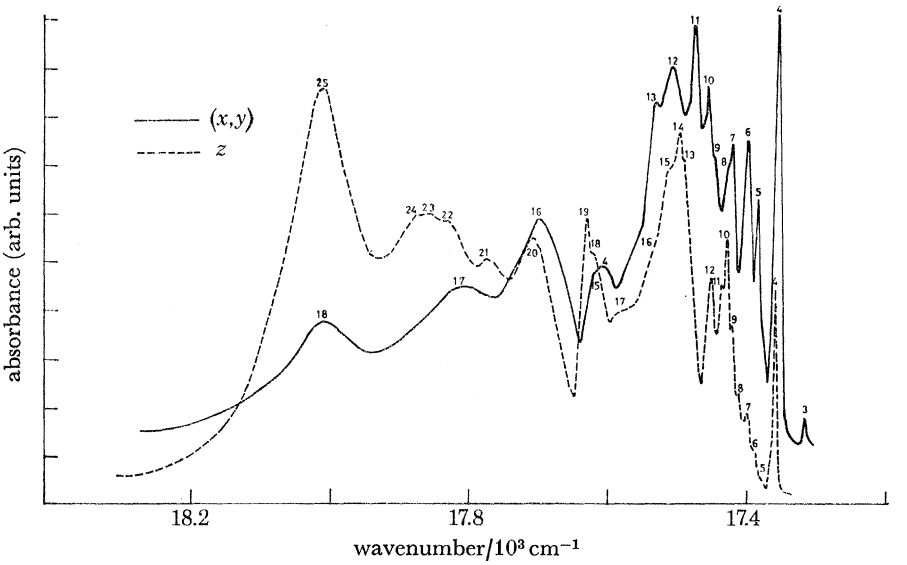

FIGURE 19. The spectrum of Cs_3CoCl_5 at 4.2 K, region VIII.

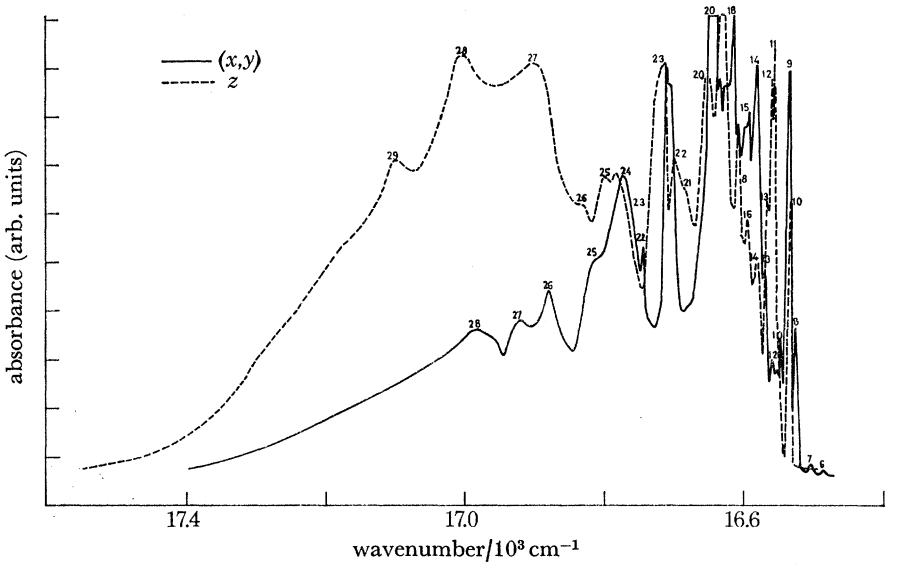

FIGURE 20. The spectrum of Cs_3CoBr_5 at 4.2 K, region VIII.

in $9xy$, $10z$ in Cs_3CoBr_5) appears to be analogous to transition A in $CsCoCl_5$ (origins in $4xy$, $4z$) and several peaks can be assigned to vibrations superimposed on these origins. In particular, frequencies corresponding to $\nu_1(a_{1g})$, $\nu_2(b_{1g})$ and $\nu_4(b_{2g})$ (see table 13) occur in both crystals. The most striking difference between the spectrum of Cs_3CoCl_5 and that of Cs_3CoBr_5 in this region is the presence in the latter of a strongly z polarized peak ($12xy$, $11z$), which is assigned to transition C. Peaks $16xy$ in Cs_3CoCl_5 and $24xy$ in Cs_3CoBr_5 are assigned to transitions B and D

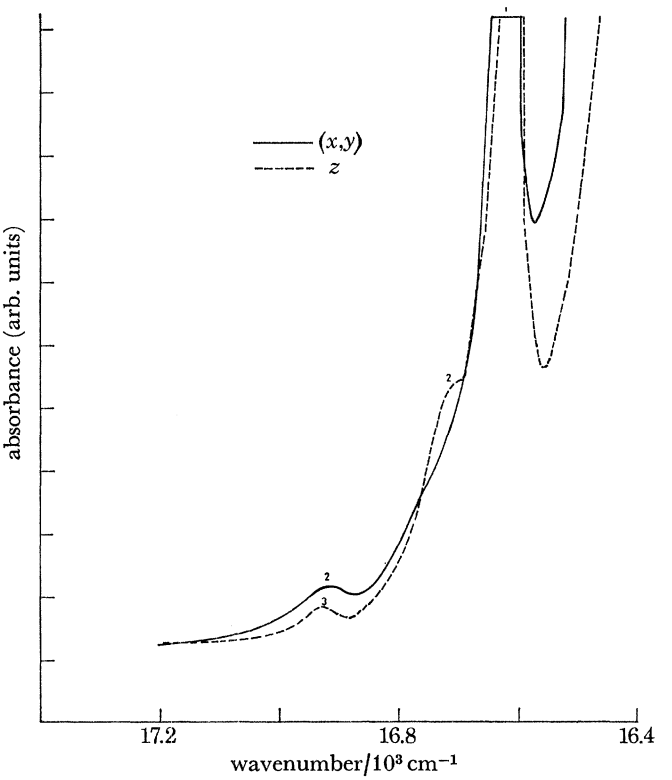

FIGURE 21. The spectrum of Cs_3CoCl_5 at 4.2 K, region IX.

respectively, and peaks $20z$ in Cs_3CoCl_5 and $24z$ in Cs_3CoBr_5 to transitions C and E respectively. The separation of these origins is $8\,cm^{-1}$ in Cs_3CoCl_5 and $13\,cm^{-1}$ in Cs_3CoCl_5. A vibrational interval corresponding to the expected value of ν_3 (see table 13) appears to be associated with both D and E, but appears as a very intense band in z polarization only.

(ix) *Region IX* (figures 21 and 22)

A few bands are resolved on the edge of the $^4A_2 \rightarrow {}^4T_1(P)$ band in both crystals. In Cs_3CoCl_5, the two intense peaks ($1xy$, $1z$) are assigned to transition A, and the weak peaks $2xy$ and $3z$ to $A + \nu_3$. The peaks above $15\,800\,cm^{-1}$ in Cs_3CoBr_5 have a similar form to the peaks in Cs_3CoCl_5 and an analogous assignment is proposed. The remaining peaks in Cs_3CoBr_5 are assigned to another transition, but the (x, y) polarized spectrum is too intense for complete measurement.

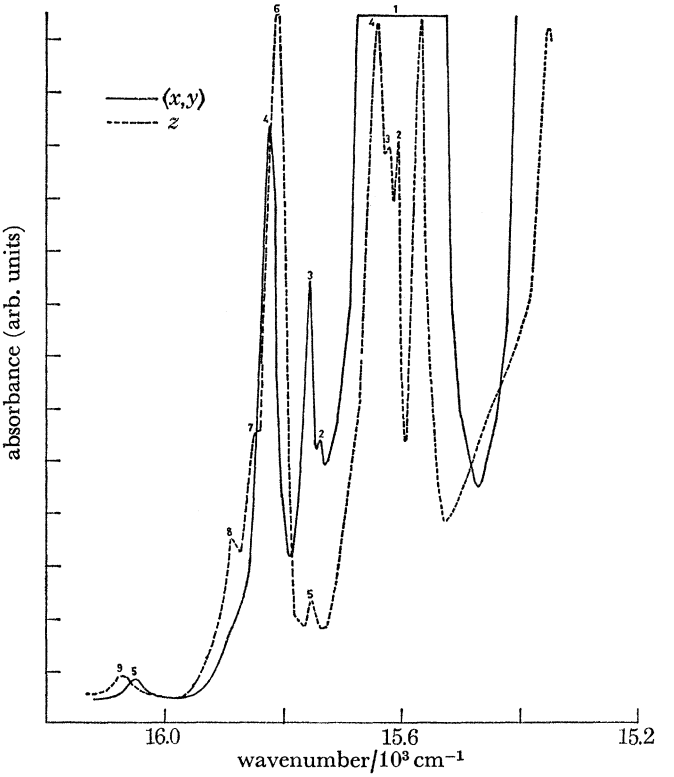

FIGURE 22. The spectrum of Cs_3CoBr_5 at 4.2 K, region IX.

(*e*) *Assignment of the spectra*

(i) *Region I* (figures 4 and 5)

This region is assigned to $^4A_2 \rightarrow {}^2T_1(F)$ by comparison with the conventional ligand-field calculation (figure 3). Under the influence of spin-orbit coupling, $^2T_1(T_d)$ gives $\Gamma_6(T_d^*)$ and $\Gamma_8(T_d^*)$. The degeneracy of the latter being further lifted by the tetragonal distortion to give $\Gamma_6(D_{2d}^*)$ and $\Gamma_7(D_{2d}^*)$. $\Gamma_6(T_d^*)$ correlates with $\Gamma_6(D_{2d}^*)$. Since the ground state $^4A_2(T_d)$ is split into Γ_6 and Γ_7 in D_{2d}^* the possible electronic transitions are $\Gamma_6 \rightarrow \Gamma_7$ and $\Gamma_6 \rightarrow \Gamma_6$ from the ground level, and $\Gamma_7 \rightarrow \Gamma_6$ and $\Gamma_7 \rightarrow \Gamma_7$ from the upper zero-field component of the ground state, although the last two transitions are expected to be weak at 4.2 K, because of the small thermal population of $\Gamma_7(^4A_2)$. The electric dipole selection rules in D_{2d}^* permit all transitions in (x, y) polarization, but only $\Gamma_6 \rightarrow \Gamma_7$ and $\Gamma_7 \rightarrow \Gamma_6$ in z.

Since the separation of transition A ($125z$) from transition B ($134xy$) in Cs_3CoBr_5 is close to the known zero-field splitting of the ground state (19), these bands may be assigned to transitions from $\Gamma_7(^4A_2)$ and $\Gamma_6(^4A_2)$ respectively, to the same excited state. Since transition A is observed in z polarization, the excited state must be $\Gamma_6(^2T_1)$. The corresponding (x, y) polarized transition must be inherently weak since it is not observed. Transition A ($85xy$) in Cs_3CoCl_5 is only present

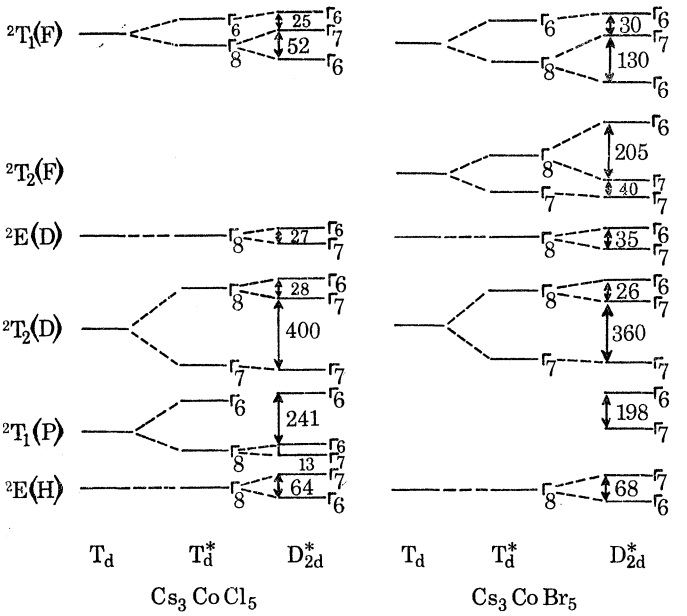

FIGURE 23. Excited state splittings in Cs_3CoCl_5 and Cs_3CoBr_5 deduced from the experimental spectra. Only those levels which could be placed from the spectra are shown. The diagram is not to scale, but the energy units are cm^{-1}.

in (x, y) polarization and may be assigned, by analogy with transition B in Cs_3CoBr_5 to $\Gamma_6(^4A_2) \rightarrow \Gamma_6(^2T_1)$. The highest energy transitions E ($87xy$ in Cs_3CoCl_5; $139xy$ in Cs_3CoBr_5), observed in (x, y) only are assigned to $\Gamma_6(^4A_2) \rightarrow \Gamma_6(^2T_1)$. One more transition, $\Gamma_6(^4A_2) \rightarrow \Gamma_7(^2T_1)$, is expected in z polarization. Most likely candidates for assignment to this transition are the origins D ($99z$ in Cs_3CoCl_5; $127z$ in Cs_3CoBr_5), which cannot be vibronic in origin because vibrational frequencies are lower in Cs_3CoBr_5 than in Cs_3CoCl_5 while the separation of D from the lower energy transitions is larger in the bromo-complex. The assignment of the weaker transitions in z polarization, B ($98z$) in Cs_3CoCl_5 and C ($126z$) in Cs_3CoBr_5, remains obscure. With the assignments we have proposed, the energy level schemes for $^2T_1(F)$ in Cs_3CoCl_5 and Cs_3CoBr_5 are as shown in figure 23.

Our conventional ligand-field calculation indicates that the dominant contributions to $^2T_1(F)$ are the doubly excited $e^2(^1E)\, t_2^5$ and singly excited $e^3t_2^4(^3T_1)$ configurations. Calculations of the spin-orbit splitting of $^2T_1$ in T_d^* (Ferguson 1963) show that the state splits with $\Gamma_6(T_d^*)$ at higher energy. Therefore the major interval must be the low symmetry splitting if $\Gamma_8(T_d^*)$.

Ferguson (1963) recorded the spectrum of $CoCl_4^{2-}$ in this region, but merely reports the presence of a band at 32 500 cm^{-1} without further analysis.

(ii) *Region II* (figures 6 and 7)

From the ligand-field calculation region II b in Cs_3CoBr_5 may be assigned to $^4A_2 \rightarrow {}^2A_2(F)$ and it is probable that the weak transition A (79*z*) in Cs_3CoCl_5 may also belong to $^2A_2(F)$. The main part of region II in Cs_3CoCl_5, and region II a in Cs_3CoBr_4 are assigned to $^4A_2 \rightarrow {}^2T_2(F)$. In D_{2d}^*, $^2A_2(T_d)$ transforms as Γ_7, transitions to which from $\Gamma_6(^4A_2)$ are allowed in both polarizations, as observed in II a. Spin-orbit coupling splits $^2T_2(T_d)$ into $\Gamma_7(T_d^*)$ and $\Gamma_8(T_d^*)$ and the degeneracy of the latter is lifted in D_{2d}^* to give Γ_6 and Γ_7 levels. In Cs_3CoBr_5, transition C (127*xy*) is present in (x, y) polarization only and may reasonably be assigned to $\Gamma_6(^4A_2) \rightarrow \Gamma_6(^2T_2)$. Transitions A (123*xy*, 113*z*) and B (124*xy*, 114*z*) occur in both polarizations and may be assigned to $\Gamma_6(^4A_2) \rightarrow \Gamma_7(^2T_2)$. Spin-orbit coupling calculations (Ferguson 1963 and present paper) predict that $\Gamma_8(T_d^*)$ will lie higher in energy than $\Gamma_7(T_d^*)$ so the energy level scheme for this region of Cs_3CoBr_5 is as shown in figure 23.

In Cs_3CoCl_5, the pattern of origins is more complex and there is no obvious correlation with the spectrum of Cs_3CoBr_5. The separations between the origins in Cs_3CoCl_5 are larger than those in Cs_3CoBr_5. If transition E (93*z*) is purely electronic then it must be assigned to $\Gamma_6(^4A_2) \rightarrow \Gamma_7(^2T_2)$ on the basis of its intensity and polarization. A similar assignment could be proposed for transitions B (70*xy*, 80*z*), C (73*xy*, 83*z*) and D (86*z*), but this is clearly impossible since only two such transitions are predicted for $^2T_2(F)$. Transition E is rather broad and might be vibronic in origin but there is no obvious connexion with an observed transition in (x, y) polarization. The apparent origins in this region of the spectrum of Cs_3CoCl_5 cannot be satisfactorily explained as transitions to the components of $^2T_2(F)$ gaining intensity by spin-orbit coupling.

(iii) *Region III* (figures 8 and 9)

In both crystals the band group in this region has a comparatively straightforward structure. The distribution of origins suggests an assignment to $^2E(D)$. Spin-orbit coupling does not lift the degeneracy of ^2E which transforms as Γ_8 in T_d^*, but the degeneracy is lifted in D_{2d}^* to give Γ_6 and Γ_7. In both crystals, the observed pattern of bands indicates that the Γ_7 component lies below Γ_6. Leask's 1.3 K spectrum of the lowest energy transition, A (51*xy* in Cs_3CoCl_5; 98*xy* in Cs_3CoBr_5), only observed in (x, y) polarization, demonstrates that it originates in $\Gamma_7(^4A_2)$. Transition B (52*xy*, 62*z* in Cs_3CoCl_5; 99*xy*, 91*z* in Cs_3CoBr_5), separated from A by the known zero-field splitting (Belgers *et al.* 1964) may be assigned to $\Gamma_6(^4A_2) \rightarrow \Gamma_7(^2E)$. The separation of C (63*z* in Cs_3CoCl_5; 92*z* in Cs_3CoBr_5) and D (53*xy* in Cs_3CoCl_5); 100*xy* in Cs_3CoBr) also corresponds to the zero-field splitting, and these transitions may be assigned to $\Gamma_7(^4A_2) \rightarrow \Gamma_7(^2E)$ and $\Gamma_6(^4A_2) \rightarrow \Gamma_6(^2E)$ respectively. The temperature dependence of D (see page 308) is consistent with this assignment. The assignment of the Γ_6 and Γ_7 components of ^2E proposed here has been confirmed for Cs_3CoCl_5 by measurement of the m.c.d. spectrum (Collingwood *et al.* 1970, unpublished).

This region of the spectrum was not examined by Ferguson (1963) and although Pelletier-Allard (1965*a*) reports many of the lines in the spectrum of Cs_3CoCl_5 between 26 000 and 27 000 cm^{-1}, she did not make any detailed assignments.

(iv) *Region IV* (figures 10 and 11)

From the conventional ligand-field calculation, and the observed distribution of origins region IV is assigned to $^4A_2 \rightarrow {}^2T_2(D)$. The splitting of $^2T_2$ under the influence of spin-orbit coupling

and low symmetry has already been described in connexion with $^2T_2(F)$. Three transitions from $\Gamma_6(^4A_2)$ are expected in (x, y) polarization and two in z polarization. The very intense, z polarized transition A ($44xy$, $54z$ in Cs_3CoCl_5; $80xy$, $74z$ in Cs_3CoBr_5) is assigned to $\Gamma_6(^4A_2) \rightarrow \Gamma_7(^2T_2)$. Transitions B and C in Cs_3CoCl_5 display the same qualitative behaviour and it is reasonable to assume assignments analogous to B and C in Cs_3CoBr_5. The transition $\Gamma_6(^4A_2) \rightarrow \Gamma_6(^2T_2)$ is not observed in either complex. On the basis of these assignments, we propose an energy level scheme for $^2T_2(D)$, in which one Γ_7 component lies several hundred cm^{-1} below the other, which is separated only by a small interval ($28\,cm^{-1}$ in Cs_3CoCl_5 and $26\,cm^{-1}$ in Cs_3CoBr_5) from Γ_6.

Ferguson (1963) recognized that in $CoCl_4^{2-}$ this group of bands belongs to ^2D, but having failed to assign the band at $26\,000\,cm^{-1}$ to $^2E(D)$, he attempted to ascribe region IV to this transition.

(v) *Region V* (figures 10 and 13)

The bands in region V are assigned to $^4A_2 \rightarrow {}^2T_1(P)$. Since $^2T_1(T_d)$ splits in D_{2d}^* into two Γ_6 levels and one Γ_7 level, the spectrum should consist of two transitions in (x, y) polarization only and one in both (x, y) and z from $\Gamma_6(^4A_2)$. Transitions A ($51z$ in Cs_3CoCl_5; $70xy$, $63z$ in Cs_3CoBr_5) can be assigned to $\Gamma_6(^4A_2) \rightarrow \Gamma_7(^2T_1)$, and transition B in Cs_3CoBr_5 ($73xy$) may be assigned to $\Gamma_6(^4A_2) \rightarrow \Gamma_6(^2T_1)$ since it is absent in z polarization. By analogy, transition C ($43xy$) in Cs_3CoCl_5 may also be assigned to $\Gamma_6(^4A_2) \rightarrow \Gamma_6(^2T_1)$. Transition B ($42xy$) in Cs_3CoCl_5 is separated from transition A by $13\,cm^{-1}$, which is well outside the experimental error. We therefore propose that transition B arises from $\Gamma_6(^4A_2) \rightarrow \Gamma_6(^2T_1)$.

Ferguson (1963) observed a weak band in this region and assigned it to transitions to ^2D, but no full assignment of the bands was given.

(vi) *Region VI* (figures 14, 15 and 16)

In Cs_3CoCl_5, region VI contains transitions to $^2T_1(H)$ and $^2E(H)$, while in Cs_3CoBr_5, $^2E(H)$ (VI b) is well-separated from $^2T_1(H)$ (VI a). Since the two transitions are separated in Cs_3CoBr_5, assignment should be more straightforward and will be discussed before that of Cs_3CoCl_5. Transition A in region VI a ($54xy$, $46z$) is strongly (x, y) polarized and may be assigned to $\Gamma_6(^4A_2) \rightarrow \Gamma_6(^2T_1)$. The assignments of B ($56xy$, $47z$) and C ($63xy$, $50z$) present a problem since both transitions are very intense in z polarization but only one z-allowed $\Gamma_6(^4A_2) \rightarrow \Gamma_7(^2T_1)$ is expected for $^2T_1$. The spin-orbit coupling calculations of § 5 predict that $\Gamma_8(^2T_1)$ lies at lower energy than $\Gamma_6(^2T_1)$ though the separation of the two components is expected to be small. The effect of low symmetry may be important. If transition C is assigned to $\Gamma_6(^4A_2) \rightarrow \Gamma_7(^2T_1)$ then the origin of B is obscure.

The separation and relative intensities of transitions A ($35xy$, $33z$) and B ($36xy$, $34z$) in region VI b of Cs_3CoBr_5 suggest that A may be assigned to a transition from $\Gamma_7(^4A_2)$ and B to a transition from $\Gamma_6(^4A_2)$, to the same excited level. Since A is moderately intense in z polarization while B is extremely weak, we propose that A is $\Gamma_7(^4A_2) \rightarrow \Gamma_6(^2E)$ and B is $\Gamma_6(^4A_2) \rightarrow \Gamma_6(^2E)$. Transition C may be assigned to $\Gamma_6(^4A_2) \rightarrow \Gamma_7(^2E)$ since it is allowed in z polarization. Thus the separation of the two low symmetry components of $\Gamma_8(^2E)$ is $68\,cm^{-1}$ wtih $\Gamma_6(^2E)$ at lower energy.

By using the pattern of bands in the two separated regions VI a and VI b of Cs_3CoBr_5 as a guide, region VI in Cs_3CoCl_5 can be subdivided into a set of peaks at higher energy commencing with $34xy$ analogous to VI a, and the sharper peaks at low energy, analogous to VI b. Transition A ($36z$), which is very weak appears $9\,cm^{-1}$ below transition B ($30xy$, $37z$) which is weak in z but

PHILOSOPHICAL TRANSACTIONS OF THE ROYAL SOCIETY A MATHEMATICAL, PHYSICAL & ENGINEERING SCIENCES

strong in (x, y). This energy difference is close to the ground state zero-field splitting, so if B is assigned to the z-forbidden transition $\Gamma_6(^4A_2) \rightarrow \Gamma_6(^2E)$ then A may be assigned to $\Gamma_7(^4A_2) \rightarrow \Gamma_6(^2E)$. Transition C ($41z$) is then $\Gamma_6(^4A_2) \rightarrow \Gamma_7(^2E)$. The excited state zero-field splitting of this band is then almost the same as that which we deduced above for $^2E(H)$ in Cs_3CoBr_5. The sharpness of the peaks and lack of vibrational progressions in this region, in both Cs_3CoCl_5 and Cs_3CoBr_5, is consistent with the strong-field composition of $^2E(H)$, which is almost completely derived from the two singly excited configurations, $e^3t_2^4(^1E)$ and $e^3t_2^4(^1A_1)$.

Transition D ($34xy$) in Cs_3CoCl_5 is analogous to transition A in Cs_3CoBr_5 (VI a) and may be assigned to $\Gamma_6(^4A_2) \rightarrow \Gamma_6(^2T_1(H))$. As in Cs_3CoBr_5 (VI a), it is not possible to give an unambiguous assignment of the intensely z polarized transitions E ($45z$) and F ($47z$).

In his spectrum of $CoCl_4^{2-}$ Ferguson (1963) assigned the bands between 21 800 and 22 600 cm^{-1} to transitions to ^2D, but he was unable to explain the observed band polarizations.

(vii) *Region VII* (figures 17 and 18)

From the conventional ligand-field calculation of § 6 the intense bands in region VII are assigned to $^2T_1(H)$ and $^2T_2(H)$, which remain close together for a wide range of parameter values. Extensive second-order interactions will therefore occur between the spin-orbit, and low-symmetry components and the resulting spectrum is expected to be complicated. Hence no meaningful analysis of the small number of very broad bands can be attempted.

(viii) *Region VIII* (figures 4 and 20)

Region VIII probably contains transitions to $^2T_2(G)$. The separation (9 cm^{-1}) of transitions A ($8xy$) and B ($9xy$, $10z$) in Cs_3CoBr_5 and the lower intensity of the former peak suggests that these transitions originate in the zero-field components $\Gamma_7(^4A_2)$ and $\Gamma_6(^4A_2)$ respectively. Since A is present in (x, y) polarization only while B is observed in both polarizations, A is assigned to $\Gamma_7(^4A_2) \rightarrow \Gamma_7(^2T_2)$ and B to $\Gamma_6(^4A_2) \rightarrow \Gamma_7(^2T_2)$. Transition A ($4xy$, $4z$) in Cs_3CoCl_5 seems to be analogous to B in Cs_3CoBr_5 and is similarly assigned. The strongly z-polarized peak $11z$ (transition C) in Cs_3CoBr_5 is assigned to a transition $\Gamma_6(^4A_2) \rightarrow \Gamma_7(^2T_2)$ on the basis of its intensity and polarization. It is possible that peak $10z$ in Cs_3CoCl_5 in the analogue of transition C in Cs_3CoBr_5.

The contrast between the sharp bands at the low energy end of region VIII and the broad bands at higher energy is quite striking and there is a marked similarity between the features in the two complexes. The energy differences of 8 cm^{-1} between B ($16xy$) and C ($20z$) in Cs_3CoCl_5 and of 13 cm^{-1} between D ($24xy$) and E ($24z$) in Cs_3CoBr_5 are close to the known zero-field splittings of the ground states of the respective crystals. However, it would be surprising if either of the lower energy members of these pairs of transitions arose from the upper zero-field component $\Gamma_7(^4A_2)$ since the peaks remain intense at 4.2 K. On the basis of their polarizations we therefore assign both pairs to $\Gamma_6(^4A_2) \rightarrow \Gamma_7(^2T_2(G))$.

If this is so, the expected z forbidden transition $\Gamma_6(^4A_2) \rightarrow \Gamma_6(^2T_2)$ remains unaccounted for. It may be one of the numerous sharp (x, y) polarized bands or, alternatively, the predicted polarization ratio of the transition may have been modified by some other interaction.

PHILOSOPHICAL TRANSACTIONS OF THE ROYAL SOCIETY A MATHEMATICAL, PHYSICAL & ENGINEERING SCIENCES

(ix) *Region IX* (figures 21 and 22)

The bands on the high energy side of the spin-allowed $^4A_2(F) \rightarrow {}^4T_1(P)$ transition may belong to other states arising from ^2G. From the ligand-field calculation $^2A_1(G)$ is predicted to lie above $^4T_1(P)$ and, in D_{2d}^*, this state transforms as Γ_6. It is possible that the intense (x, y) polarized peak $1xy$ (transition A) in Cs_3CoBr_5 may be assigned to the transition $\Gamma_6(^4A_2) \rightarrow \Gamma_6(^2A_1)$. No clear assignment of the higher energy transition B $(4xy, 6z)$ in Cs_3CoBr_5 and A $(1xy, 1z)$ in Cs_3CoCl_5 can be given.

(*f*) *General discussion of the spectra*

Although a complete assignment of the entire set of transitions in the two crystals has not been achieved, a good correlation has been obtained between separate regions of the spectra and both the number and relative disposition of the predicted crystal field states. The measurement of the spectrum of Cs_3CoBr_5, in addition to that of Cs_3CoCl_5, has proved an invaluable aid to assignment. The over-all similarity between the two spectra indicated by figure 2 is maintained within the detailed spectrum of each region, though the ratio of vibronic intervals to spin-orbit and low symmetry splittings varied markedly. The smaller vibronic intervals in the bromide made its spectrum somewhat easier to interpret than that of the chloride, but for both crystals the availability of comprehensive Raman data made it possible to assign unambiguously the components arising from spin-orbit or low symmetry splittings of the cubic field states in some of the regions, while for others, differences between the observed and expected pattern of origins have prevented a full assignment. The energy-level schemes which we have proposed for each region are collected in figure 23 and the assignments are tabulated in tables 14 and 15. In this section we collect some general observations on the assignments.

For transitions to ^2F, the low symmetry splitting of $\Gamma_8(T_d^*)$ is of a similar magnitude to the spin-orbit splitting of the cubic field state and is greater for the bromo-complex than for the chloro-complex. Both splittings are about $50\ cm^{-1}$ in Cs_3CoCl_5 and $100\ cm^{-1}$ in Cs_3CoBr_5. For $^2E(D)$, the low symmetry splitting is $27\ cm^{-1}$ in Cs_2CoCl_5, slightly smaller than in Cs_3CoBr_5 $(35\ cm^{-1})$. Splitting of a similar order is observed for $^2T_2(D)$, but for this state there is no significant difference between the values observed in two complexes. The large spin-orbit splitting of $^2T_2(D)$ $(400\ cm^{-1})$ makes the assignments particularly clear. Although transitions to $^2T_1(P)$ are weak and ill-defined, it appears once again that the low symmetry splitting $(13\ cm^{-1})$ is much smaller than the spin-orbit splitting $(200\ cm^{-1})$.

No satisfactory analysis of the transitions to $^2T_1(H)$ could be obtained either in Cs_3CoCl_5 or Cs_3CoBr_5, but the two components of $^2E(H)$ have been assigned. This state splits in the opposite sense from $^2E(D)$ with a separation considerably greater than that observed for $^2E(D)$. Because of the close proximity of $^2E(H)$ to $^2T_1(H)$ at higher energy, second-order interactions between the components of these states may affect their energies. It is possible that $\Gamma_6(^2E(H))$ is pushed to low energy by interaction with the two Γ_6 components of $^2T_1(H)$. The pattern of transitions to the remaining components of ^2H, and to ^2G is very complex and unambiguous assignment was not possible.

An interesting comparison can be made between the bands assigned to $^2T_1(F)$ and those assigned to $^2T_1(H)$, and between the bands assigned to $^2T_2(F)$ (in Cs_3CoCl_5) and those assigned to $^2T_2(G)$. Transitions to $^2T_1(F)$ and to $^2T_1(H)$ give fairly sharp bands with more strongly z polarized peaks than can be explained within the proposed D_{2d}^* energy level scheme. The bands corresponding to transitions to $^2T_2(F)$ (in Cs_3CoCl_5) and to $^2T_2(G)$ both begin with very sharp

TABLE 14. ASSIGNMENTS OF THE DOUBLET SPECTRUM OF $CoCl_4^{2-}$

		present work (Cs_3CoCl_5)				Ferguson (1963) (Cs_2CoCl_4)
region	transition	free ion	c.f. (R.S.)	T_d^*	D_{2d}^*	
I	A	^2F	$^2T_1$	Γ_6	Γ_6	$^2T_1(F)$
	B	^2F	$^2T_1$	—	—	
	C	^2F	$^2T_1$	Γ_8	Γ_7	
	D	^2F	$^2T_1$	—	—	
	E	^2F	$^2T_1$	Γ_6	Γ_6	
II	A	^2F	$^2A_2$	—	—	
	B	^2F	$^2T_2$	—	—	
	C	^2F	$^2T_2$	—	—	
	D	^2F	$^2T_2$	—	—	
III	A	^2D	^2E	Γ_8	Γ_7†	
	B	^2D	^2E	Γ_8	Γ_7	
	C	^2D	^2E	Γ_8	Γ_6†	
	D	^2D	^2E	Γ_8	Γ_6	
IV	A	^2D	$^2T_2$	Γ_7	Γ_7	$^2E(D)$
	B	^2D	$^2T_2$	Γ_8	Γ_6†	
	C	^2D	$^2T_2$	Γ_8	Γ_7	
V	A	^2P	$^2T_1$	Γ_8	Γ_7	
	B	^2P	$^2T_1$	Γ_8	Γ_6	
	C	^2P	$^2T_1$	Γ_6	Γ_6	
VI	A	^2H	^2E	Γ_8	Γ_6†	$^2T_2(D)$
	B	^2H	^2E	Γ_8	Γ_6	
	C	^2H	^2E	Γ_8	Γ_7	
	D	^2H	$^2T_1$	—	—	
	E	^2H	$^2T_1$	—	—	
	F	^2H	$^2T_1$	—	—	
VII	A	^2H	—	—	—	$^2H+{}^2P$
	B	^2H	$^2T_1$	—	—	
	C	^2H	$^2T_2$	—	—	
	D	^2H	—	—	—	
VIII	A	^2G	$^2T_2$	—	—	
	B	^2G	$^2T_2$	—	—	
	C	^2G	$^2T_2$	—	—	
IX	A	^2G	—	—	—	^2G

† From $\Gamma_7(^4A_2)$.

peaks, but have broad, strongly z polarized peaks at high energy. To make any more precise comments about these features it may be necessary to move away from the 'oriented gas' model of the crystals, which has been used throughout the foregoing sections, and to take explicit account of interactions between the molecular anions. Although a factor group analysis of the vibrational spectra of the two crystals was carried out, the possible effect of intermolecular interactions on the number and polarization of the electronic transitions has not been considered. A considerable amount of information is available about the magnitudes of electronic factor group (Davydov) splittings in organic molecular crystals (see, for example, Craig & Walmsley 1968) but the overwhelming proportion even of that work relates to transitions which are allowed both by oribtal and spin selection rules. In one of the few pieces of work on spin-forbidden transitions in organic molecular crystals, Hochstrasser (1967) located the factor group components of the lowest energy triplet transition in pyrazine, finding a splitting between them of 6.4 cm^{-1}.

TABLE 15. ASSIGNMENT OF THE DOUBLET SPECTRUM OF $CoBr_4^{2-}$ IN Cs_3CoBr_5

region	transition	free ion	c.f. (R.S.)	T_d^*	D_{2d}^*
I	A	^2F	$^2T_1$	Γ_8	Γ_6†
	B	^2F	$^2T_1$	Γ_8	Γ_6
	C	^2F	$^2T_1$	Γ_7	Γ_7
	D	^2F	$^2T_1$	—	—
	E	^2F	$^2T_1$	Γ_6	Γ_6
IIa	A	^2F	$^2T_2$	Γ_7	Γ_7
	B	^2F	$^2T_2$	Γ_8	Γ_7
	C	^2F	$^2T_2$	Γ_8	Γ_6
IIb	A	^2F	$^2A_2$	Γ_7	Γ_7
III	A	^2D	^2E	Γ_8	Γ_7†
	B	^2D	^2E	Γ_8	Γ_7
	C	^2D	^2E	Γ_8	Γ_6†
	D	^2D	^2E	Γ_8	Γ_6
IV	A	^2D	$^2T_2$	Γ_7	Γ_7
	B	^2D	$^2T_2$	Γ_8	Γ_6
	C	^2D	$^2T_2$	Γ_8	Γ_7
V	A	^2P	$^2T_1$	Γ_8	Γ_7
	B	^2P	$^2T_1$	Γ_6	Γ_6
VIa	A	^2H	$^2T_1$	—	—
	B	^2H	$^2T_1$	—	—
	C	^2H	$^2T_1$	—	—
VIb	A	^2H	^2E	Γ_8	Γ_6†
	B	^2E	^2E	Γ_8	Γ_6
	C	^2H	^2E	Γ_8	Γ_7
VII	A	^2H	—	—	—
	B	^2H	$^2T_1$	—	—
	C	^2H	$^2T_2$	—	—
	D	^2H	—	—	—
VIII	A	^2G	$^2T_2$	—	—
	B	^2G	$^2T_2$	—	—
	C	^2G	$^2T_2$	—	—
	D	^2G	$^2T_2$	—	—
IX	A	^2G	$^2A_1$	Γ_6	Γ_6
	B	—	—	—	—

† From $\Gamma_7(^4A_2)$.

The only available information on factor group splittings of spin forbidden transitions in inorganic crystals concerns Cr_2O_3, in which the metal ions are expected to experience a greater interaction than in our case, because they are directly bridged by oxide ions. For example, the Neel temperature of Cr_2O_3 is 308 K (Van der Ziel 1967), while that of Cs_3CoCl_5 is only 0.59 K (Wielinga *et al.* 1967). The most recent estimate of the separation of the Davydov components of the ^2E excited state in Cr_2O_3 is 180 cm^{-1} (Allen, McFarland & White 1969). It is to be expected that the Davydov splittings of the spin forbidden transitions in the 'molecular' crystals Cs_3CoCl_5 and Cs_3CoBr_5 will be closer in magnitude to those of pyrazine than to those for the continuous lattice Cr_2O_3. The definitive experiment which would distinguish Davydov effects from other types of perturbation would be a determination of the spectrum of $CoCl_4^{2-}$ diluted in Cs_3ZnCl_5, but no such spectra, in the region of the spin forbidden transitions, have ever been reported.

In sum, the major groups of bands lying between 16 000 and 33 000 cm^{-1} in the spectra of

Cs_3CoCl_5 have been assigned, both as to spin-orbit and Russell–Saunders parentage. Taken in conjunction with the information already available on the quartet transitions, we thus have available a large set of experimentally validated excited state energies, term symmetries and intensities, against which the theoretical model constructed in §§ 2 and 3 may be tested.

5. Correlation of spectral assignments with the theory

Our aim in this section is to use the state energies, term symmetries and intensities of the ligand-field transitions of CoX_4^{2-}, independently determined by the experiments on Cs_3CoCl_5 and Cs_3CoBr_5 in § 4, to test the set of approximations to the molecular orbital-based integrals of electron repulsion and spin-orbit coupling set out in §§ 2 and 3. After appropriate validation of the basic scheme one may use a least-squares fitting procedure to extract the orbital population parameters n_e, n_{t_2} and n_π and hence estimate eigenvectors for the molecular orbitals of the ligand-field manifold. In cubic complexes of the 3d elements the major splittings between the observed ligand field states are determined by the orbital energy difference between e and t_2, and by changes in interelectron repulsion on excitation. A more subtle test of our theory is to calculate the magnitude of the much smaller splittings brought about by spin-orbit coupling since, as we indicated in § 3, integrals of the spin-orbit operator may equally be written down in terms of molecular orbital eigenvectors. Also, since the electric-dipole intensity of spin-forbidden ligand-field transitions in non-centrosymmetric complexes comes principally from second-order interaction, via spin-orbit coupling, with the spin-allowed transitions, the relative intensities of the former may also prove a valuable assignment tool. It is partly for this reason that we have devoted particular attention to the doublet states of CoX_4^{2-} in § 4.

(*a*) *Electron repulsion: term baricentres*

Because the electron repulsion energy for the 3d complexes which we are considering here is much greater than the spin-orbit coupling energy, it is convenient to examine first the correlation between the cubic field Russell–Saunders term energies predicted by the molecular orbital model and the baricentres of the quartet and doublet ligand-field transitions identified in § 4.

As mentioned in § 4 (*e*), to obtain some preliminary orientation among the very complicated sequence of transitions, we carried out conventional crystal field calculations on the CoX_4^{2-} chromophores, using a least-squares procedure to extract the parameters giving the best fit to the spectrum. We begin with an outline of the results of these calculations. Because the molecular orbital-based calculations, which include charge transfer as well as ligand-field states, are necessarily carried out in a strong field basis, the conventional crystal-field calculations also employ the strong-field scheme. This contrasts with some earlier work (Jesson 1968) on CoX_4^{2-}, but if the complete ligand field matrices are diagonalized the resulting energies will be the same.

For the limited purpose of identifying the major regions of absorption, it is sufficient to use a two-parameter model of the ligand field, comprising the $t_2 - e$ subshell separation Δ, and a factor β, the nephelauxetic factor, scaling the free ion interelectron repulsion parameters. The Racah parameters for Co^{2+} to be scaled in this fashion were taken from Watson's (1959) s.c.f. calculations. The s.c.f. values are slightly larger than those obtained by fitting the atomic spectrum of Co^{2+} (e.g. the ratio C (observed)/C (s.c.f.) is 0.915 for ^4F (Ferguson 1963)) so Watson's parameters were therefore scaled first by this factor, giving the following values for the average of configurations (d^7) of Co^{2+}: A 181 050 cm^{-1}, B 1153 cm^{-1}, C 4259 cm^{-1}.

The term baricentres used in the fit were those whose low symmetry and spin-orbit components were identified in tables 2 and 3, and presented schematically in figure 23. In addition the baricentres of the three quartets of $CoCl_4^{2-}$ were taken from the work of van Stapele *et al.* (1966) and Jesson (1968), who used Cs_3ZnCl_5 as a host lattice. Unfortunately no comparable data have been recorded on $CoBr_4^{2-}$ in Cs_3ZnBr_5 so for the baricentres of the quartets of the latter ion we have relied on spectra measured at 4 K in $[N(C_2H_5)_4]_2ZnBr_4$ (Grant 1970) and the original room temperature solution spectra of Cotton *et al.* (1961).

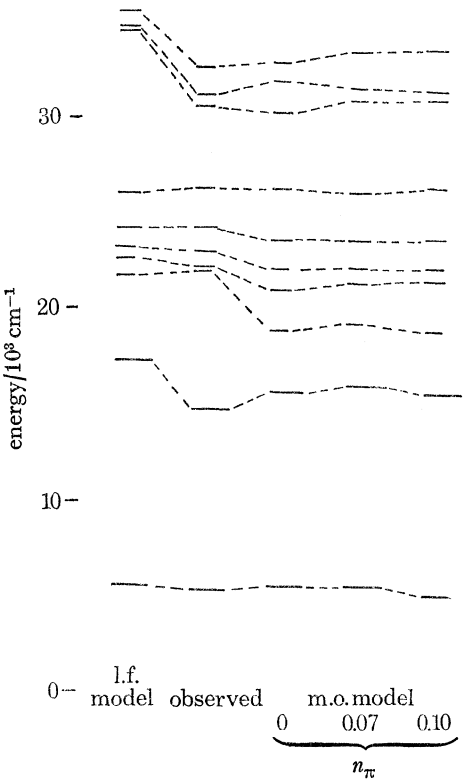

FIGURE 24. Baricentres of the ligand field terms of $CoCl_4^{2-}$, as observed in Cs_3CoCl_5 and calculated by the conventional ligand field model ($\Delta = 3230\,cm^{-1}$, $\beta = 0.77$) and the molecular orbital model ($n_\pi = 0, 0.07, 0.10$).

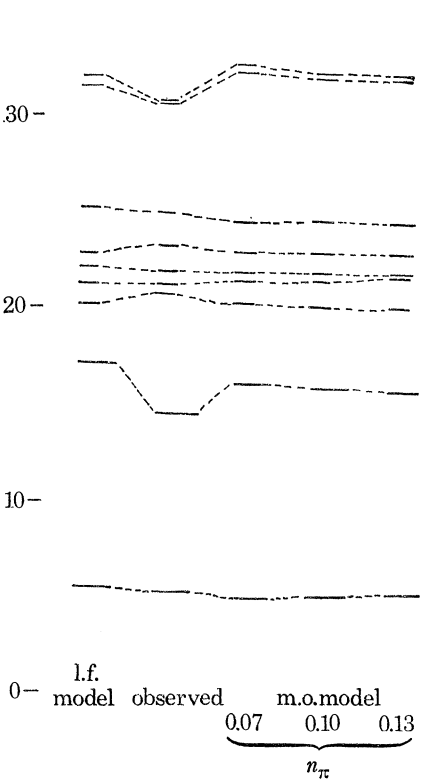

FIGURE 25. Baricentres of the ligand field terms of $CoBr_4^{2-}$, as observed in Cs_3CoBr_5 and calculated by the conventional ligand field model ($\Delta = 3080\,cm^{-1}$, $\beta = 0.73$) and the molecular orbital model ($n_\pi = 0.07, 0.10, 0.13$).

The assignment of the quartets is not in doubt, so that by taking approximate values of Δ and β from the baricentres of the two $^4T_1$ one may carry out least-squares fits on the doublet baricentres. Including the five doublet baricentres between 20 000 and 26 000 cm^{-1}, since these are the ones whose assignments are best defined by the site-group and spin-orbit splittings described in § 4 (*e*), one obtains excellent fits, with standard deviations of 325 cm^{-1} for the chloride and 196 cm^{-1} for the bromide. Good correlation is also achieved with the baricentres of the other doublets not included in the fit, leading to the schematic sets of assignments in figures 24 and 25. These figures also contain the results of fits carried out using the molecular orbital model, but before considering these in greater detail, two interesting deficiencies of the conventional crystal field calculation deserve mention. The first is that when the doublets between 20 000 and 26 000 cm^{-1} are fitted with the greatest precision, the energies of those above 30 000 cm^{-1} are

TABLE 16. OBSERVED ENERGIES OF BARICENTRES OF CUBIC LIGAND-FIELD STATES IN $CoCl_4^{2-}$, AND THOSE CALCULATED BY THE MOLECULAR ORBITAL MODEL, TOGETHER WITH VALUES OF Δ AND THE POPULATION PARAMETERS (cm^{-1})

		calculated		
	observed	$n_\pi = 0$	$n_\pi = 0.07$	$n_\pi = 0.10$
$^2A_2$	30 732	30 407	31 047	31 100
$^4T_1(F)$	5 470	5 682	5 738	5 314
$^4T_1(P)$	14 840	15 799	16 177	15 827
$^2E(2)$	22 061	19 011	19 380	19 033
$^2E(3)$	26 391	26 405	26 217	26 481
$^2T_1(3)$	22 274	21 102	21 507	21 568
$^2T_1(4)$	23 090	22 205	22 322	22 272
$^2T_1(5)$	32 745	32 988	33 569	33 698
$^2T_2(3)$	24 378	23 757	23 709	23 849
$^2T_2(4)$	31 320	31 984	31 743	31 636
n_t		0.8177	0.8305	0.8320
n_e		0.9048	0.8873	0.9075
Δ (cm^{-1})		60 159	40 622	53 116
F (eq. (5.2))		4.113	4.472	3.597
standard dev. (cm^{-1})		906	945	850

TABLE 17. OBSERVED ENERGIES OF BARICENTRES OF CUBIC LIGAND-FIELD STATES IN $CoBr_4^{2-}$, AND THOSE CALCULATED BY THE MOLECULAR ORBITAL MODEL, TOGETHER WITH VALUES OF Δ AND THE POPULATION PARAMETERS (cm^{-1})

		calculated		
	observed	$n_\pi = 0.07$	$n_\pi = 0.10$	$n_\pi = 0.13$
$^2A_2$	30 720	32 401	32 161	32 129
$^4T_1(F)$	5 300	4 980	5 148	5 292
$^4T_1(P)$	14 590	16 187	16 026	15 879
$^2E(2)$	20 810	20 350	20 200	20 233
$^2E(3)$	25 010	24 644	24 680	24 598
$^2T_1(3)$	21 350	21 459	21 577	21 781
$^2T_1(4)$	22 010	21 961	21 974	22 029
$^2T_2(3)$	23 280	22 985	22 996	23 013
$^2T_2(4)$	30 840	32 766	32 404	32 286
n_t		0.8664	0.8619	0.8615
n_e		0.8751	0.8717	0.8685
Δ (cm^{-1})		8 925	9 686	7 773
F (from eq. (5.2))		3.100	2.702	2.420
standard dev. (cm^{-1})		1 015	949	895

always overestimated. This may be the result, either of interaction between these levels and the adjacent charge transfer states, or of our incomplete knowledge of the spectrum of gaseous Co^{2+}, leading to inaccurate estimates of the free ion electron repulsion parameters. The second point is that if one uses the energies of the two $^4T_1$ alone to define values of Δ and β, the doublets are all placed uniformly too high, while the energies of the two $^4T_1$ predicted by the fits based on the observed energies of the doublets alone are also too high. If one attempts to fit quartets and doublets together the least-squares procedure converges to fits having standard deviations much larger than if the doublets alone are fitted. The values of Δ and β, together with the standard deviations of all the methods of fitting the spectrum, are collected in table 16.

Before we can begin fitting the CoX_4^{2-} spectra to extract eigenvectors using the molecular orbital ligand field model, estimates are required of one-centre electron repulsion integrals for

cobalt and halogen, and also the two-centre integrals. The average ligand Coulomb and exchange integrals J_{av} and K_{av}, and the metal-ligand distances, which occur in the expressions of table 11, are given in table 17. The J_{av} and K_{av} were obtained from Clementi's wavefunctions (Clementi 1964) while the Co—Cl bond length was taken from the crystal structure of Cs_3CoCl_5 (Figgis *et al.* 1964). No experimental data are available on the Co—Br bond length in $CoBr_4^{2-}$, so it was estimated from the known change in copper–halogen bond distance between Cs_2CuCl_4 and Cs_2CuBr_4 (Morosin & Lingafelter 1960, 1961). To make allowance for the charge dependence of the one-centre metal integrals, they were interpolated between the $Co^+(^3F)$ and $Co^{2+}(^4F)$ parameters of Watson (1959), scaled down as before for electron correlation:

	A	B	C
$Co^{2+}(^4F)$	181 607 cm^{-1}	1 158 cm^{-1}	4 280 cm^{-1}
$Co^{+}(^3F)$	167 280 cm^{-1}	1 042 cm^{-1}	3 803 cm^{-1}

No allowance was made for the charge dependence of J_{av} and K_{av}. The charge q on the cobalt is $(5-n_d)$, where n_d is the number of d-electrons. If the e orbital is ignored, being a closed shell,

$$n_d = 6(1-n_t) + 3n_t = 6 - 3n_t \tag{5.1}$$

so that q, taken as positive, is $(3n_t - 1)$.

In order to limit the complexity of the fitting problem the atomic orbital basis set is truncated by neglecting the 4p orbital on the cobalt and the *ns* orbitals on the halide ions. Our justification for excluding 4p is that the lowest excited state of Co^{2+} containing 4p, $3d^6(^5D)4p$, ^6D lies almost 100 000 cm^{-1} above the $3d^7$, ^4F ground state. Also, the final result for n_σ will implicitly contain the ligand *s* as well as $p\sigma$ contributions. Apart from Δ, the expressions of the tables contain n_t, n_e, n_π and n_σ, the two former factors being the Mulliken populations of the d-electrons in the t_2 and e molecular orbitals, and the latter two the populations of the $p\pi$ and $p\sigma$ orbitals (with the proviso about *ns* above) due to a single electron in the t_2 molecular orbital. As a result of neglecting 4p, we have $n_t + n_\pi + n_\sigma = 1$, and hence n_σ need no longer be considered an independent parameter.

The aim of the least-squares calculation is to find those values of the four disposable parameters which minimize the function

$$F = \sum_t [f_{calc}(t) - f_{obs}(t)]^2 W(t), \tag{5.2}$$

where the summation is over all the observables denoted t, and $W(t)$ is the weight attached to each. In the present case, the f_{calc} and f_{obs} are the calculated and observed energies of the baricentres of the cubic ligand-field terms. The simplest type of iterative calculation to find the minimum value of F would be that of systematically varying the parameters. However, in the present very complex instance, convergence was found to be extremely slow, and a method using partial derivatives, the so-called Newton–Raphson–Gauss method (Whittaker & Robinson 1944; Brown & Taylor 1965) was finally employed. For details, the reader is referred to Bird (1969), appendix A. The iterative calculations were performed using a programme written in Fortran for the Oxford University KDF 9, which prints out the set of computed band positions, parameter values and F factor after each set of iterations, proceeding with successive cycles of calculations until F is minimized. As data, the programme is supplied with the one- and two-centre integrals, together with their charge increments, a set of observed baricentres with weighting factors, and starting values for Δ and the population parameters. To avoid the possibility of convergence towards local minima in F different starting values of Δ and the population parameters were employed in repeated sets of calculations.

PHILOSOPHICAL TRANSACTIONS OF THE ROYAL SOCIETY A MATHEMATICAL, PHYSICAL & ENGINEERING SCIENCES

Before describing the results of the calculations for $CoCl_4^{2-}$ and $CoBr_4^{2-}$, one or two general points about the sensitivity of the fitting process, and the resulting strategy of the fits should be mentioned. The first is that, because the relevant equations (table 7) contain the extremely large Racah A parameter, the calculated baricentre energies are extremely sensitive to small changes in n_e and n_t. Such changes may be compensated, in the course of the fitting process, by variation of A, but the result is that A becomes 'ill-conditioned'. For example, the direction in the parameter space along which the error function F does not alter may be typically

$$A - 0.00038n_\pi + 0.0012n_e + 0.00025n_t. \tag{5.3}$$

Speciously good fits may therefore sometimes be obtained with quite widely varying values of A, though in practice trends towards particular ranges of A may be discerned as the fitting proceeds. A second problem concerns n_π, which sometimes fluctuated widely throughout the fitting process. Sets of fits were therefore made, setting n_π to different constant values and assessing the effect on F and on the other freely varying parameters.

The calculated energies of the cubic-field Russell–Saunders terms calculated for various fixed values of n_π compared with the experimental energies for $CoCl_4^{2-}$ in table 16 and $CoBr_4^{2-}$ in table 17. These tables also give the values of A and the population parameters extracted from each fit, together with the minimum value of the least-squares function F and the standard deviation in each case. Figures 16 and 17 present the observed and calculated spectra pictorially, so that the level of agreement can be more easily judged. In the course of calculating the spectrum, the program evaluates numerical values for all the electron repulsion integrals defined in table 11. No estimates of these generalized electron repulsion integrals based on the analysis of experimental spectra appear ever to have been given in the literature, so despite their bulk we give in table 5 sets of the integrals involving t_1, t_2 and e molecular orbitals obtained from the fitting calculations set out in tables 16 and 17.

From the orbital population parameters, m.o. coefficients may be calculated. If we define the coefficients as follows, taking the d, σ and π orbital combinations from table 12:

$$\left.\begin{aligned} |t_2\rangle &= c_4|3d\rangle + c_5|\sigma\rangle + c_7|\pi\rangle, \\ |e\rangle &= c_1|3d\rangle + c_2|\pi\rangle, \end{aligned}\right\} \tag{5.4}$$

then the orbital populations are in turn expressed:

$$\begin{aligned} n_t &= c_4^2 - (2\sqrt{3})\, c_4 c_5 S(d, p\sigma) + \tfrac{2}{3}\sqrt{(2)}\, c_4 c_7 S(d, p\pi) \\ n_\pi &= c_7^2\{1 + \tfrac{1}{6}S(p\sigma, p\sigma) + \tfrac{11}{16}S(p\pi, p\pi) + \tfrac{2}{3}\sqrt{(2)}\, c_4 c_7 S(d, p\pi) - \tfrac{2}{3}\sqrt{(2)}\, c_5 c_7[S(p\pi, p\pi) - S(p\sigma, p\sigma)]\}, \\ n_e &= c_1^2 + \tfrac{2}{3}\sqrt{(6)}\, c_1 c_2 S(d, p\pi). \end{aligned} \tag{5.5}$$

The overlap integrals required to evaluate these expressions were calculated from Clementi's (1964) wavefunctions for Cl and Br, and Watson's (1959) for Co^{2+}. The coefficients are listed in table 19. The significance of these coefficients, and of the A values in tables 16 and 17 is discussed below.

TABLE 18. NUMERICAL VALUES OF THE GENERALIZED MOLECULAR ORBITAL ELECTRON REPULSION INTEFGRALS DEFINED IN TABLE 11, OBTAINED BY LEAST-SQUARES FITTING THE CoX_4^{2-} SPECTRA (TABLES 5.1 AND 5.2) (THE UNITS ARE cm^{-1})

(*a*) $CoCl_4^{2-}$

	a	*b*	*c*	*d*
$n_\pi = 0$	144 210	134 446	1 619	143 253
$n_\pi = 0.07$	152 806	142 083	1 677	146 944
$n_\pi = 0.10$	151 506	140 909	1 689	147 700
	e	*f*	*g*	*h*
$n_\pi = 0$	165 049	6 887	3 789	809
$n_\pi = 0.07$	163 890	6 817	4 029	873
$n_\pi = 0.10$	167 139	7 009	4 081	887
	i	*j*	*mk*	*lm*
$n_\pi = 0$	1 402	5 507	56 235	56 779
$n_\pi = 0.07$	1 448	5 400	56 444	56 704
$n_\pi = 0.10$	1 419	5 229	56 471	56 743
	mm	*nn*	*pu*	*uq*
$n_\pi = 0$	59 933	0	− 76	0
$n_\pi = 0.07$	59 833	0	− 84	− 3
$n_\pi = 0.10$	59 833	0	− 73	− 39
	uu	*vv*	*zz*	*aa*
$n_\pi = 0$	442	73	73	38
$n_\pi = 0.07$	441	60	144	42
$n_\pi = 0.10$	440	62	181	36
	tx	*xx*	*yy*	*bb*
$n_\pi = 0$	− 1690	7 083	218	495
$n_\pi = 0.07$	− 506	7 071	1 104	545
$n_\pi = 0.10$	− 171	7 071	1 505	474
	ar	*bs*	*bt*	*sy*
$n_\pi = 0$	− 4	23	− 506	− 39
$n_\pi = 0.07$	− 23	113	− 104	176
$n_\pi = 0.10$	− 22	115	24	249
	rz	*qv*	*uy*	*ty*
$n_\pi = 0$	− 23	9	27	− 181
$n_\pi = 0.07$	8	10	119	− 202
$n_\pi = 0.10$	18	1	139	− 25

(*b*) $CoBr_4^{2-}$

	a	*b*	*c*	*d*
$n_\pi = 0.07$	156 528	145 339	1 679	146 337
$n_\pi = 0.10$	155 235	144 172	1 659	145 293
$n_\pi = 0.13$	155 132	144 088	1 649	144 899
	e	*f*	*g*	*h*
$n_\pi = 0.07$	158 724	6 556	4 045	875
$n_\pi = 0.10$	157 683	6 497	4 049	881
$n_\pi = 0.13$	156 882	6 450	4 080	894
	i	*j*	*mk*	*lm*
$n_\pi = 0.07$	1 513	5 610	52 659	52 789
$n_\pi = 0.10$	1 468	5 533	52 677	52 774
$n_\pi = 0.13$	1 420	5 573	52 719	52 761

TABLE 18 (*cont.*)

(*b*) $CoBr_4^{2-}$

	mm	*nn*	*pu*	*uq*
$n_\pi = 0.07$	54 345	0	−91	−26
$n_\pi = 0.10$	54 345	0	−93	−36
$n_\pi = 0.13$	54 345	0	−96	−47
	uu	*vv*	*zz*	*aa*
$n_\pi = 0.07$	404	49	125	46
$n_\pi = 0.10$	404	50	160	47
$n_\pi = 0.13$	404	51	193	48
	tx	*xx*	*yy*	*bb*
$n_\pi = 0.07$	−306	6 170	933	559
$n_\pi = 0.10$	−21	6 170	1 276	575
$n_\pi = 0.13$	296	6 170	1 614	589
	ar	*bs*	*bt*	*sy*
$n_\pi = 0.07$	−24	114	−49	163
$n_\pi = 0.10$	−29	136	72	248
$n_\pi = 0.13$	−34	156	207	336
	rz	*qv*	*yv*	*ty*
$n_\pi = 0.07$	10	6	109	−110
$n_\pi = 0.10$	21	−2	127	53
$n_\pi = 0.13$	33	−14	142	283

TABLE 19. MOLECULAR ORBITAL COEFFICIENTS DERIVED FROM THE LIGAND-FIELD SPECTRA OF $CoCl_4^{2-}$ AND $CoBr_4^{2-}$ (THE NOTATION IS THAT OF EQUATION (5.4))

(*a*) $CoCl_4^{2-}$

	e		t_2		
	c_1	c_2	c_4	c_5	c_7
$n_\pi = 0$	0.9611	−0.3316	0.9225	0.4846	−0.0628
$n_\pi = 0.07$	0.9580	−0.3517	0.9413	0.3474	−0.2831
$n_\pi = 0.10$	0.9645	−0.3307	0.9378	0.2992	−0.3312

(*b*) $CoBr_4^{2-}$

$n_\pi = 0.07$	0.9467	−0.3749	0.9468	0.3146	−0.2830
$n_\pi = 0.10$	0.9450	−0.3796	0.9432	0.2585	−0.3306
$n_\pi = 0.13$	0.9435	−0.3838	0.9403	0.1612	−0.3697

(*b*) *Spin-orbit coupling: intensities and fine-structure of terms*

The calculations described in § 5 (*a*) give a good overall account of the energies of the baricentres of the cubic-field Russell–Saunders terms in tetrachloro- and tetrabromocobaltates, and lead to estimates of the m.o. coefficients appropriate to the t_2 and e ligand-field orbitals. In § 3 we gave a brief description of the way in which matrix elements of the molecular spin-orbit operator could be expressed in terms of m.o. coefficients and atomic spin-orbit coupling constants. Thus we may now make use of the coefficients obtained by fitting the baricentres of the ligand-field terms to calculate numerical values for the one-electron reduced matrix elements of table 12 and then, by the methods of Griffith (1962), the many-electron matrix elements. A computer program (for details see Bird 1969, appendix D) has been written to carry out these operations, and to diagonalize the resulting matrices. It is sufficiently general that interactions between charge transfer and ligand-field states, and even between charge transfer states, may be treated,

but for the present we consider only the ligand-field manifold. The program uses Griffith's (1962) equations (10.14) and (10.18) to find the coefficients to the one-electron reduced matrix elements $\langle \frac{1}{2}t_2 \| su \| \frac{1}{2}t_2 \rangle$ and $\langle \frac{1}{2}t_2 \| su \| \frac{1}{2}e \rangle$, which are then punched out separately to avoid repeating the calculation. The final matrices are comparable to those of Eisenstein (1961) except for the hole formalism for $(t_2e)^3$.

The atomic spin-orbit coupling constants needed in the calculation were taken without scaling as $\zeta_{3d} = 515\,\mathrm{cm}^{-1}$ for Co^{2+}, from Dunn's (1961) compilation, and $\zeta_{3p} = 590\,\mathrm{cm}^{-1}$ (chlorine) and $\zeta_{4p} = 2460\,\mathrm{cm}^{-1}$ (bromine) from Jørgensen (1962). Earlier results, fitting the spin-orbit fine structure of the charge transfer bands of IrX_6^{2-} (Bird, Day & Grant 1970), indicated that the halogen spin-orbit coupling constants need not be scaled for charge dependence.

In addition to the eigenvalues of the spin-orbit matrices, which may be compared directly with the observed energies of transitions to the individual spin-orbit components of the ligand-field bands (§ 4), the eigenvectors may also be employed in calculations of the dipole strengths of these transitions, defined as

$$D = (3/\lambda(a)) \Sigma |\langle a | m_x | j \rangle|^2,$$

where m_x is the x-component of the electric-dipole operator, and the summation is over all components of the ground state a (degeneracy $\lambda(a)$) and the excited state j. From the $^4A_2$ ground state of CoX_4^{2-} transitions are spin- and electric-dipole-allowed only to $^4T_1$, a sole singly excited example of which, $e^3t_2^4(^3T_1)^4T_1$, exists within the ligand-field manifold. The dipole strengths of the individual spin-orbit components of $^4T_1$ – for example, $\langle {}^4A_2\Gamma_8\kappa | m_x | {}^4T_1\Gamma_6\alpha \rangle$ – are simply obtained by expanding the wavefunctions

$$|ShJt\tau\rangle = \sum_{M\theta} \langle ShM\theta | ShJt\tau \rangle \, |ShM\theta\rangle, \tag{5.6}$$

using the coupling coefficients $\langle ShM\theta | ShJt\tau \rangle$ given by Griffith (1961). We then have

	Γ_6	Γ_7	$\frac{3}{2}\Gamma_8$	$\frac{5}{2}\Gamma_8$
D	$\frac{1}{6}$	$\frac{1}{6}$	$\frac{1}{3}$	$\frac{1}{3}$

in units of m^2, where $m = \langle {}^4A_2 \| m \| {}^4T_1 \rangle$. In the ligand field spectrum there are, of course, two $^4T_1$ transitions, so that the dipole strength indicated here will largely be shared between them. Further, though smaller, admixtures of $^4T_1$ occur in the remaining ligand-field states formally labelled doublets, brought about by off-diagonal elements of the spin-orbit operator. In general, there are two mechanisms by which the spin-forbidden transitions may gain intensity: mixing of $e^3t_2^4(^3T_1)^2T_2$ into the ground-state or of $e^3t_2^4(^3T_1)^4T_1$ into the doublet wavefunction. The former will be ignored in the present treatment. Thus the electric-dipole matrix element of a formally spin-forbidden transition becomes

$$\langle {}^4A_2\Gamma_8\kappa | m_x | \alpha({}^2ht\tau) + \beta({}^4T_1t\tau) \rangle, \tag{5.7}$$

where β is small. Consequently $D \sim \beta^2({}^4T_1t\tau)$. With U' states the situation is slightly more complicated since both $\frac{3}{2}\Gamma_8$ and $\frac{5}{2}\Gamma_8$ can contribute. However, writing

$$|\Gamma_8\rangle = a|\tfrac{3}{2}\Gamma_8\rangle + b|\tfrac{5}{2}\Gamma_8\rangle \tag{5.8}$$

one may show that

$$D = \tfrac{1}{3}(a^2 + b^2)\, m^2, \tag{5.9}$$

the cross terms cancelling.

The state reduced matrix element m is easily related to the one-electron reduced matrix element $\langle e \| m \| t_2 \rangle$; in fact $m = \langle e \| m \| t_2 \rangle$. To express $\langle e \| m \| t_2 \rangle$ in terms of m.o. coefficients we use

TABLE 20. ENERGIES (E/cm^{-1}) AND DIPOLE STRENGTHS (D/10^{-7} nm^{-2}) OF TRANSITIONS TO THE SPIN-ORBIT COMPONENTS OF THE LIGAND-FIELD STATES OF CoX_4^{2-}, AS CALCULATED BY THE MOLECULAR ORBITAL METHOD

The left-hand column lists the Russell–Saunders term having the largest eigenvector in each spinor state.

(*a*) $CoCl_4^{2-}$

(i) Γ_6 excited states

	$n_\pi = 0$		$n_\pi = 0.07$		$n_\pi = 0.10$	
	E	D	E	D	E	D
$^4T_2$	2 946	1	2 840	12	2 496	11
$^4T_1$	4 957	77	5 023	1 780	4 760	1 988
$^2T_1$	13 237	10	13 857	0	13 601	2
$^2A_1$	14 264	33	15 216	1 270	14 814	1 458
$^4T_1$	16 453	574	16 944	12 923	16 570	15 507
$^2T_1$	18 634	1	18 898	67	18 507	106
$^2T_1$	20 930	3	21 902	59	21 770	54
$^2T_1$	22 555	1	22 960	24	22 934	33
$^2T_1$	33 498	0	34 543	4	34 397	5

(ii) Γ_7 excited states

	$n_\pi = 0$		$n_\pi = 0.07$		$n_\pi = 0.10$	
	E	D	E	D	E	D
$^4T_2$	3 230	0	3 083	7	2 731	7
$^4T_1$	5 770	94	5 832	2 136	5 572	2 388
$^4T_1$	15 782	554	16 216	13 341	15 838	16 132
$^2T_2$	16 289	23	16 814	322	16 703	251
$^2T_2$	18 465	0	18 649	3	18 415	4
$^2T_2$	23 521	1	23 653	19	23 700	21
$^2A_2$	30 399	0	32 130	0	31 854	0
$^2T_2$	32 341	0	32 831	6	32 468	7
$^2T_2$	50 468	1	51 638	20	51 879	25

(iii) Γ_8 excited states

	$n_\pi = 0$		$n_\pi = 0.07$		$n_\pi = 0.10$	
	E	D	E	D	E	D
$^4A_2$	116	—	132	—	−150	—
$^4T_2$	2 836	4	2 730	72	2 387	70
$^4T_2$	3 159	2	3 045	45	2 714	44
$^4T_1$	5 290	164	5 354	3 790	5 091	4 243
$^4T_1$	5 858	185	5 916	4 212	5 655	4 715
^2E	13 430	5	13 492	33	13 259	41
$^2T_1$	14 057	11	14 257	320	14 027	486
$^4T_1$	15 779	1 101	16 210	26 942	15 831	32 483
$^4T_1$	16 011	68	16 561	23 436	16 200	32 277
$^2T_2$	16 127	1 142	16 616	4 037	16 550	290
$^2T_2$	18 317	3	18 463	112	18 135	219
$^2T_1$	18 467	5	18 815	246	18 464	299
^2E	19 225	2	20 133	50	19 700	70
$^2T_1$	21 029	16	21 891	349	21 916	357
$^2T_1$	22 070	1	22 626	0	22 438	8
$^2T_2$	23 934	1	24 137	45	24 189	49
^2E	26 559	1	26 295	30	26 469	32
$^2T_2$	32 174	0	32 658	7	32 270	9
$^2T_1$	33 199	1	34 272	23	34 142	29
^2E	47 939	0	49 470	6	49 137	6
$^2T_2$	50 546	1	51 619	19	51 865	24

TABLE 20 (*cont.*)

(*b*) $CoBr_4^{2-}$

(i) Γ_6 excited states

	$n_\pi = 0.07$		$n_\pi = 0.10$		$n_\pi = 0.13$	
	E	*D*	*E*	*D*	*E*	*D*
$^4T_2$	2 668	9	2 647	11	2 567	17
$^4T_1$	4 601	2 163	4 782	3 164	4 834	4 024
$^2T_1$	14 287	1	14 147	1	14 181	1
$^2A_1$	15 486	1 867	15 387	3 000	15 338	5 924
$^4T_1$	16 583	16 172	16 456	21 847	16 397	25 774
$^2T_1$	19 144	114	18 999	204	19 017	246
$^2T_1$	21 408	56	21 496	68	21 657	75
$^2T_1$	22 052	38	22 085	64	22 209	109
$^2T_1$	33 961	3	33 759	5	33 688	8

(ii) Γ_7 excited states

	$n_\pi = 0.07$		$n_\pi = 0.10$		$n_\pi = 0.13$	
	E	*D*	*E*	*D*	*E*	*D*
$^4T_2$	2 711	4	2 674	5	2 632	8
$^4T_1$	5 182	2 319	5 354	3 355	5 503	4 368
$^4T_1$	15 976	17 948	15 801	24 807	15 612	31 437
$^2T_2$	16 624	0	16 710	0	16 931	5
$^2T_2$	18 791	45	18 652	80	18 793	78
$^2T_2$	22 690	24	22 678	37	22 651	61
$^2A_2$	32 372	0	32 123	0	32 062	0
$^2T_2$	32 858	2	32 518	3	32 410	5
$^2T_2$	51 054	24	50 767	38	50 641	59

(iii) Γ_8 excited states

	$n_\pi = 0.07$		$n_\pi = 0.10$		$n_\pi = 0.13$	
	E	*D*	*E*	*D*	*E*	*D*
$^4A_2$	− 118	—	− 136	—	− 168	—
$^4T_2$	2 587	58	2 561	72	2 465	100
$^4T_2$	2 758	31	2 740	38	2 702	56
$^4T_1$	4 863	4 446	5 023	6 493	5 116	8 338
$^4T_1$	5 238	4 600	5 410	6 664	5 572	8 664
^2E	13 984	34	13 872	50	14 035	230
$^2T_1$	14 695	768	14 583	1 355	14 667	3 357
$^4T_1$	15 973	35 860	15 798	49 637	15 609	62 851
$^4T_1$	16 279	34 164	16 131	47 123	16 017	58 329
$^2T_2$	16 369	410	16 455	72	16 609	7
$^2T_2$	18 823	355	18 675	651	18 713	981
$^2T_1$	18 933	258	18 781	398	18 883	242
^2E	20 387	32	20 260	52	20 295	69
$^2T_1$	21 442	393	21 541	557	21 671	743
$^2T_1$	22 094	9	22 131	8	22 202	3
$^2T_2$	23 148	49	23 117	76	23 223	135
^2E	24 785	26	24 840	36	24 793	62
$^2T_2$	32 714	3	32 346	5	32 218	8
$^2T_1$	33 907	17	33 728	28	33 608	46
^2E	49 879	0	49 491	0	49 520	2
$^2T_2$	50 768	23	50 442	38	50 331	58

the simple dipole-length approximation such that, in the l.c.a.o. expansion of the dipole matrix elements between m.os all two-centre terms are neglected (Mulliken 1949). Thus, if ϕ_{b_m} and ϕ_{c_n} are atomic orbitals m, n centred on atoms b, c

$$\langle \phi_{b_m} | r | \phi_{c_n} \rangle = \pm \delta_{bc} \delta_{mn} R, \tag{5.10}$$

where $\pm R$ is the projection of the distance of ligand i from the metal on to the coordinate axes. With this approximation, we have in the present instance

$$\langle \mathrm{e} \| m \| \mathrm{t}_2 \rangle = c_2 c_7 R, \tag{5.11}$$

the coefficients being those defined in equation (5.4).

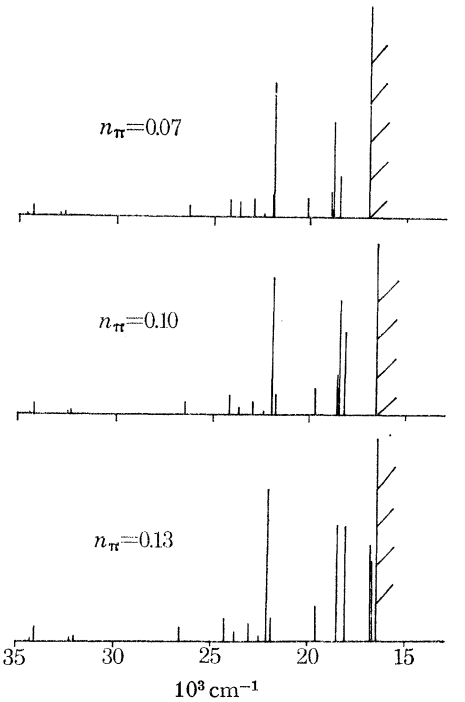

FIGURE 26. Calculated doublet spectrum of $CoCl_4^{2-}$ including spin-orbit coupling. The heights of the lines are proportional to the dipole strengths.

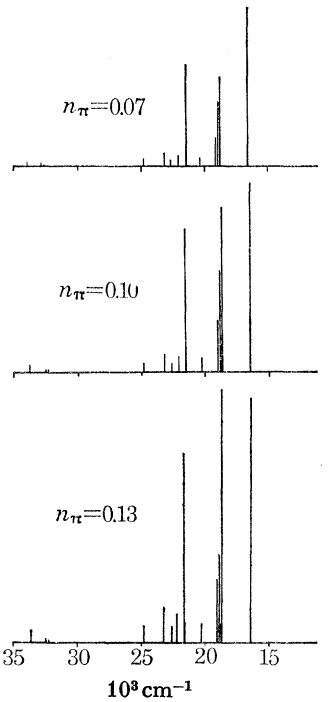

FIGURE 27. Calculated doublet spectrum of $CoBr_4^{2-}$ including spin-orbit coupling. The heights of the lines are proportional to the dipole strengths.

In table 20 we list the eigenvalues resulting from diagonalization of the spin-orbit matrices using the m.o. coefficients of table 19, which were in turn derived from least-squares fitting the Russell–Saunders terms to the experimental baricentres. Also listed in table 20 are the dipole strengths of the transitions and the Russell–Saunders term making the largest eigenvector contribution to each spinor state. In several instances the mixing of adjacent Russell–Saunders states by the spin-orbit coupling is such that the parentage of the resulting states may only be stated approximately. The major features in the predicted absorption spectrum in the region of the spin-forbidden transitions are also indicated in figures 26 and 27. In these figures the heights of the lines are proportional to the dipole strengths, except for the weakest transitions, whose dipole strengths have been exaggerated by a factor of two to render them visible on the diagram.

Comparing the predicted spectra of figures 26 and 27 with the experimental observations of figure 2 it is clear that the molecular orbital method has proved capable of giving an excellent

overall picture of the spin-forbidden region of the ligand-field spectrum, with regard both to the positions and relative intensities of the spin-orbit components. Thus for example $\Gamma_8(^2T_1)$ near 22 000 cm^{-1} is indeed the most intense transition, with the exception of the band group at 18 000–18 500 cm^{-1}. In the chloride the latter group is better reproduced by the higher values of n_π, which, throughout the calculations, lead to a rapid increase in the intensities of all the transitions. In the bromide, on the other hand, it is the lowest n_π (0.07) which gives the closest agreement between the relative intensities of $\Gamma_8(^2T_1)$ and the 18 000 cm^{-1} group. We now comment in detail on the relation between theory and observation for each of the band groups in turn, using the labelling of the spectral regions from figure 2 and tables 14 and 15.

Region I. Calculation and the observed polarizations agree that this region contains $^2T_1$, the sign of the spin-orbit splitting being correctly reproduced. In agreement with the calculation it is also the most intense of the three band systems of regions I and II, which correlate with ^2F in the weak field limit.

Region II. In the chloride the problem in this region is the location of the $^2A_2$ transition. In the bromide $^2A_2$ is the single vibronic progression comprising region II b but in the chloride it appears to comprise only one very weak line (79*z*). It is of interest that throughout the calculations $^2A_2$ is predicted to have zero dipole strength. The calculation correctly assigns the remainder of this region as $^2T_2$, though the sign of the spin-orbit splitting does not agree with that observed in the bromide, though from the analysis of the experimental spectrum there appears to be a particularly complicated vibronic situation. In the chloride the detailed assignment of the low symmetry and spin-orbit levels remains unclear.

Region III. The single Γ_8 level of region III has moderate intensity in both compounds, in agreement with the calculation. The assignment of this band system as Γ_8 has been fully confirmed by magnetic circular dichroism (Collingwood *et al.* 1971).

Region IV. This region, diffuse in the chloride, is sharp and well resolved in the bromide, where the observed site-group splittings and polarizations indicate a Γ_8 level lying about 400 cm^{-1} above a Γ_7 in complete agreement with the spin-orbit calculation. The Γ_7 component is more intense relative to Γ_8 in the bromide, also as required by the calculation.

Region V. In accord with the spin-orbit calculation this region contains a Γ_6 and a Γ_8 origin. Experimentally, in both compounds Γ_8 lies below Γ_6, an order which agrees with the calculation only for the chloride. Indeed, the molecular orbital calculation yields $\Gamma_6 > \Gamma_8$ independently of n_π for the chloride, while in the bromide calculation the two levels remain close, and actually invert as n_π varies. Experimentally, the separation between the Γ_6 and Γ_8 is about 200 cm^{-1} in both compounds.

Region VI. As predicted by the calculation region VI is more intense than any of the higher frequency doublets. Analysing the spectra, we proposed that in Cs_3CoCl_5 this region contains both $^2T_1$ and ^2E, but that they become separated from one another in Cs_3CoBr_5, where they have been labelled as VI a and VI b respectively. Taking the simpler situation in the bromide, the calculation correctly reproduces the weaker Γ_8, coming from ^2E, at lower energy than the composite envelope containing both components of $^2T_1$. However, the calculation overestimates the separation between the two band systems VI a and VI b: experimentally they are about 600 cm^{-1} apart, but the calculation places them nearly 1200 cm^{-1} from each other. In contrast, the two spin-orbit components of $^2T_1$ (VI a) lie no more than 50 cm^{-1} apart for all values of n_π, while in the observed spectrum their origins are about 120 cm^{-1} apart, in the opposite sense. It should be remarked, however, that the site-group splitting of the Γ_8 component is substantial,

PHILOSOPHICAL TRANSACTIONS OF THE ROYAL SOCIETY A MATHEMATICAL, PHYSICAL & ENGINEERING SCIENCES

and that there is strong coupling to non-totally symmetric vibrational modes in this state, so vibronic coupling may be exercising some influence on the energy separations of these components. In Cs_3CoCl_5 the situation is complicated by the near-degeneracy of ^2E and $^2T_1$, a feature which is unfortunately not reproduced by the calculation, which places the two Γ_8 components 1750 cm^{-1} apart. On the other hand, the order of the Γ_6 and Γ_8 components is predicted correctly.

Region VII. This region is broad and diffuse both in the chloride and the bromide. All calculations on both compounds agree in placing a $^2T_1$ and $^2T_2$ close together at this point. The combined oscillator strengths of the four resulting spin-orbit levels is correctly predicted as greater than that of any of the other band systems, with the exception only of those levels almost degenerate with the quartets. As we have already commented above, the high intensity of these bands in the chloride, compared with region VI, is best accounted for by the higher values of n_π (e.g. 0.13), a lower value such as 0.07–0.10 being more appropriate to the bromide.

Regions VIII and IX. No satisfactory empirical analysis of regions VIII and IX could be made either in Cs_3CoCl_5 or Cs_3CoBr_5. The calculation predicts further very intense components of $^2T_2$ and $^2T_1$ parentage and, at slightly lower energy, $^2A_1$. We believe on balance that the former comprise region VIII and the latter region IX, but the vibronic structure in the observed spectra is so complicated that this proposal is quite tentative.

(*c*) *Remarks on factors influencing the quality and sensitivity of the fits: significance of the parameters extracted*

In § 5 (*a*) brief comments were made about some of the problems connected with the least-squares fitting process. Before discussing the chemical significance of the orbital populations and energy differences obtained, some more detailed remarks about the interrelation between the parameters are required. The most striking feature of the parameter values of tables 16 and 17 is the large value of Δ, compared with that extracted from a conventional crystal field analysis. For example, the values producing the fits in the left-hand columns of figures 24 and 25 are 3230 cm^{-1} ($CoCl_4^{2-}$) and 3080 cm^{-1} ($CoBr_4^{2-}$), compared with values from the molecular orbital analysis of 40 000–60 000 cm^{-1} ($CoCl_4^{2-}$) and 7700–9700 cm^{-1} ($CoBr_4^{2-}$). This difference is in part due to the different definitions of Δ in the two models, a point we take up again below. It is clear, however, that quite apart from that, any difference in covalence between e and t_2 will serve to increase Δ in the course of finding the best fit to the spectrum using the molecular orbital model. For example, if one starts the fitting process from a region of the parameter space close to that suggested by a conventional crystal field approach (i.e. n_e and n_t equal, and Δ about 3000 cm^{-1}) any increase in the covalency of t_2 compared with e means that electron repulsion in the former is reduced and, unless Δ increases, electrons may be transferred from e to t_2. The molecular orbital fits indeed converge to values of n_e greater than n_t, as expected.

Another possible explanation for the high values of Δ is that the metal Racah parameters have been overestimated since the effect of bonding between the metal 4*s* and ligand orbitals has been ignored. If the metal Racah parameters are reduced uniformly by 10 %, the fits converge to somewhat smaller values of Δ, but the standard deviations are at least 50 % greater than those listed in tables 16 and 17. We therefore conclude that the magnitudes of the Racah parameters used previously have been reliably estimated.

The other parameter whose fitted values are unexpected is n_π. In both $CoCl_4^{2-}$ and $CoBr_4^{2-}$ the best fits, as gauged by the standard deviations, are obtained for the larger values of n_π, primarily because increasing n_π decreases the energy of $^4T_1(P)$, which is consistently overestimated

throughout. One possible reason for the bad reproduction of the $^4T_1(P)$ energy is that the off-diagonal matrix element linking it with $^4T_1(F)$ is being overestimated. This matrix element, which is equal to $2\sqrt{(3)}\,i$ (table 7), may be reduced by increasing n_π since the expression for i (table 11 (h)) contains a term $(2n_\sigma - n_\pi)$. The largest term in the expression for i, however, is $n_t\sqrt{(n_e n_t)}$ B, which also becomes smaller as $n_t < n_e$. From table 16 we see that n_t indeed becomes smaller the higher Δ becomes. From a number of fits, starting in different regions of the parameter space, with and without constraints, it seems clear that to reproduce the main features of the ligand field spectrum with the particular set of molecular orbital approximations described here, large values of both Δ and n_π are essential. It remains to examine the chemical significance of the parameters, and their relationship to those obtained from molecular orbital calculations.

There has been much discussion about the definition of the crystal- or ligand-field splitting parameter, $10Dq$ or Δ, most recently by Richardson and his colleagues (Soules, Richardson & Vaught 1971; Richardson *et al.* 1971) in connexion with their open-shell s.c.f.-m.o. calculations on octahedral fluoride chromophores of the 3d elements. No calculations at the level of sophistication of Richardson's appear to have been performed on the tetrahedral d^7 ions, whose spectra we have used as examples in this paper. Only the most general comments are therefore possible.

Semi-empirical ligand-field theory views Δ as an orbital energy difference, so that neglecting configuration interaction, the energy of a transition from $e^n t_2^m(Sh)$ to $e^{n-x}t_2^{m+x}(S'h')$ is given by

$$E = x\Delta + G(e^{n-x}\,t_2^{m+x}; S'h') - G(e^n\,t_2^m; Sh) = x\Delta + \Delta G,$$

where ΔG is the change in electron repulsion energy accompanying the transition. Thus for example our least-squares fit places the spin-orbit baricentre of $^4T_2$ in $CoCl_4^{2-}$ 3090 cm^{-1} above the $^4A_2$ ground-state when n_π is fixed at 0, close to the experimentally observed baricentre (Van Stapele *et al.* 1966) at 2922 cm^{-1}. In conventional ligand-field theory, which assumes that the transition changes the occupation of otherwise fixed 3d atomic orbitals, for this particular transition $\Delta G = 0$, and Δ is equal to the ligand-field 10Dq. However, in the more general molecular orbital theory the e and t_2 orbitals have different radial extensions, and ΔG is no longer zero. Indeed, as we have noted earlier, it contains contributions from the Racah A parameters, which are of the order of 160 000–180 000 cm^{-1} (§ 5 (a)), so that very small changes in ΔG have a big effect on the value of Δ which best fits the observed transition energy. In the case of the $(e^4t_2^3)\,^4A_2 \rightarrow (e^3t_2^4)\,^4T_2$ transition of $CoCl_4^{2-}$, from the diagonal elements of table 7, modified to take account of hole-electron equivalence using equation (2.8a), we find the transition energy

$$\begin{aligned} E &= \Delta + G(e^3t_2^4; {}^4T_2) - G(e^4t_2^3; {}^4A_2) \\ &= \Delta + (a + 4b - 2c - 2d - 3e + 5f + g + h - 2j) + (b + 2d - 2g - 4h - j) - (3b - 3j) \\ &= \Delta + a + 2b - 2c - 3e + 5f - g - 3h. \end{aligned}$$

The values of the electron repulsion parameters $a \ldots j$ obtained from the least-squares fit with $n_\pi = 0$ are listed in table 18 and indicate that the predicted transition energy of 3090 cm^{-1} is the sum of opposed contributions of 60 159 cm^{-1} from the orbital energy difference Δ and 57 069 cm^{-1} from the change in electron repulsion ΔG. It is clear therefore that in our model Δ may be viewed as the transition energy in the field of the ligand ions plus the transition metal core, a molecular orbital analogue of the crystal field $10Dq$. For each of the orbitals e and t_2 it then contains the sum of the kinetic energy, core potential energy and Coulomb and exchange interaction with all the orbitals except these two.

Richardson (Soules *et al.* 1971) has made a similar partition of the energy difference between

the states $^3A_{2g}$ and $^3T_{2g}$ arising from his calculation on the NiF_6^{4-} chromophore. When a basis set containing only 3d orbitals on the metal is employed, he finds that the calculated energy of this transition, which is also equal to $10Dq$ at the crystal-field level of approximation, is given by opposing contributions of 40 700 cm^{-1} from the orbital energy difference between t_{2g} and e_g, and 32 840 cm^{-1} from the change in electron repulsion energy. Richardson's theoretically derived results are therefore of very much the same magnitude as those which we have derived by least-squares fitting our somewhat simpler n.d.d.o. model to experimental spectra.

The scheme for approximating electron repulsion integrals which we have described in this paper, together with the matrices set out in tables 6–9, enable a similar molecular orbital analysis to be carried out on the ligand-field spectra of most other octahedral and tetrahedral transition metal complexes. Orbital energy differences and molecular orbital eigenvectors could thus be evaluated, for direct comparison with those found, either by conventional ligand-field methods or molecular orbital calculations. In the present paper we have limited ourselves to ligand-field spectra, but the integral approximations which we have derived for combinations of e, t_1 and t_2 orbitals also make possible, for the first time, a fully quantitative treatment of charge transfer spectra, and of the interactions between ligand-field and charge transfer configurations. This point will be taken up separately in later papers.

References

Allard, N. 1961 *C. r. hebd. Séanc. Acad. Sci., Paris* **252**, 3970
Allen, J. W., McFarlane, R. M. & White, R. L. 1969 *Phys. Rev.* **179**, 523.
Ballhausen, C. J. & Jørgensen, C. K. 1955 *Acta. chem. scand.* **9**, 397.
Ballhausen, C. J. & Gray, H. B. 1964 *Molecular orbital theory*. New York: Benjamin.
Balt, S. 1967 *Rec. Trav. chim. Pays-Bas* **86**, 1025.
Belgers, H. G., Bongers, P. F., Van Stapele, R. P. & Zijlstra, H. 1964 *Phys. Lett.* **12**, 81.
Berman, R., Brock, J. C. F. & Huntley, D. J. 1964 *Cryogenics* **4**, 333.
Berman, R. & Huntley, D. J. 1963 *Crygoenics* **3**, 70.
Bird, B. D. & Day, P. 1968 *J. chem. Phys.* **49**, 392.
Bird, B. D. 1969 D.Phil. thesis, Oxford University.
Bird, B. D., Day, P. & Grant, E. A. 1970 *J. chem. Soc.* **A**, 100.
Blume, M. & Watson, R. E. 1962 *Proc. R. Soc. Lond.* A **270**, 127; 1963, **271**, 565.
Brown, T. H. & Taylor, R. L. 1965 *J. chem. Phys.* **42**, 3979.
Clementi, E. 1964 *J. chem. Phys.* **41**, 303.
Collingwood, J. C., Day, P. & Denning, R. G. 1971 *Chem. Phys. Lett.* **10**, 274.
Condon, E. V. & Shortley, G. H. 1935 *The theory of atomic spectra*. Cambridge University Press.
Cotton, F. A., Goodgame, D. M. L. & Goodgame, M. 1961 *J. Am. chem. Soc.* **83**, 4690.
Craig, D. P. & Walmsley, S. H. 1968 *Excitons in molecular crystals*. New York: Benjamin.
Dreisch, T. & Trommer, W. 1937 *Z. phys. Chem.* B **37**, 37.
Dunn, T. M. 1961 *Trans. Faraday Soc.* **57**, 1441.
Eisenstein, J. C. 1961 *J. chem. Phys.* **34**, 1628.
Ferguson, J. 1963 *J. chem. Phys.* **39**, 116.
Figgis, B. N., Gerloch, M. & Mason, R. 1964 *Acta crystallogr.* **17**, 506.
Figgis, B. N. 1966 *Introduction to ligand fields*. New York: Interscience.
Gilson, T. R. 1970 Personal communication.
Grant, E. A. 1970 D.Phil. thesis, Oxford University.
Griffith, J. S. 1960 *Molec. Phys.* **3**, 285.
Griffith, J. S. 1961 *The theory of transition metal ions*. Cambridge University Press.
Griffith, J. S. 1962 *The irreducible tensor method for molecular symmetry groups*. Englewood Cliffs: Prentice-Hall.
Hochstrasser, R. M. 1967 *J. chem. Phys.* **47**, 1015.
Jesson, J. P. 1968 *J. chem. Phys.* **48**, 161.
Jørgensen, C. K. 1962 *Prog. inorg. Chem.* **4**, 73.
Jørgensen, C. K. 1971 *Modern aspects of ligand field theory*. North Holland.
Koide, S. & Pryce, M. L. H. 1958 *Phil. Mag.* **3**, 607.
Lohr, L. L. 1966 *J. chem. Phys.* **45**, 3611.

PHILOSOPHICAL TRANSACTIONS OF THE ROYAL SOCIETY A MATHEMATICAL, PHYSICAL & ENGINEERING SCIENCES

Lohr, L. L. 1971 *J. chem. Phys.* **55**, 27.
Misetich, A. A. & Buch, T. 1964 *J. chem. Phys.* **41**, 2524.
Misetich, A. A. & Watson, R. E. 1966 *Phys. Rev.* **143**, 335.
Morosin, B. & Lingafelter, E. C. 1960 *Acta crystallogr.* **13**, 807.
Morosin, B. & Lingafelter, E. C. 1961 *J. phys. Chem.* **65**, 50.
Mulliken, R. S. 1949 *J. Chim. phys.* **46**, 497.
Mulliken, R. S. 1955 *J. chem. Phys.* **23**, 1833.
Nicholson, B. J. 1970 *Adv. Chem. Phys.* **18**, 249.
Pelletier-Allard, N. 1965*a* *C.r. hebd. Séanc. Acad. Sci., Paris* **260**, 2170.
Pelletier-Allard, N. 1965*b* *C.r. hebd. Séanc. Acad. Sci., Paris* **261**, 1259.
Pople, J. A., Santry, D. P. & Segal, G. A. 1965 *J. chem. Phys.* **43**, S129.
Powell, H. M. & Wells, A. F. 1935 *J. chem. Soc.* 359.
Racah, G. 1942 *Phys. Rev.* **61**, 186.
Racah, G. 1943 *Phys. Rev.* **63**, 367.
Richardson, J. W. & Rundle, R. E. 1956 *Theoretical study of the electronic structure of transition metal complexes.* Oak Ridge (Tenn.): U.S. Atomic Energy Comission Technical Information Service.
Richardson, J. W., Soules, T. F., Vaught, D. M. & Powell, R. R. 1971 *Phys. Rev.* B **4**, 1721.
Ruedenberg, K. A. 1951 *J. chem. Phys.* **19**, 1433.
Soules, T. F., Richardson, N. W. & Vaught, D. M. 1971 *Phys. Rev.* B **3**, 2186.
Stoneman, C. 1964 Ph.D. thesis, University of London.
Tanabe, Y. & Sugano, S. 1954 *J. phys. Soc. Japan* **9**, 753.
Tanabe, Y. 1960 *Prog. theor. Phys.* (*Kyoto*), Suppl. 14, 17.
Van der Ziel, J. P. 1967 *Phys. Rev. Lett.* **18**, 237.
Van Stapele, R. P., Belgers, H. G., Bongers, P. F. & Zijlstra, H. 1966 *J. chem. Phys.* **44**, 3719.
Watson, R. E. 1959 Techn. Report no. 12, *Solid State and Mol. Theory Group.* Cambridge (Mass): M.I.T.
Weakliem, H. A. 1962 *J. chem. Phys.* **36**, 2117.
Whittaker, E. & Robinson, G. 1944 *The calculus of observations.* London: Blackie and Son.
Wielinga, R. F., Blöte, H. W. J., Roest, J. A. & Huiskamp, W. J. 1967 *Physica* **34**, 223.
Wigner, E. 1959 *Group theory and its application to the quantum mechanics of atomic spectra.* London: Academic Press.

PHILOSOPHICAL TRANSACTIONS OF THE ROYAL SOCIETY A MATHEMATICAL, PHYSICAL & ENGINEERING SCIENCES